Phase I Final

# HIGH TEMPERATURE ZERO DROP THYRATRON TUBE PROGRAM

Prepared for
Jet Propulsion Laboratory
4800 Oak Grove Drive
Pasadena, California
Attention: Mr. T. J. Williams

Contract JPL 951352

EOS Report 7016 - Phase I 1 February 1966

Prepared by

Wm J Kearns

W. J. Kearns

**This work was performed for the Jet Propulsion Laboratory, California Institute of Technology, sponsored by the National Aeronautics and Space Administration under Contract NAS7-100.**

Approved by

A. O. Jensen, Manager
ELECTRO-OPTICAL TECHNOLOGY LABORATORY

Approved by

George R. White

George R. White, Manager
OPTICAL-ELECTRONICS GROUP

ELECTRO-OPTICAL SYSTEMS, INC. - - PASADENA, CALIFORNIA
A Subsidiary of Xerox Corporation

CONTENTS

CONTENTS (contd)

## 1. INTRODUCTION

This report describes the Phase I work on JPL Contract 951352. The 12-month contract is concerned with the development of a high-temperature power conditioning system for a 150-watt thermionic converter generator consisting of thyratrons, a high-temperature transformer, and associated circuitry. Two schemes were investigated: (1) high-temperature, metal-ceramic thyratrons and a high-temperature inverter transformer mounted adjacent to the thermionic converter generator to eliminate the need for high-current bus bars from the generator to the load (a low-current, low-temperature grid-drive circuit will be located a safe distance from the heat source); and (2) high-temperature ceramic thyratrons mounted directly behind the thermionic-converter generator but connected to a low-temperature transformer and grid circuit by high-current bus bars. In both approaches, the thyratron cathode was heated by thermal energy from the generator cavity, the thermal energy absorbed by the thyratron being used to provide electron emission and work-function adjustment to effect zero-drop operation. This thermal energy would normally be considered rejected heat from the solar concentrator.

The program, as planned, was divided into two phases. The first phase of 3 months duration was an analytical study of both schemes. The study compared the relative merits of the integrated tube and transformer approach with the more conventional low-temperature transformer approach. It also included the design, fabrication, and testing of a low-current cesium device to determine deionization times and other discharge parameters to be expected in the thyratron. Quantitative knowledge of such parameters is not available in the literature. Phase II, to be started after JPL approval of the results of Phase I,

was to be of 9 months duration. During this phase, a high-temperature ceramic thyratron, a high-temperature transformer, and dc to dc converter circuits will be designed according to the criteria established in Phase I. At least four high-temperature thyratrons, two high-temperature transformers, and one complete dc to dc converter of each type described above will be fabricated and tested.

The effort for this reporting period was applied toward the initial investigation of the three areas of interest, namely, the thyratron design and deionization time test vehicle, the high-temperature transformers, and the inverter circuit analysis. The program schedule has been altered so that Phase I and Phase II are each of 6 months duration. No change in the overall program objectives has been made.

## 2. THYRATRON ANALYSIS AND DESIGN

The characteristics of the thyratron required for efficient dc to dc conversion at an input of 2.8 volts are given in Table 2-I.

**TABLE 2-I**

DESIRED THYRATRON CHARACTERISTICS

| | |
|---|---|
| Forward Tube Drop | 0 ±0.1V |
| Forward Conduction Current | 100 A |
| Minimum Forward Blocking Voltage | 20 V |
| Maximum Forward Blocking Current at 20V | 0.1 A |
| Peak Inverse Voltage | 20 V |
| Maximum Reverse Current (at 20V) | 0.1 A |
| Deionization Time | < 125 microsecond |
| Firing Time | < 10 microsecond |
| Maximum Grid Drive Power | 0.25 W Average |

### 2.1 Design Criteria

The tube characteristics listed in Table 2-I are described below in terms of the physical parameters which determine these ratings.

#### 2.1.1 Forward Tube Drop

The forward tube drop is defined as the voltage appearing across the thyratron between anode and cathode when the tube is conducting in the forward direction. This drop is determined by several factors which can be expressed by Eq. (A) where

$$\phi_c - \phi_a - V_s - V_p - V_g = 0 \qquad \text{(A)}$$

$\phi_c$ and $\phi_a$ are the cathode anode work functions, $V_s$ is the total sheath drop, $V_p$ is the plasma drop, and $V_g$ is the [illegible] across the grid aperture. $V_s$, the total sheath drop, is equal to $V_{c_s} + V_{a_s}$ (Fig. 2-1(b)). In practice, the sum of $V_s$, $V_p$ and $V_g$ ranges between 0.5 and 1.5 volts, the smaller value applying to the relatively close spacing and open grid structure to be used in the thyratron. It is essential that both grid and anode back emission be minimized, and this can be accomplished only by keeping the grid and anode relatively cool, say below 700°C. Under these conditions, the grid and anode work functions will be 1.8 volts. These values when put into Eq. (A) yield a required cathode work function of 2.3 to 2.8 volts. The details of balancing the cathode work function (i.e., temperature and cesium pressure to establish the correct emission current level to handle the load current) will be discussed in Subsection 2.1.2.

### 2.1.2 Effect of Grid on Tube Drop

The addition of a third element between the emitter and collector of a gas diode introduces considerable complexity into the energy level diagram applicable to the diode. Figure 2-1 (a) shows the potential distribution through the axis of a thyratron grid hole prior to breakdown with a negative voltage, $V_g$, applied to the grid. As can be seen from the diagram, the work function of the grid is very important in establishing the height of the potential barrier and minimizing the amount of applied voltage needed to prevent electron flow to the anode during the OFF cycle. Care must be taken to keep the total grid potential (i.e., the sum of $\phi_g + V_g$) below the point where a breakdown in the interelectrode region between either the grid and cathode or grid and anode might take place. Figure 2-1 (b) shows the potential distribution through the axis of the grid hole after breakdown. In this case, the grid is well shielded from the plasma by a plasma sheath and is no longer effective in controlling the discharge. With attention

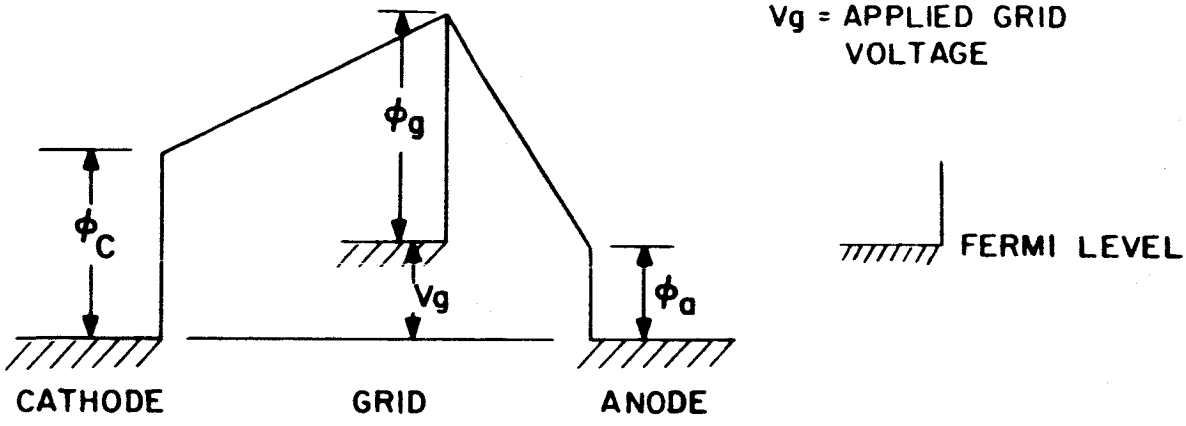


a. Potential distribution before conduction

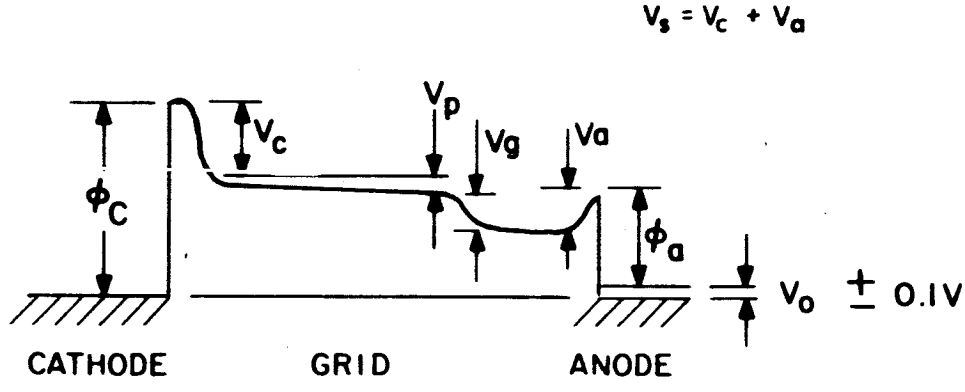


b. Potential distribution during conduction

FIG. 2-1 POTENTIAL DISTRIBUTIONS THROUGH AXIS OF GRID

to the design of the grid aperture and interelectrode spacing, the potential drop through the grid sheath can be reduced to a minimum so that no more than 0.1 to 0.4 volt is added to the usual plasma drop occurring in a cesium diode.

### 2.1.3 Current Capacity

The design goal for the thyratron is 100 amperes although the actual circuit in which it will be used will be only a nominal 50 ampere circuit. The original intention was to use a molybdenum cathode operating at a current density of about 5 $A/cm^2$. However, the emission curves for cesium or rhenium shown in Fig. 2-2 indicate that 10 $amps/cm^2$ can be obtained at cesium pressures well below 1 torr with a cathode temperature of 1277°C and cathode work function of 2.3V. Choosing this operating point will allow adjustment of the several parameters which control the tube characteristics, namely, cesium pressure and cathode temperature to adjust the work function difference for zero tube drop. Operating with low cesium pressure (< 1 torr) assures high frequency operating capability as will be discussed in the next section.

### 2.1.4 Turn OFF Time (Deionization Time)

#### 2.1.4.1 Grid Aperture Design

The problems of controlling the discharge are a function of grid design including the effects of aperture design and temperature control.

To minimize the plasma drop through the sheath, it is very important that the discharge utilize all the cross-sectional area of the openings in the electrode which separate the anode and cathode. When this condition obtains, the discharge is called a "spread discharge." When the current goes through only one aperture, the discharge is said to be "constricted." These two conditions are illustrated in Figs. 2-3 (a) and 2-3 (b). It is obvious that a spread discharge is a more desirable operating mode

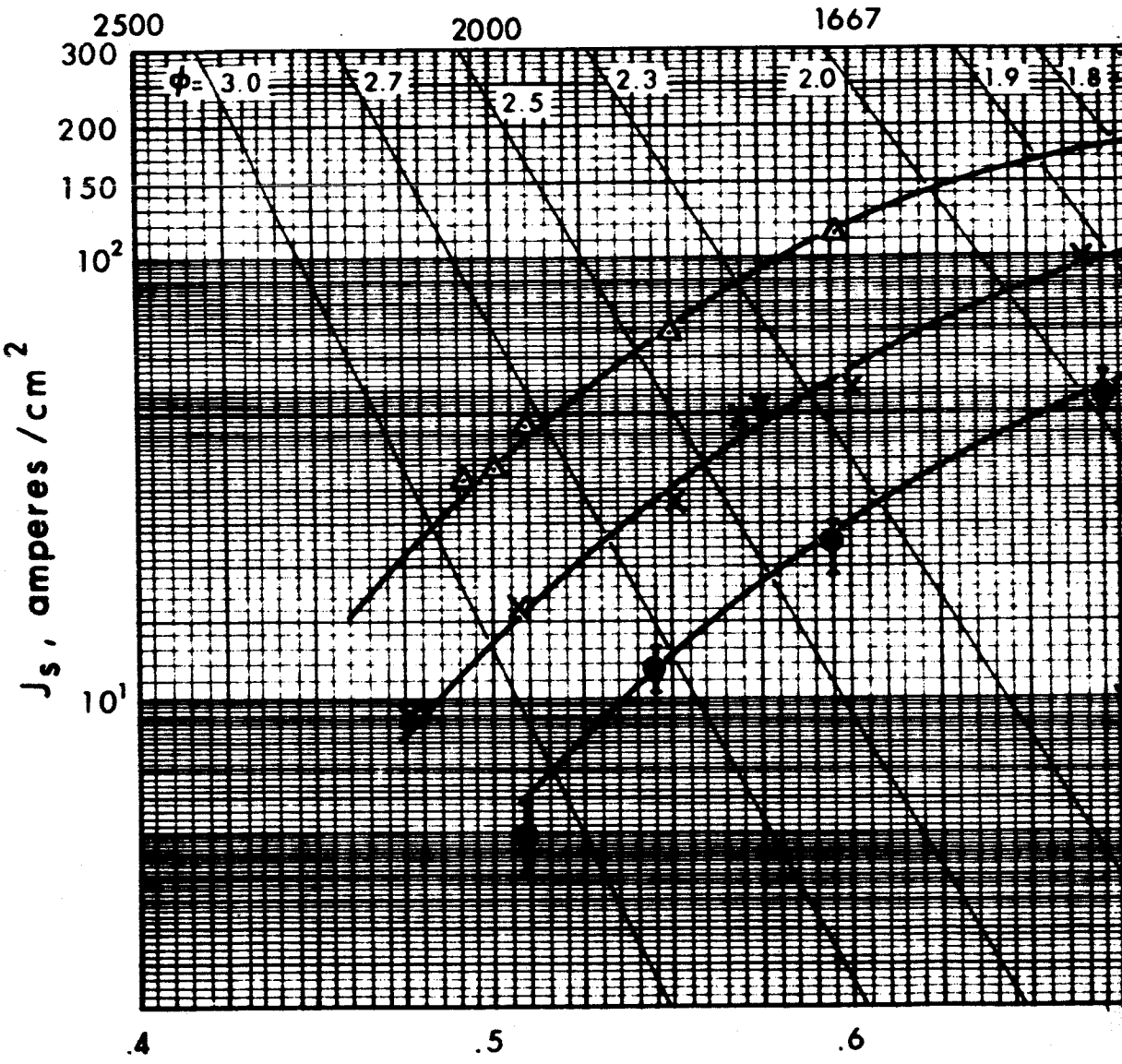
2500
2000
1667
300
200
150
$10^2$
$10^1$
$\phi$= 3.0
2.7
2.5
2.3
2.0
1.9
1.8
$J_s$, amperes /cm$^2$
.4
.5
.6
100

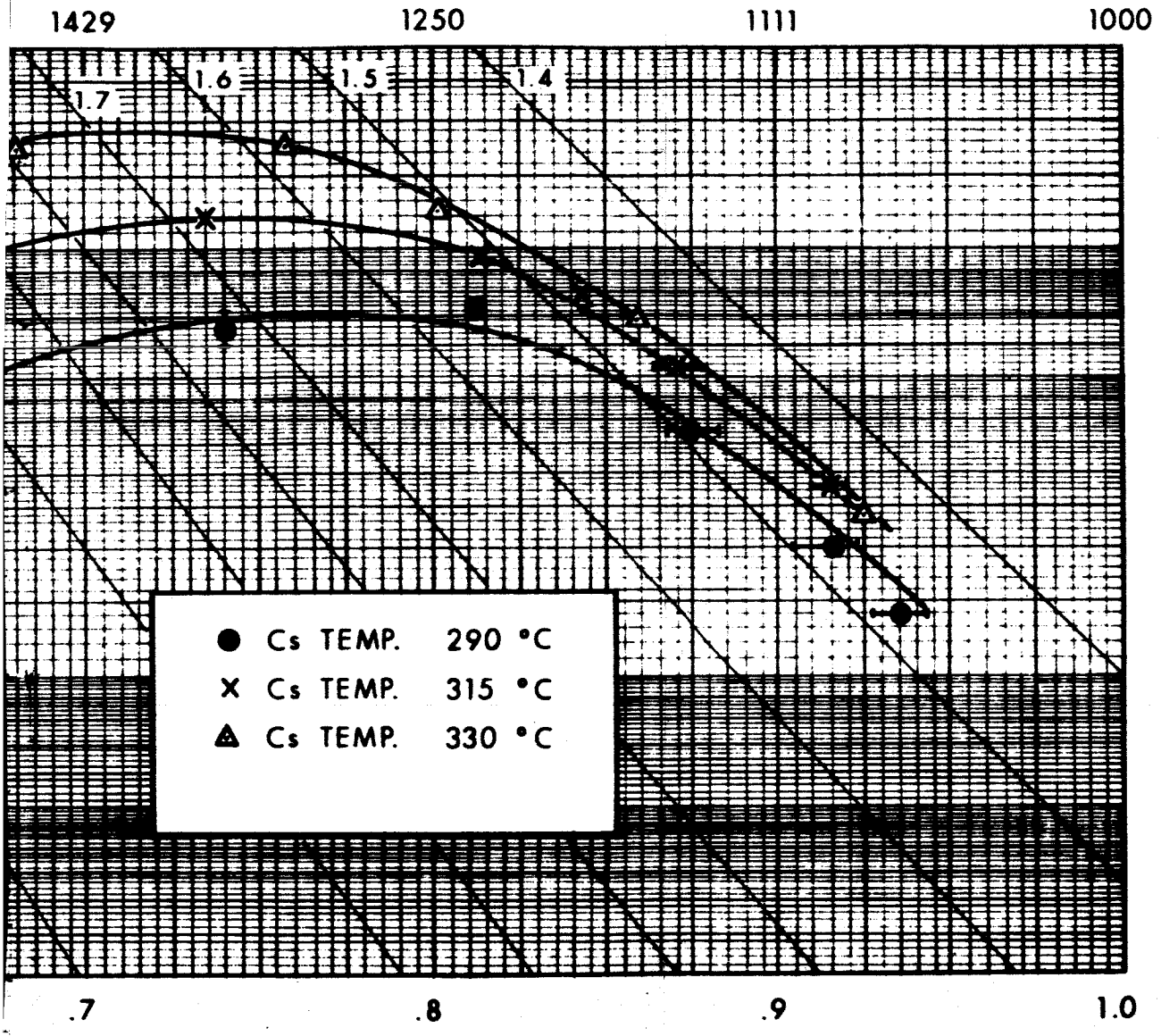


FIG. 2-2 SATURATED ELECTRON EMISSION FROM POLYCRYSTALLINE RHENIUM



2

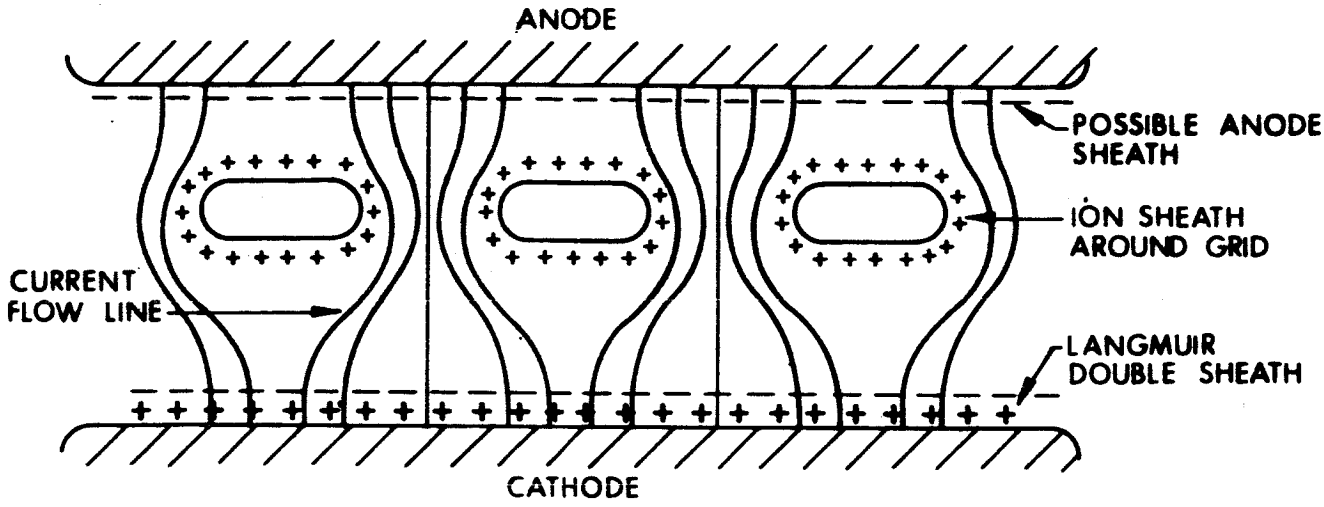


a. SPREAD DISCHARGE

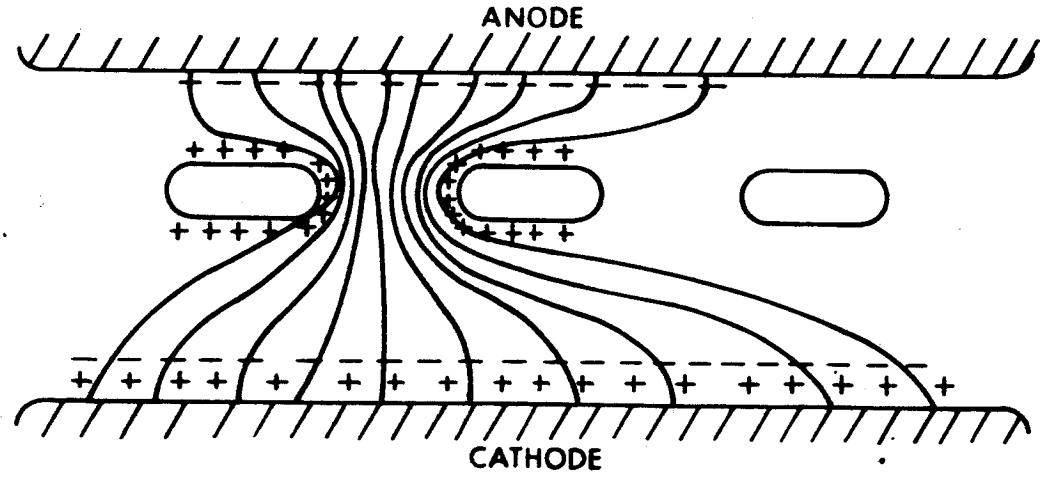


b. CONSTRICTED DISCHARGE

FIG. 2-3 CURRENT FLOW FOR CONSTRICTED AND SPREAD DISCHARGES THROUGH GRID APERTURE

for a controllable discharge tube, since all the grid holes are carrying current and the plasma loss is minimized. To estimate the condition of pressure and aperture dimension required to insure the spread discharge condition, one can apply the "Fetz criterion" originally worked out by Fetz[1] for mercury vapor and later by Kok[2,3] for the noble gases. It should, in principle, apply also to cesium vapor. The critical pressure-aperture relationship is given by:

$$p s_e r_o = 2\sqrt{m/M}$$

where:

- $p$ = pressure in torr
- $s_e$ = differential ionization coefficient (ionization probability) in ion pairs/cm torr
- $r_o$ = grid aperture radius in cm
- $\sqrt{m/M}$ = mass ratio of electron to the $Cs^+$ ion (or $Cs_2^+$ ion, whichever actually occurs in the discharge)

Therefore, when $p s_e r_o < 2\sqrt{m/M}$, the discharge is spread. When $p s_e r_o > 2\sqrt{m/M}$, the discharge is constricted, and all the current tends to concentrate in one opening.

Using a range of ionization probability[4] $0.01 \leq s_e \leq 1$, and a pressure range $0.05 \leq p \leq 1$ yields the following range of allowable grid aperture for a mass ratio $\sqrt{m/M}$ of 1/500.

$$\text{For} \begin{cases} p = 1 \text{ torr} \\ s_e = 1 \text{ ion pair/cm torr} \end{cases} \quad r_o < \frac{1}{250} \text{ cm}$$

$$\text{For} \begin{cases} p = 0.05 \text{ torr} \\ s_e = 0.01 \text{ ion pair/cm torr} \end{cases} \quad r_o < 8 \text{ cm}$$

The above pressure range certainly encompasses all useful values for thyratron operation. A desirable operating pressure from an emission standpoint is 0.5 torr and a reasonable grid aperture size is 0.2 cm. Putting these quantities into the Fetz criterion yields a value of 0.04 for $s_e$, a value within the range of the differential ionization coefficient $0.01 \leq s_e \leq 1.0$ ion pair/cm torr.

The greatest uncertainty in such a calculation is always the ionization coefficient. The early work of Hull, Berger, and Westbrook[5] demonstrated grid control with larger apertures than 0.2 cm. Kearns and Pehek[6] also demonstrated grid control in spread discharges in rubidium vapor whose ionization coefficient is almost identical with cesium in the low-energy range encountered in a plasma. This early work has shown that grids with large apertures (2 to 4 mm) are effective in controlling the discharge, thus justifying the lower values of $s_e$ as those most characteristic of a low density cesium vapor plasma.

2.1.4.2 Ionization Processes

The discussion in Subsection 2.1.4 is based on single electron-impact ionization. Pollock and Jensen[7] have suggested that the formation of the $Cs_2^+$ ion by photon absorption at the resonance levels 3521Å and 3043Å and/or two stage impact ionization at ~ 1.45 eV is primarily responsible for space-charge neutralization in the high-temperature thermionic converter. As the emitter temperature is lowered, the photon flux from the cathode decreases and the ionization process becomes more a two stage electron-impact process. However, even at the relatively low cathode temperature of 1300 to 1500°C anticipated for the thyratron, some photoexcitation will occur. The magnitude of the photoexcitation effect on the arc drop of the thyratron will certainly be negligible at the lower emitter temperature, but it may have an effect on the starting characteristics and the "hold-off" voltage of the tube. It is felt, however, that the dominant ionization process in the thyratron will probably be an electron impact two stage mechanism.

2.1.4.3 Problems of Grid Control

One of the most serious problems of grid control, that of grid emission, was mentioned in Subsection 2.1.1. Two other problems are: (1) recovery of grid control (deionization), and (2) voltage hold-off.

Recovery of grid control can be brought about in several ways. The usual method is to design the tube so that tube pressure and interelectrode spacings allow the ions from the plasma to reach the wall or electrode surfaces quickly by ambipolar diffusion and become neutralized in a short time compared to the time the tube is in the negative portion of the applied voltage cycle. In the type of circuit to be used for this converter, there is a short portion of time when the anode voltage approaches zero or even goes negative with respect to the cathode. During this time, the grid regains control due to a combination of deionizing processes taking place in the tube and to the action of a negative grid pulse which can be applied to the grid to sweep ions from the interelectrode space.

Fortunately, the voltages encountered in the circuit probably will never exceed 10 volts in any polarity. For this reason, it is not inconceivable that current cutoff could be achieved by grid action alone. For example, methods for interrupting an established plasma by combined electric and magnetic fields have been proposed by Jensen.[8] The low internal voltages of the zero drop thyratron make the tube particularly amenable to such crossed-field grid control action. However, the design of the thyratrons as proposed for this program is based on electrostatic grid firing techniques used in conventional thyratrons. To determine what the upper frequency limit of grid control is achievable in a cesium thyratron two approaches were investigated and the results compared. The first approach was to calculate the theoretically attainable grid control frequency from available data in the literature. The second was to make actual deionization time measurements in a specially designed vehicle.

#### 2.1.4.4 Calculation of Plasma Decay Time

An approach to estimating the deionization time of the interelectrode region of the thyratron (grid-anode region) can be made by simplifying the geometry to that of an infinite plane

electrode system with the space between electrodes filled with plasma at a charge density $n_e = n_p$ which would prevail for the highest current to be conducted; $n_e$ and $n_p$ are the electron and ion densities. This infinite electrode geometry now permits a one-dimensional solution to the ambipolar diffusion equation.

$$\frac{\partial n}{\partial t} = D_a \nabla^2 n \tag{1}$$

where n is the charge density ($n = n_e = n_p$) and $D_a$ is the ambipolar diffusion coefficient. The one-dimensional solution to this equation gives the particle density at any time t

$$n\ (x,\ y,\ z,\ t) = n_o\ (x,\ y,\ z)\ \exp\ (-t/\tau) \tag{2}$$

where $\tau$ is the decay constant. The coefficient $D_a$ is assumed to be constant and (1) can be written as

$$\nabla^2 n = \left(\frac{-1}{D\tau}\right) n. \tag{3}$$

Equation (3) is a classical eigenvalue problem with various standard solutions depending upon the boundary conditions as established by the geometry. The plane parallel geometry chosen above suggests the solution for rectangular geometry where

$$n(x) = \sum_k n_k \cos\left(\frac{x}{\Lambda_k}\right) \tag{4}$$

where $$\Lambda_k^2 = D_a \tau_k. \tag{5}$$

$\Lambda$ is called the characteristic diffusion length and the subscript k refers to the diffusion mode; for each $\Lambda_k$ there is a corresponding decay time $\tau_k$, $\tau_1$ being the time for the fundamental mode. For the infinite plane case the ratio of $\tau_1/\tau_2 = 9$ and for $\tau_1/\tau_3 = 25$ , , , so that for all practical purposes, all higher order decay modes can be neglected.

Putting the boundary condition n = 0 at x = ± L/2, where L is the distance between planes, into (4) yields

$$\cos\left(\frac{L\Lambda_k}{2}\right) = 0$$

and

$$\frac{L\Lambda_k}{2} = (2K-1)\frac{\pi}{2} \tag{6}$$

which for k = 1

$$\Lambda = \frac{L}{\pi}. \tag{7}$$

Putting (7) into (5) yields finally for $\tau_1 = \tau$, the first order decay time

$$\tau = \frac{1}{D_a}\left(\frac{L}{\pi}\right)^2. \tag{8}$$

Before a decay time can be determined, a value for $D_a$, the ambipolar diffusion coefficient, is required. If the ion and electron mobilities are known, $D_a$ can be calculated from Equation (9)

$$D_a = \frac{\mu_+ D_- + \mu_- D_+}{\mu_+ + \mu_-} \tag{9}$$

where $\mu_+$ and $\mu_-$ are the ion and electron mobilities and $D_+$ and $D_-$ are the ion and electron diffusion constants. $D_a$ can also be expressed as

$$D_a = D_+ \frac{T_-}{T_+} = D_- \frac{\mu_+}{\mu_-} \tag{10}$$

and by the Einstein Relation

$$D_- = \frac{k}{e} T_- \tag{11}$$

where $T_- \gg T_+$, k is the Boltzmann constant, and e is the electronic charge.

Equation (11) is the most useful one, since only $\mu_+$ and the specification of electron temperature are required. Equations (10) and (11) are reasonably correct when $T_e \gg T_+$, $\mu_- \gg \mu_+$ and the mobility is constant over a range of temperature and electric field. However, when $T_e = T_+$, $D_a = 2D_+$ which contradicts (10) as written. The correction term shown in (12) takes the change in electron temperature into account and corrects

$$D_a = \mu_+ \frac{k}{e} T_e \left[1 + \frac{T_+}{T_e}\right] \tag{12}$$

the values obtained in equations (10) and (11).

The most believable data on ionic mobilities appears to be that of Chanin and Steen[10,11] which is reproduced in Table II which also compares their values with other workers.

The values for $\mu_o$ are for a gas density equivalent to 760 torr at 0°C and for zero fields. Equation (13) will correct the values to the conditions found in the thyratron, i.e., gas temperature of 1000°K and pressure of 1 torr

$$\mu_+ = \mu_o \left(\frac{760}{P}\right) \left(\frac{T}{273}\right) \tag{13}$$

Equation (3) has been solved for the decay time (deionization time) which is the time for the plasma to have decayed to $\frac{1}{e}$ of its original value and the results are shown in Fig. 2-4. The two extreme values of $\mu_o$ were chosen from Table 2-II and extreme values of electron temperature $T_-$ which should encompass those found in the thyratron were assumed to cover the possible theoretically attainable decay times. An electron temperature of 2000°K represents very nearly thermal equilibrium between ions and electrons; the temperature of 11600°K is the electron temperature likely to be encountered in the plasma at a plasma potential of one volt. Either or both of these conditions are not too unreasonable and may be encountered for various pressure and current conditions in the thyratron.

## TABLE 2-II

COMPARISON OF EXPERIMENTAL AND THEORETICAL MOBILITIES IN CESIUM

| Experimental $\mu_o$ ($cm^2/V$ sec) | | | Theoretical $\mu_o$ ($cm^2/V$ sec) | |
|---|---|---|---|---|
| Chanin and Steen[10,11] (579-679° K) | Dandurand and Holt[12] $Cs_2^+$ | Chen and Raether[13] $Cs^+$ (450-550° K) | Langevin[14] polarization limit $Cs_2^+$ ($T + 0^2$ limit) | Charge Exchange calculation $Cs^+$ (T = 300° K) |
| 0.21 ($Cs_2^+$) | | | | 0.074 |
| | 0.065 | 0.4 | 0.203 | 0.036 |
| | | | | 0.038 |
| 0.075 ($Cs_+$) | | | | 0.055 |

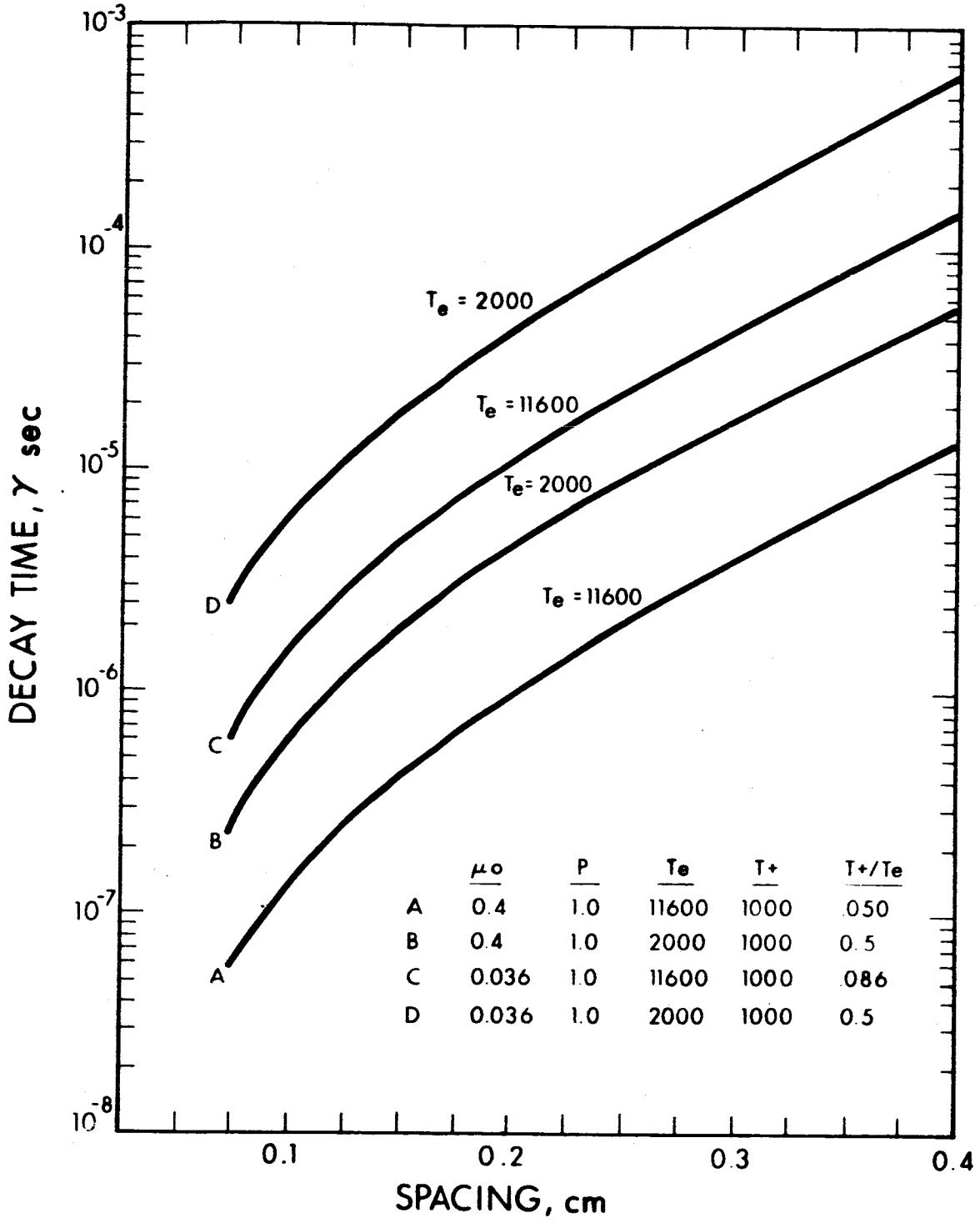


FIG. 2-4 SPACING VERSUS DECAY TIME

From equation (13) the product of $\mu_+ p$ is essentially constant at any given temperature. However, calculations of $D_a$ based on this relationship often give unrealistically high values at low pressure ranges. The calculated decay times as a function of pressure are shown in Fig. 2-5 for the four cases as follows: (A) the upper limit of mobility and the upper limit on electron temperature; (B) the upper limit of mobility and the lower limit on electron temperature; (C) the lower limit on mobility and the upper limit on electron temperature and finally (D) the lower limits of both mobility and electron temperature.

Now it is an experimentally observed fact that the drift velocity of ions in their own gas[15] is a proportional to $\sqrt{E/P}$ for E/P greater than 50. Thus, the 45 degree section of curves A through D which show the decay times for the diffusion controlled mode, must change slope at some points, i.e., from one to one-half to conform to the $\sqrt{E/P}$, mobility controlled, regime. For the two plasma temperatures shown, the ions will be diffusion controlled for pressure greater than 0.04 torr in the case of the electron temperature $T_-$ of 2000°K and for pressures greater than 0.2 torr for the 11600°K electron temperature case. These limits were calculated by expressing the electron temperatures in equivalent volts and solving for the pressure which satisfies

$$\frac{E}{P} = 50. \tag{14}$$

The decay time is then determined by equation 15,

$$= \frac{L}{v} = \frac{L}{B\sqrt{\frac{E}{P}}} \tag{15}$$

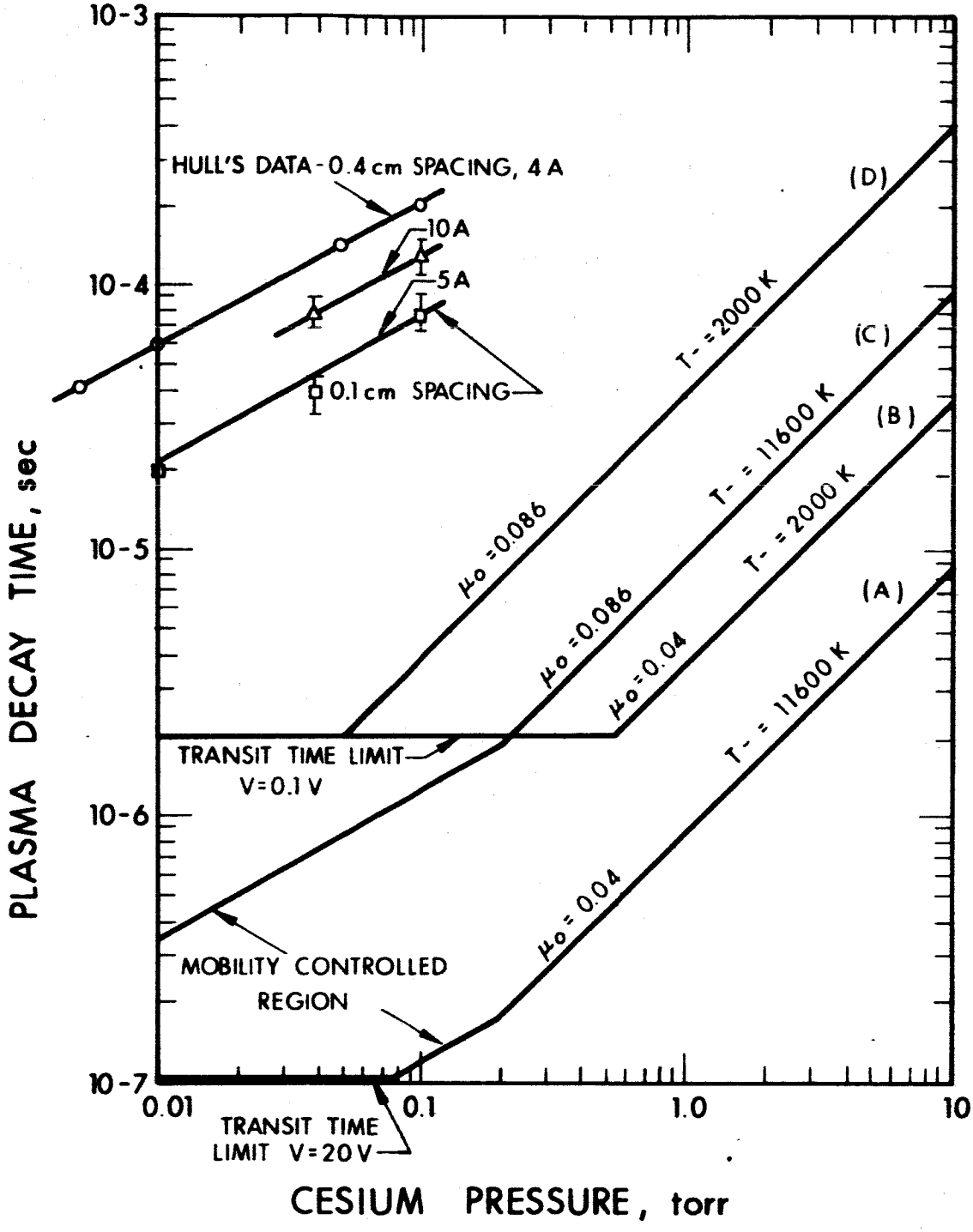


FIG. 2-5 CALCULATED DECAY TIME AS A FUNCTION OF PRESSURE

where v is the ion velocity in cm/sec, B is a proportionality constant, E is the impressed field in volts/cm and p is the pressure in torr. If $\tau$ is measured in such a way that for most of the recovery period $E/P > 50$, then

$$\tau = \frac{L}{B}\sqrt{\frac{P}{E}} \tag{16}$$

The portion of the curve for each case is shown in Fig. 2-5 as lines with a slope of one-half.

A further limitation on the lower limit of decay time is the ion transit time. It is obvious that in the low pressure limit, the decay time cannot be any less than the ion transit time in the gap. This time can be calculated from equation (17)

$$t = \frac{L}{\sqrt{\frac{2\ eV}{300M}}} = \frac{L}{v} \tag{17}$$

where t is the minimum ion transit time, v is the ion velocity in cm/sec, V is the applied voltage in volts, or for zero field conditions, the voltage equivalent of the thermal energy of the ion, e is the electronic change in cgs units and M is the mass of the cesium ion in grams. V will range, therefore, from 0.1V for thermal energies to as high as 2 volts for maximum applied voltage with corresponding limits on t of $2 \times 10^{-6}$ and $1 \times 10^{-7}$ sec, respectively, for an anode-cathode spacing, L, of 0.1 cm (0.040 inch). These limits are drawn in Fig. 2-5 as horizontal lines.

2.1.4.5 Measurement of Plasma Decay Time

Measurements on the decay time of cesium plasmas in a geometry similar to that to be encountered in the actual thyratron were made in the deionization time test vehicle described in Section 3. The results of the measurements for two different load currents are presented in Fig. 2-6 along with the results of the early work of Hull, et al[5] on a cesium vapor thyratron operating at 4 amp

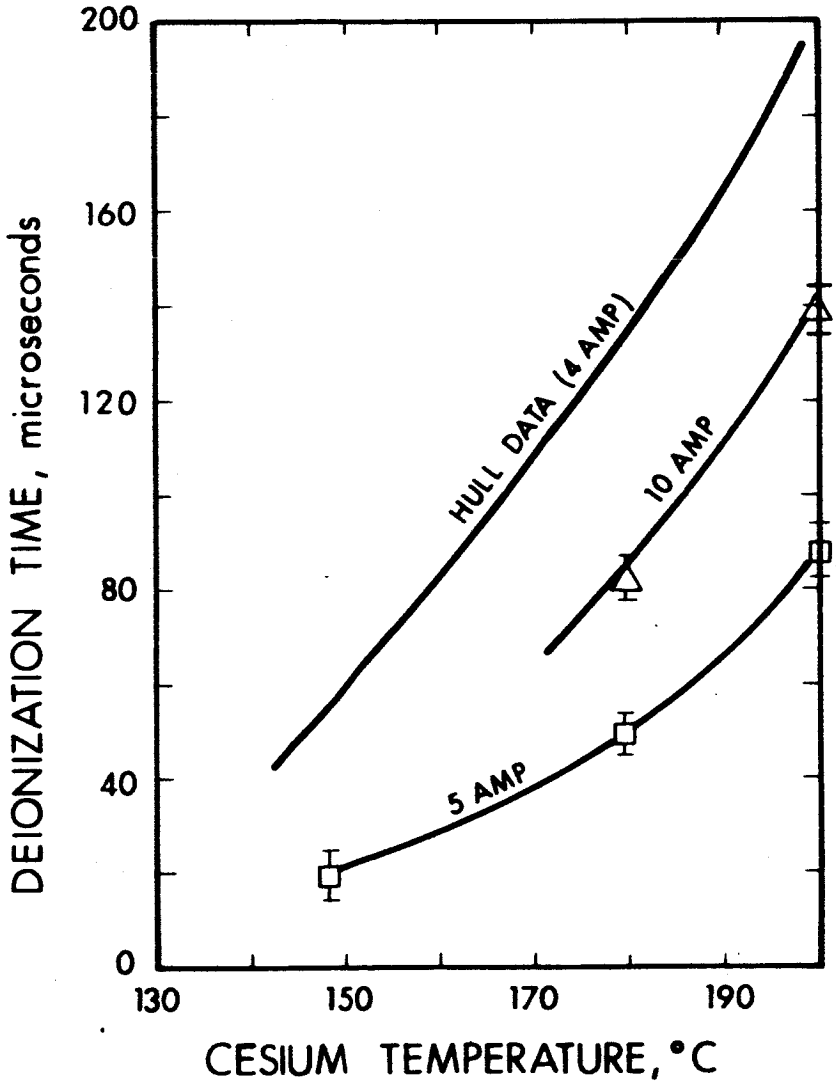


FIG. 2-6 MEASURED DEIONIZATION TIME AS A FUNCTION OF CESIUM TEMPERATURE

load current. The lower deionization times of the recent measurements reflect the closer spacing of 0.1 cm as compared with 0.4 cm spacing of Hull's tube.

The results are more interesting however when they are plotted on Fig. 2-5 for direct comparison with calculated values. All three curves for the experimental data appear to have slopes of one-half indicating that the recovery process is definitely mobility controlled. This is certainly to be expected for Hull's data since his applied voltage was 125 volts and the criterion of equation 14 was easily met. The deionization test vehicle on the other hand is operating very close to the point where the recovery time is diffusion limited. The effect of current on the recovery time is quite apparent also. However, from this data it does appear that, with proper attention to spacing, the desired recovery time to permit circuit operation between 1000 and 1600 cycles can be achieved.

Typical oscillograms of the measurement of deionization time are shown in Fig. 2-7. The deionization times as plotted in Figs. 2-5 and 2-6 are those for which the application of a negative voltage for a duration of the discharge of a charged capacitor through the load resistor enabled the tube to regain control and hold off a forward voltage. The hash at the extreme left in Fig. 2-7 (a) is switch noise which is discussed in Subsection 3.4. Figure 2-7 (b) is quite interesting in that it shows a case where the tube recovered and held off a forward voltage for a time long compared to the turn-off time and finally broke down again probably due to a voltage transient in the circuit.

### 2.1.5 Voltage ratings

The problem of voltage hold-off involves the inter-electrode spacing, grid emission, and vapor pressure of the cesium. The voltage hold-off capability of an electrode system in a gas is given as a function of pd product (pressure in torr x spacing in cm).

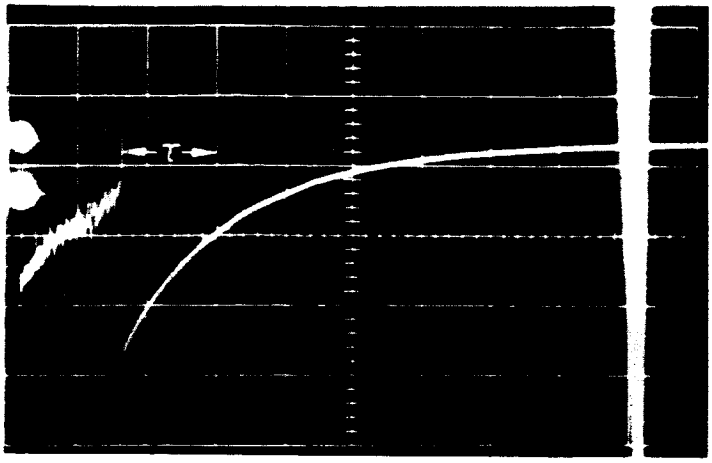


(a)

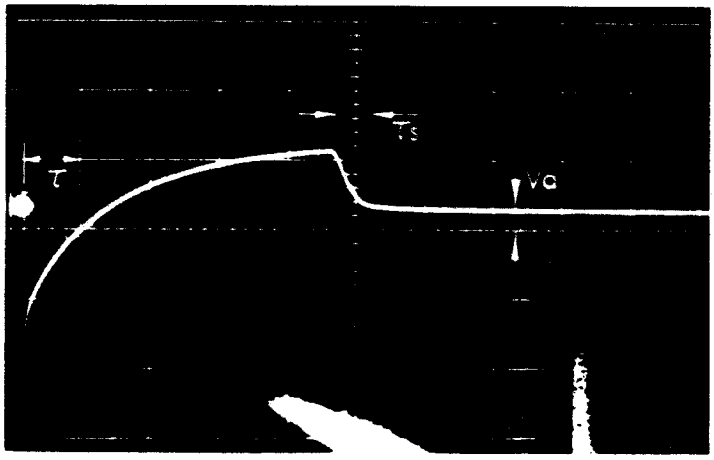


(b)

FIG. 2-7 TYPICAL OSCILLOGRAM OF DEIONIZATION TIME MEASUREMENTS

Because cesium is used often in devices where electrode temperatures are high enough to emit fairly high currents, data on breakdown under these conditions is most useful in the design of a practical device. Figure 2-8 shows a representative curve of voltage versus pd for the case where the electrodes can emit up to 10 $mA/cm^2$, depending on the degree of cesium average. This curve is included in the report because it is the only available data on cesium voltage breakdown for any electrode system. The curve, however, may or may not be directly applicable to thyratron design because it is not known how important the temperature of the electrodes is in determining voltage ratings of devices.

Forward and inverse voltage measurements were made on the deionization time test vehicle. At the highest pressure reached in the measurement of 0.1 torr and with an anode-grid gap of 0.1 cm, the pd is 0.02 torr/cm. The observed hold-off voltage was 20 volts forward and at least 40 volts inverse, considerably higher than the 6 volts predicted by the curve of Fig. 2-8. The discrepancy is possibly due to the fact that the electrodes in the deionization time device were at a maximum temperature of 360°C as compared with temperatures between 415 and 470°C of the electrodes in the device used to obtain the data shown in Fig. 2-8.

### 2.1.6 Turn-on Time

The turn-on time is the time required to initiate a discharge and bring the current up to its full value. For most discharges in gases this time varies from 1 to $10^{-3}$ microseconds. For the cesium vapor thyratron working at very low voltages the ion and electron velocities will be much lower than usual and longer times can be expected. However, a good estimate is 10 microseconds, which is much less than that which would cause any circuit difficulties.

This estimate is verified in the oscillogram of Fig. 2-7 (b) which shows an actual tube starting where the current built up to five amperes from zero in about 20 microseconds.

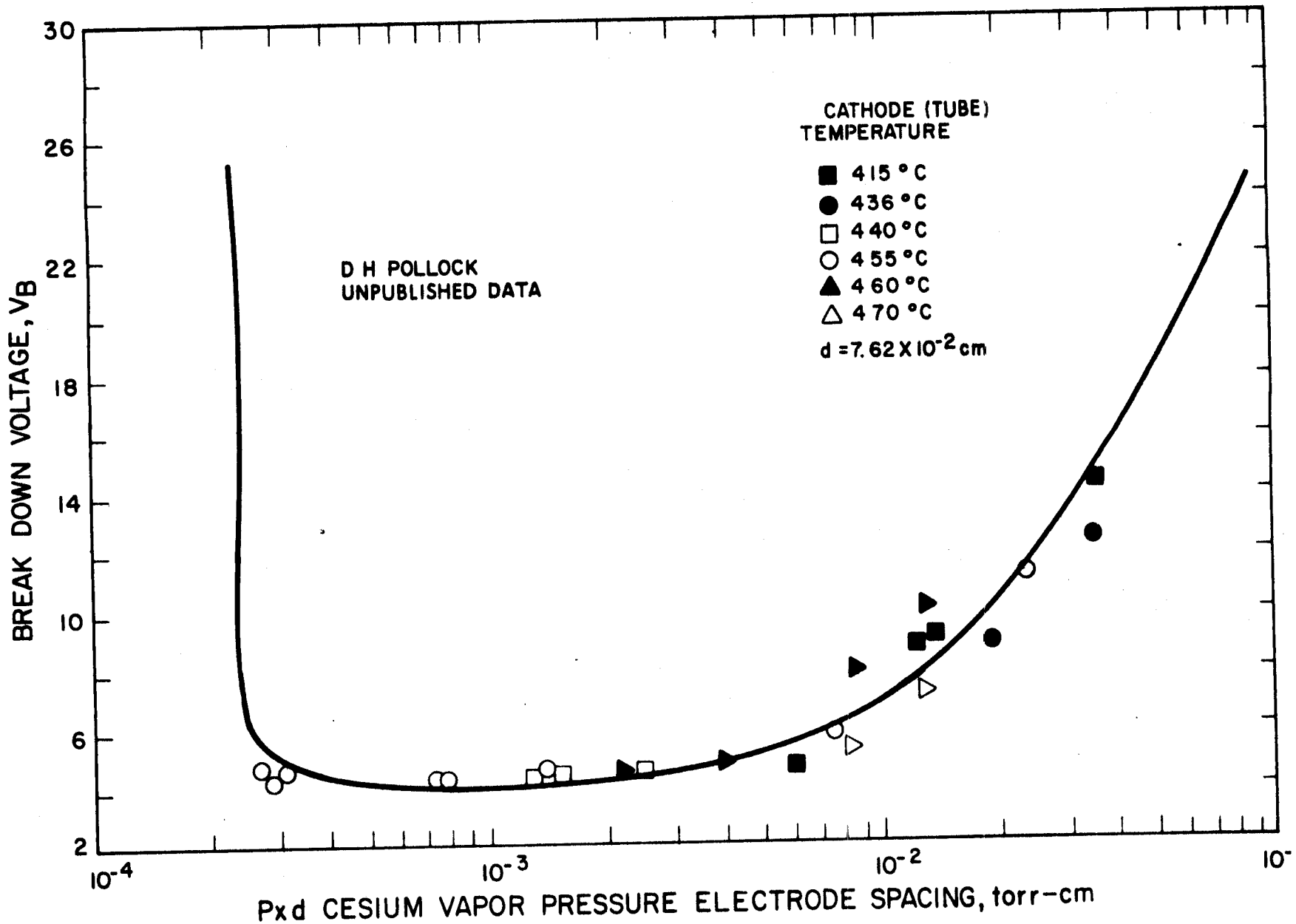


FIG. 2-8 BREAKDOWN VOLTAGE IN CESIUM VAPOR

For accuracy in starting measurements, care must be taken to insure that the inductance of the circuit does not interfere with the measurement. Only moderate care with the breakdown time measurement was applied in these initial measurements. The time as measured, therefore, is a maximum due to the possibility of some inductance effects. While future starting time measurements can be improved in accuracy, it can safely be concluded now that the thyratron starting time is adequately fast for proper circuit operation. It may even be much more desirable, from a circuit point of view, for the rise time to be as slow as 10 or 20 microseconds rather than a fraction of a microsecond as in usual thyratrons, in order to avoid generating transients which might be a source of electrical interference.

### 2.1.7 Grid Drive Power

Due to the requirement that very low grid emission is required for reliable control action, negligible power will be required by the grid. The grid loading will come from the interelectrode capacity, possible leakage currents, and perhaps a microampere or so of grid emission, but the total grid drive power required will be milliwatts at most. Grid emission, per se, is not expected to contribute significantly to the grid drive power.

### 2.1.8 Problem Areas

The principal problem areas will be the adjustment of proper electrode operating temperatures at load conditions and possible grid emission effects.

## 2.2 Proposed Thyratron Structure

A schematic of the configuration proposed for the thyratron is shown in Fig. 2-9. It consists of a cylindrical, internal cathode which is heated by radiation from the thermal cavity. The external cylinder of the thyratron is the anode, which is integral with its radiator. Between the two is interposed the grid or control electrode, also with its integral radiator structure. The electrode radiators

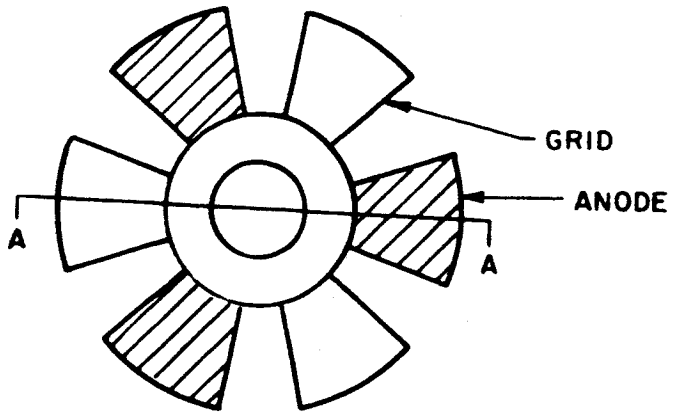


(a) VIEW SHOWING STAGGERED ORIENTATION OF GRID AND ANODE RADIATORS

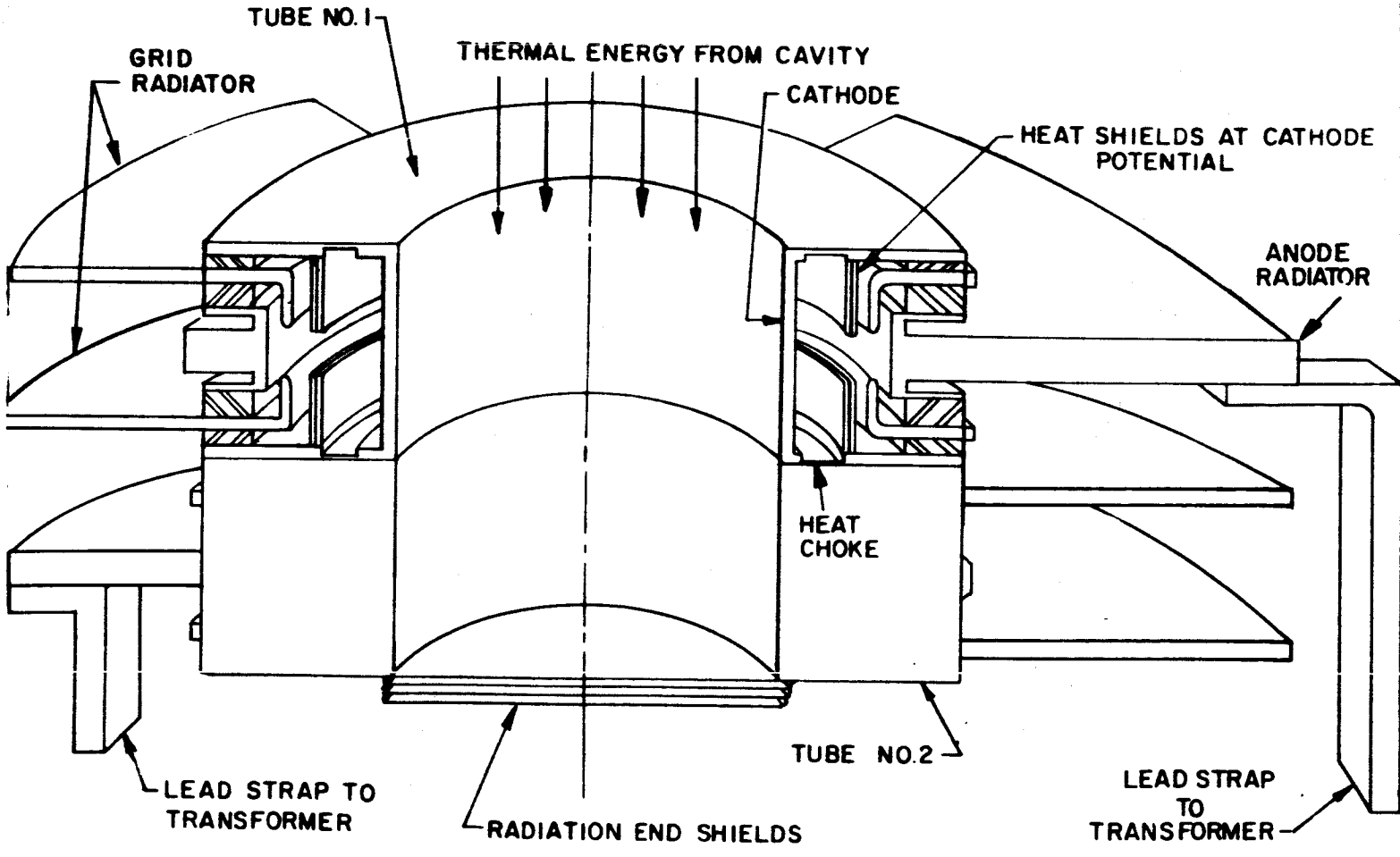


(b) SECTION A-A THROUGH THYRATRONS

FIG. 2-9 PROPOSED THYRATRON STRUCTURE

are important since the only way to establish proper electrode temperatures is by radiation of thermal energy. The anode has, in addition to the radiator, a connection directly to the transformer or to high-current leads for connection to low-temperature circuitry. If a high-temperature transformer is used, it will be so arranged that the high-current winding will act partially as a heat sink for the anode and partially as a heat dissipation device for the transformer itself. Since the tube and transformer are used in a balanced circuit, two thyratrons are required for proper operation of the inverter. Two similar diodes, mounted coaxially as shown in Fig. 2-9, serve as the two elements in the inverter circuit. In the case of the high-temperature transformer, the transformer and its leads are an integral part of the tube configuration. Essentially standard seal configurations utilizing the materials and technologies developed on previous converter programs will be used to make the thyratron tubes.

## 3. DEIONIZATION TIME TEST VEHICLE

The original intention in making the deionization time test measurements was to construct a relatively simple ceramic tube and associated test circuitry to obtain required cesium vapor deionization characteristics with a minimum of time and effort. Such measurements were required because a careful literature search revealed very little applicable data for cesium under the geometry and pressure conditions expected in the thyratron. The most directly useful information was obtained from the work by Hull, Berger, and Westbrook[5] for an early 200 ampere cesium thyratron development program. The cesium pressures for the Hull thyratron were lower and the spacings much wider than those planned for the zero drop tube. The Hull thyratron deionization time data are given in Fig. 2-5 as a function of cesium temperature and pressure.

Almost all recent work on cesium plasma studies is concerned with steady-state cesium discharges and very little with plasma initiation or decay. Measurements on the mobilities of cesium ions in cesium and the drift velocities of electrons in cesium have been made by Chanin and Steen.[10,11] These quantities can be used to calculate a range of deionization times for an assumed geometry by making assumptions the boundary conditions as discussed in Subsection 2.1.4.4. However, there is a considerable variation in the published data as Chanin and Steen point out, and there is always the question of which ion, $Cs^+$ or $Cs_2^+$, is involved in the deionization process. Therefore, the deionization time measurements were essential to the design of a practical cesium vapor thyratron.

During the course of the deionization time measurements, the simplified approach developed several complications. The first deionization test vehicle had some inherent problems which required modifications of materials and design. The two devices are described below.

## 3.1 Deionization Time Test Vehicle Design No. 1

The design of the first test vehicle is shown in Fig. 3-1. To expedite the program, the design dimensions were based on available niobium flanges and ceramics, constituting the long lead-time items. The primary purpose of the tube was to determine deionization times in a cesium plasma contained in a volume approximating that of the final device. The anode-to-grid space of 0.040 inch and the grid-to-cathode spacing of 0.100 inch were maximum spacings to be expected in the final device. Since the deionization is proportional to the plasma volume, all measured deionization times will be maximum values.

The test device was essentially a wide-spaced converter with a grid interposed between emitter and collector (cathode and anode) and insulated by the two ceramic insulators. The grid was made of heavy molybdenum with temperature control being provided by a heater brazed as shown in Fig. 3-1, or a cooling surface which can be bolted to the grid disc through the holes provided on the periphery. The emitter will be heated by electron bombardment in the same manner as thermionic converters. The temperature is monitored by means of a thermocouple inserted into a well in the back surface of the tantalum disc. The anode temperature can also be individually controlled by heating or cooling the anode radiator and support clamps. The magnitude of temperature control for each element, while somewhat limited by the tube's structural aspects affecting heat transfer, should be adequate for the deionization time measurements.

In the actual converter working at very low forward voltage drops, the effect of electrode work functions may be important. However, for the deionization time measurements such electrode potential can be compensated by external potentials and will not influence the measured plasma decay times in any way. More important phenomena in the operation of both the test device and the final design are grid emission and possibly back emission from the anode. These two effects are temperature sensitive and are the primary basis for the electrode

# DEIONIZATION TIME VEHICLE (NO. 1)

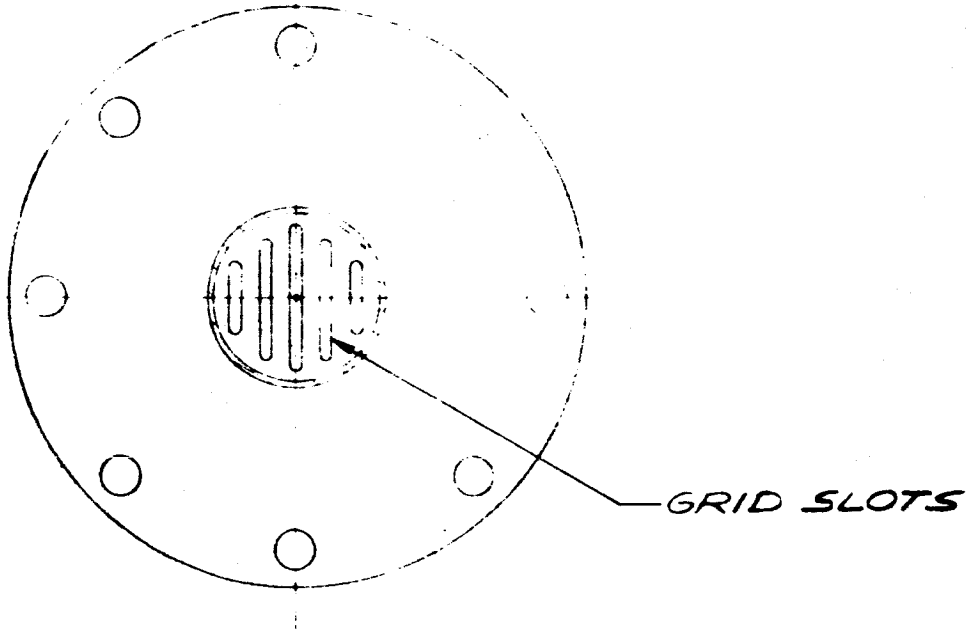


## SECTION A-A

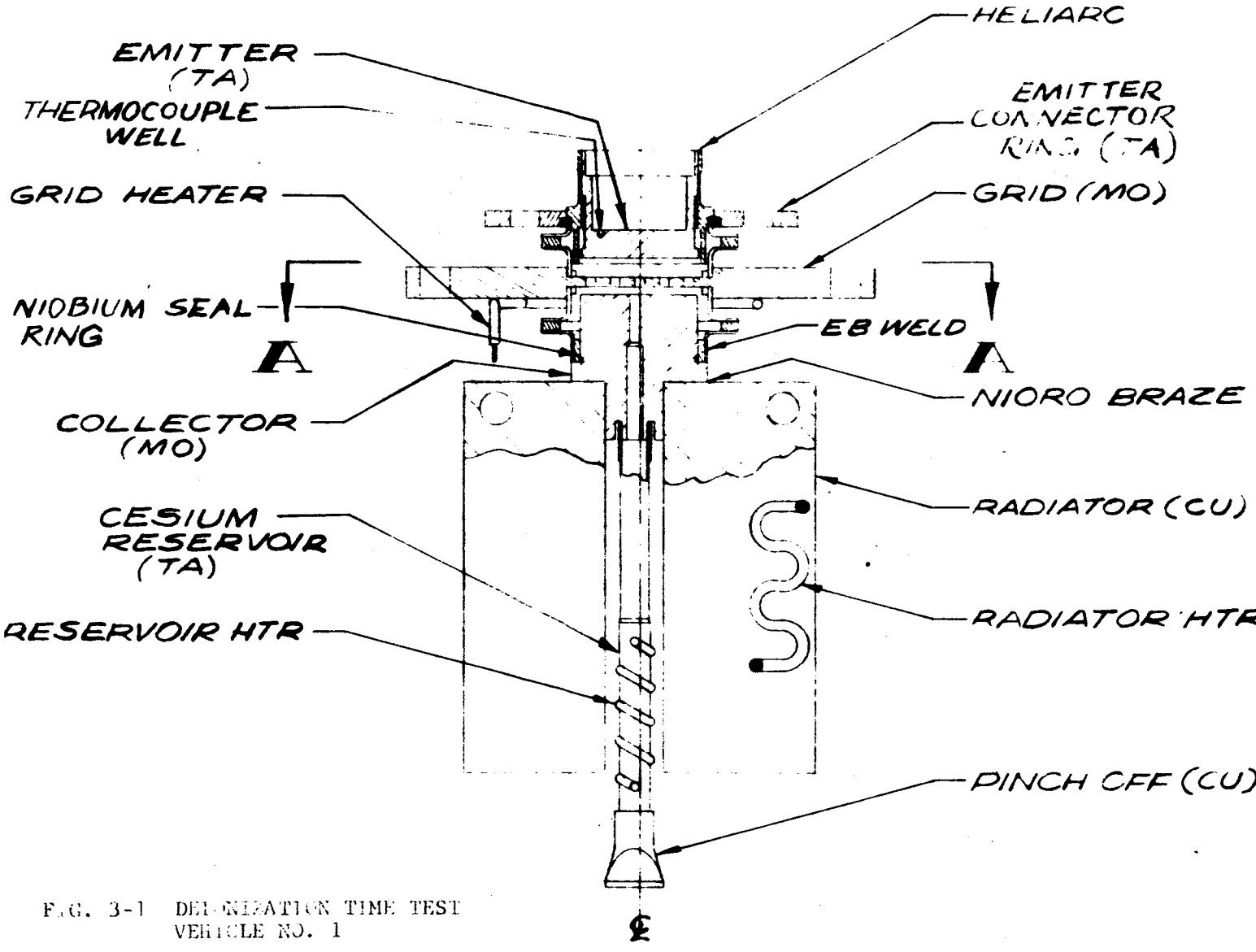


FIG. 3-1 DEIONIZATION TIME TEST VEHICLE NO. 1

temperature control discussed above. Thus, in addition to deionization time data, the tube should provide information of the effect of inverse emission on the recovery time and operation of a three-element structure in cesium vapor.

The problems in fabricating the first design were due to materials and brazing temperature problems. The procedure followed to assemble the tube started with the titanium brazing of the subassemblies consisting of (1) the heat choke envelope, emitter connector ring, and seal flange; (2) grid, tantalum-clad heater, and two seal flanges; (3) collector, cesium reservoir and heater, and niobium seal ring (see Fig. 3-1). Each individual subassembly was titanium-brazed in high vacuum, leak checked and found to be vacuum tight. Subassemblies (1) and (2) were then brazed together to form a seal assembly using active alloy seal to bond the ceramic insulators to the metal parts. Both seal brazes were tight, but the braze operation caused a leak to appear at one of the seal flange joints at the grid, resulting in rejection of the seal assembly. Because the grid was difficult to machine, it was salvaged by machining the defective seal. The above procedure was repeated to make another seal assembly. This time a seal was not vacuum tight, again causing rejection of the seal assembly.

The grid was again salvaged and the grid subassembly (grid plus two seal flanges) was titanium brazed. This time the titanium seal cracked due to the formation of a stable beta phase in the titanium caused by dissolved molybdenum diffusing into the titanium braze volume. The beta titanium has a different coefficient of thermal expansion than the alpha titanium; this resulted in the cracking and leaking of the joint. Because of these difficulties, a new grid structure was made using tantalum as described in the next section.

### 3.2 Deionization Time Test Vehicle No. 2

The molybdenum grid was used in the above structure because there was no tantalum stock of the proper thickness available when the work was begun. When the tantalum was received, the grid was made essentially to the same configuration as the molybdenum grid. Tantalum has two advantages over molybdenum in that its thermal expansion coefficient closely matches niobium and alumina, and it is not as soluble in titanium as is molybdenum; titanium-brazed joints can be temperature cycled more safely with this metal combination. Another grid subassembly was made successfully with the tantalum grid, as was subassembly (2), the grid flange assembly, using the salvaged tantalum emitter connector ring. However, the seal assembly leaked after brazing and microscopic examination showed that the ceramic was not completely wet by the active braze alloy. As before, the tantalum grid and emitter plate were salvaged from the seal assembly and the parts were prepared for another attempt.

The collector or anode electrical connection was changed from the first design to simplify the construction as shown in Fig. 3-2. However, due to repeated reworking, several critical parts became unusable and a new start was required.

### 3.3 Deionization Time Test Vehicle No. 3

Because of the problems associated with the first two designs, it was decided not to use any of the old parts except the tantalum grid and to redesign the device for easier, more reliable assembly.

Due to the seal problems it was decided to modify the structure slightly so that each seal braze consisting of a ceramic ring and two seal flanges could be made as subassemblies. Since each ceramic metal seal was fabricated independently of the other braze operations, a defective seal braze did not spoil a complete assembly. Two more seal brazes were made successfully and the envelope assembly was completed by copper brazing the subassemblies together.

# DEIONIZATION TIME VEHICLE (NO.2)

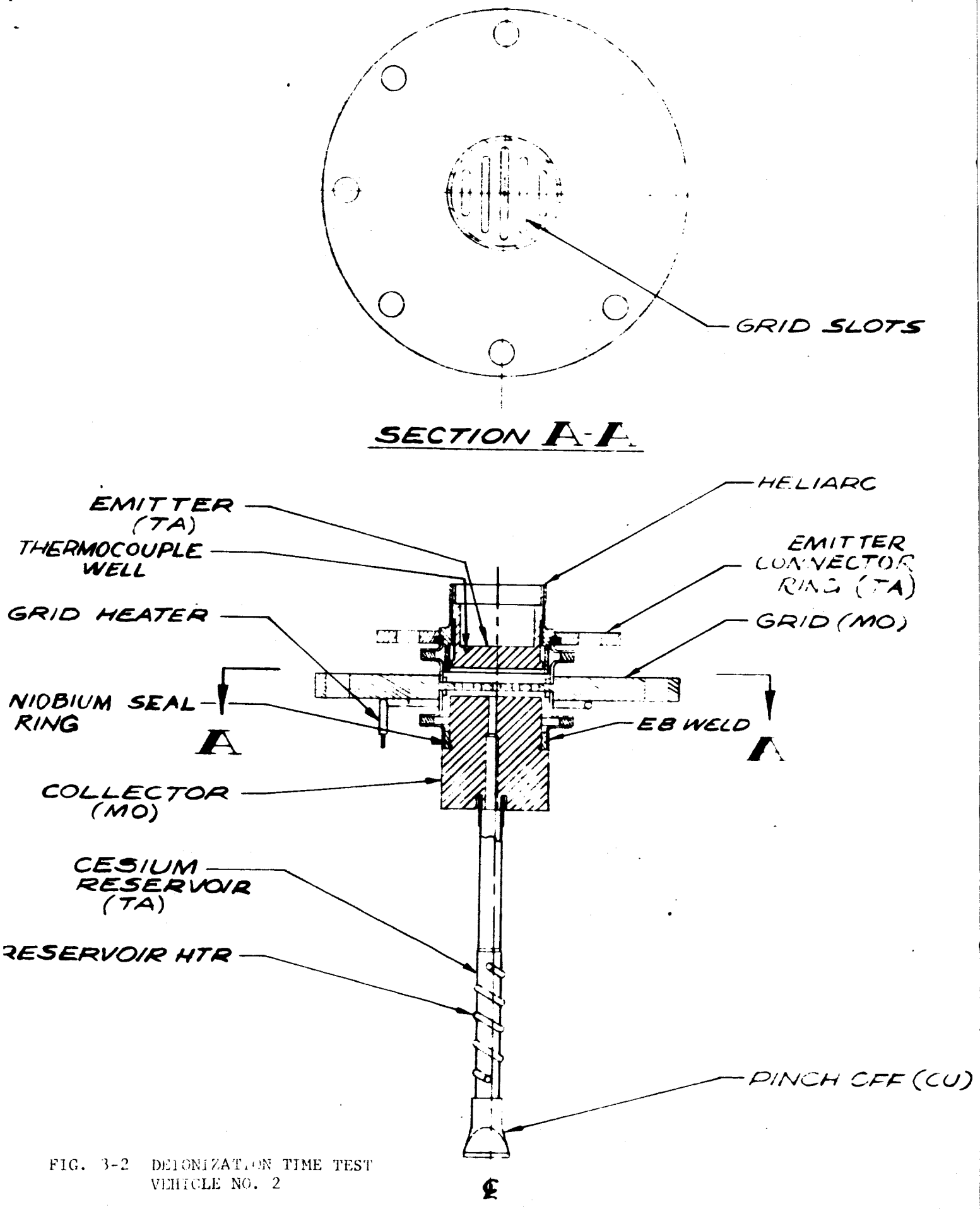


FIG. 3-2 DEIONIZATION TIME TEST VEHICLE NO. 2

Another change was made in the design to simplify the testing procedure as shown in Fig. 3-3. The collector clamp was replaced with heavy copper clamps which fit around the collector shank of existing converters to cool it and to serve as the collector (anode) electrical connector. This clamp also was equipped with electrical heaters in case it was necessary to heat the collector (anode) rather than cool it to prevent parasitic cesium reservoir formation at cool spots in the tube.

This third model was assembled with only one mishap. The copper brazes of the niobium seal flanges to the anode and cathode subassemblies leaked because the copper did not completely wet the tantalum. The device was rebrazed vacuum tight using nicoro solder. Nicoro was chosen for the braze material because it was an alloy with the proper melting point which contained enough nickel to provide the required wetting action on the tantalum to make a vacuum tight joint. The principal objection to nicoro was that, in order to obtain the necessary low melting point (960°C) a relatively high percentage of silver is required, (nicusil is 71.15 percent silver, 28.1 percent copper and 0.75 percent nickel) and silver is attacked by cesium. The rate of attack was slow enough, however, that a useful life of 100 to 300 hours was possible on the deionization time test vehicle which was more than adequate to get the required data.

### 3.4 Deionization Time Measurements

The test circuit chosen for determining the deionization time is one patterned after that used by A. W. Hull[5] in his work on early cesium vapor thyratrons. The operation of the circuit, shown in Fig. 3-4, is described below. With all the potentials connected as shown, switch $S_2$ momentarily connects the grid to the anode to start the tube. After starting, the anode voltage drops from the supply voltage to the arc drop value. Switch $S_2$ then reconnects the grid to its adjustable bias source. $S_1$ is then operated to connect capacitor C to the negative side of the line, thereby charging it to twice the thyratron supply voltage.

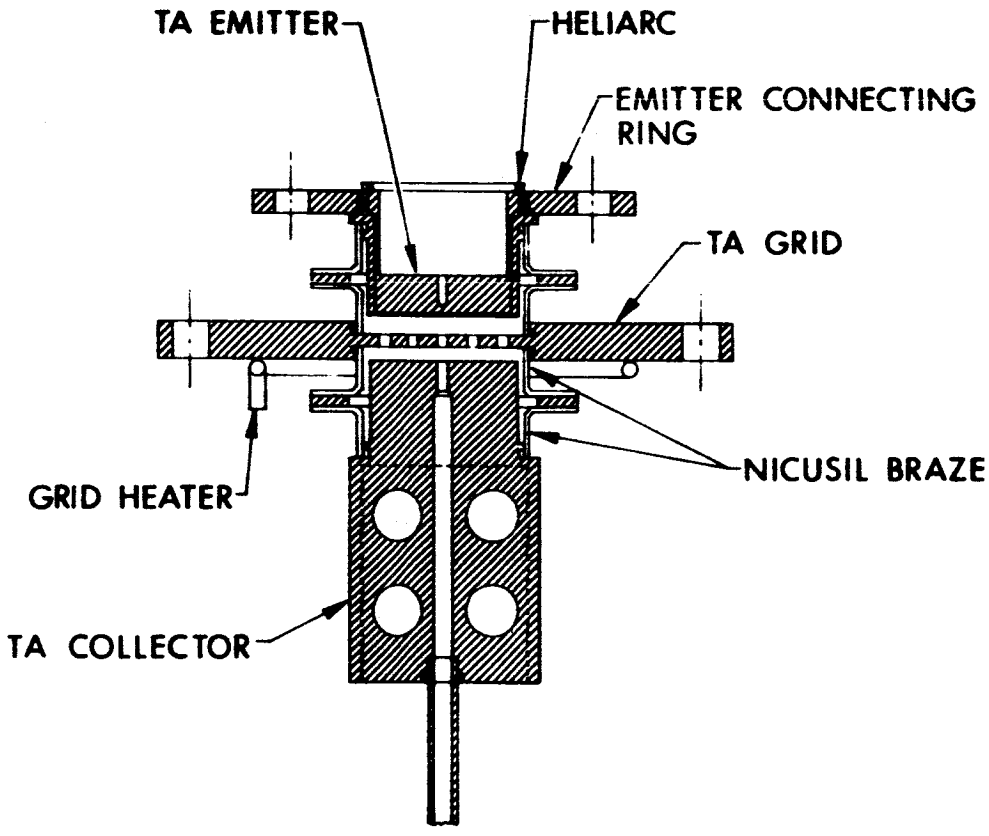


FIG. 3-3 DEIONIZATION TIME TEST VEHICLE NO. 3

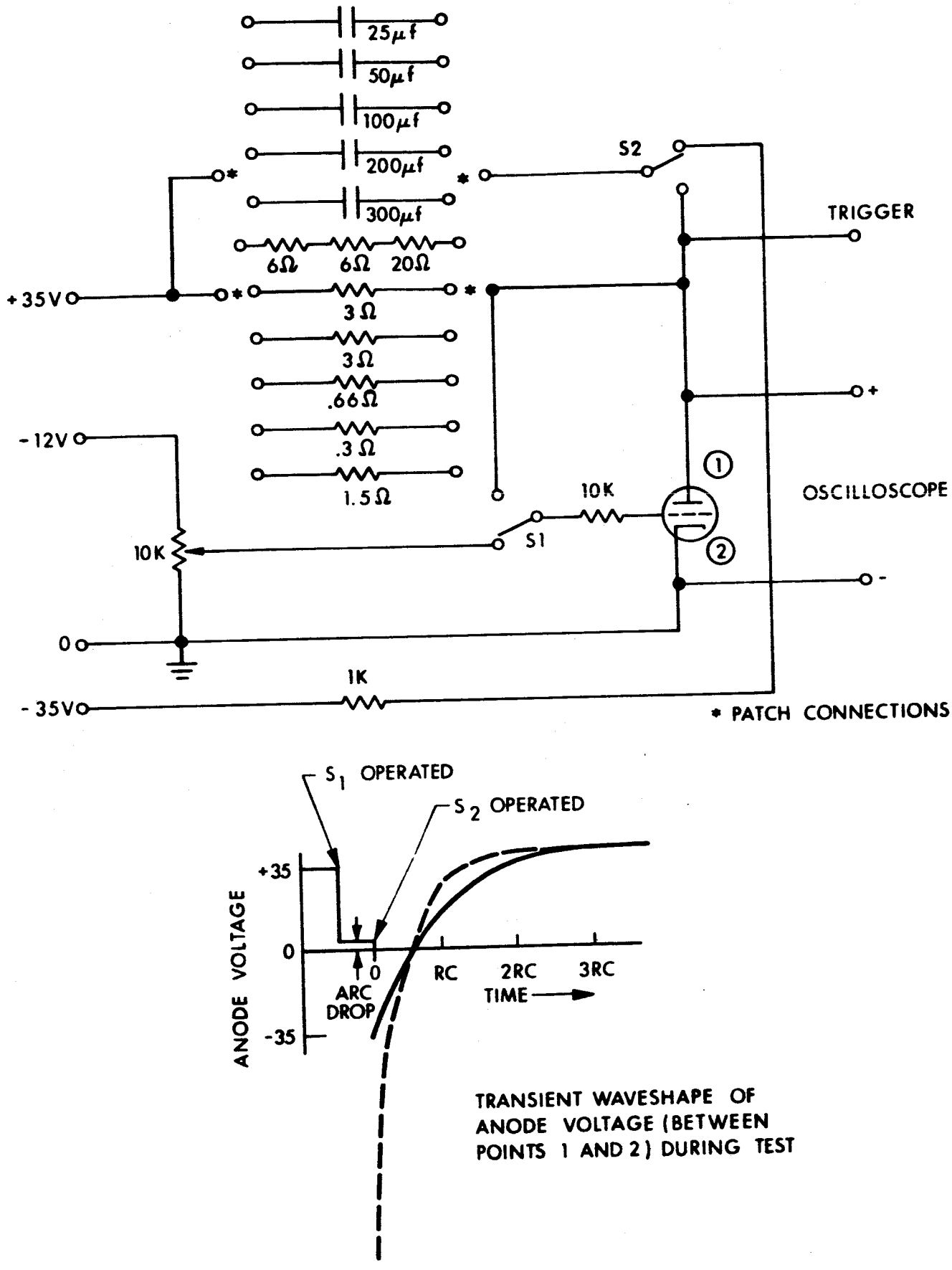


FIG. 3-4 ELECTRICAL CIRCUIT USED FOR DETERMINATION OF DEIONIZATION TIME IN CESIUM VAPOR TUBES

To measure the deionization time, capacitor C is varied to provide various RC time constant values, and switch $S_1$ is used to connect the charged capacitor to the anode, driving it momentarily negative. The anode voltage returns to its supply voltage in a time determined by the value of RC. If the tube has deionized or recovered, the full anode voltage can be applied to the tube without conduction recurring since the grid is biased to prevent arc initiation. By systematically varying R and C, the value of RC for which the tube does not deionize can be determined.

Since the thyratron in this program is operating at low voltages, the supply voltage values shown in Fig. 3-4 are considerably lower than those used in the original circuit. By selecting a high charging voltage for C, the discharge curve (rise of voltage on the anode) will be approximately linear as shown by the dotted line in Fig. 3-4.

Typical oscillograms of deionization time measurements are shown in Fig. 2-7. The deionization time is defined as the minimum time between the application of a negative anode voltage and the point where the anode goes positive such that a rising positive voltage does not restart the tube. This time is shown as $\tau$ in Fig. 2-7. The minimum time is obtained by systematically varying R and C in Fig. 3-4 by various parallel circuit value combinations until the tube no longer recovers after the application of the negative voltage. Figure 2-7(b) is interesting in that it is a case where almost total recovery was obtained and then the tube fired due to a voltage transient in the circuit. The rate of fall of tube voltage is approximately equal to or greater than the buildup of current in the circuit and thus is a crude measure of starting time $\tau_s$. Refined measurements of $\tau_s$ would probably show that the current buildup is probably at least twice as fast as the voltage decrease since it takes some time for a plasma carrying full dc load current to reach its minimum operating voltage.

### 3.4.1 Circuit Problems

The simplicity of the circuits of Fig. 3-4 is offset by a few difficulties which, while they do not prevent taking reasonably accurate data, do limit the range of operation of the device under test. Low load resistances of a fraction of an ohm are required for low anode voltage high current operation. The 0.3 ohm resistor of Fig. 3-4 should be changed to a variable, water cooled load similar to those used on thermionic converters for load currents over 10 amperes. In this way using a fixed capacitance, RC can be varied smoothly over the required range.

The most annoying problem was associated with the contact bounce of switch $S_1$. The rough portion of the oscillogram of Fig. 2-7(a) covering the first 100 microseconds is due to the contacting time of the switch. A mercury wetted contact switch would probably perform satisfactorily if one is available for high current operation. Lacking such a switch, the toggle switch $S_1$ was replaced with a knife switch. The knife switch was an improvement but in a relatively short time it too developed switching noise. This is not surprising if the initial current from the capacitor is considered. For a load of 0.3 ohm and a charging voltage of -20 volts, the current at moment the switch is closed is 66 amperes.

An approach to deionization time measurement, which is free from the limitations described above, is to use a variable frequency ac generator capable of driving the test device at 20 to 30 amperes with at least 5 volts output. A sine wave oscillator driving a quality amplifier of 150 watts output will accomplish this result nicely if the proper impedance matching transformer, which does not saturate on the dc flowing in the load circuit, can be obtained. Efforts to utilize this method of deionization measurement will be made in the next phase.

## 4. FIGURE OF MERIT FOR THYRATRON

In order to assess properly the relative merits of the thyratron over the solid state device, some criteria are required which are meaningful enough that a realistic appraisal of one system over the other can be made. In particular, it is desirable to be able to compare directly a high temperature thyratron with a transistor or switching diode. However, such a comparison is analogous to the fluorescent light as related to the incandescent light. For example, in ordinary circumstances, i.e., room temperature and pressure, the fluorescent light is far superior in terms of lumens per watt. Under extreme conditions of temperature or where radio noise is a concern only an incandescent lamp is suitable and regardless of efficiency, it often is the only suitable light source. To adapt the fluorescent lamp to extreme thermal environments for instance, would require thermal shielding which adds to the weight and complexity of the lamp installation. Thus, the desirable features of the lamp are obtained only at the expense of increased system complexity. If the usual index of lumens/watt is used in this instance, the fluorescent lamp would still be attractive. The index in this case is not a reliable criterion for comparison.

Viewed in such a light, the best method of comparison and hence "Figure of Merit" for the thyratron is the extent to which it helps to solve a particular power conditioning problem and the appropriate criterion would be "watts per pound" for the dc to dc conversion process which is associated with each system being compared under the same conditions. Thus, the weight of auxiliary components, bus bars, and support weights required to make the system work at a given power level and efficiency would be accounted for with respect to the ability of the system to meet its goals. This criterion would also

include the generator and support size which might produce obscuration; such obscuration would appear as a reduced thermal efficiency which in turn lowers the electrical output of the system. A similar statement applies to the thermal drive requirements of the thyratron. Therefore, the criterion which will be used in this program which best describes the relative performance of the thyratron versus solid state power conversion system is given by:

$$F = \text{Figure of Merit} = \frac{\text{Dc output power}}{\text{Total system weight}}$$

Such a figure has meaning only for a specific operating condition. The one system parameter that has the greatest effect on F is the temperature of the system at the location of the thyratron or solid state device. F versus temperature for various devices and operating conditions is discussed in Subsection 7.3 and listed in Table 7-II.

## 4.1 Thermal Drive Requirement

For the thyratron to operate properly, a minimum amount of thermal energy is required to furnish the electron emission current. The greatest portion of this power depends upon the amount of current and the work function of the cathode surface and is given by the products of work function and load current plus a contribution to the cathode work function of $1.72 \times 10^{-4}$ Te where Te is the emitter temperature. An absolute maximum on cathode work function is about 2.8 volts and a value for the energy term at 1600K is 0.27V. Therefore, for a constant load current of 100 amperes, a total of 307 watts of electron cooling is taken from the cavity. Another amount of heat due to radiation losses and cesium conduction total about 70 watts, giving a total thermal drive requirement of about 377 watts for two tubes at 100 amperes. For the immediate application requiring 50 amperes load current, the thermal drive requirement is about 220 watts. A detailed thermal analysis is given in Subsection 4.3.

## 4.2 Effect of Thyratron on Heat Source

The heat load imposed upon the thermal source by the addition of the thyratrons is a direct cost to the system and enters into thermal efficiency calculations with no efficiency factors modifying it. For example, a 1500 watt thermal energy concentrator operates at about 10 percent overall solar power to electrical power efficiency to provide 150 watts electrical output at the 4-diode-generator terminals. A solid state dc-dc converter will condition this full 150 watts of power for use in power distribution circuits.

For the same 1500 watt solar source, if thyratrons are used for the dc-dc converter with the same electrical efficiency as the solid state circuit, the electrical power output will be decreased somewhat because the thyratron will have extracted some heat from the solar source. For example, for a thyratron heating requirement of 200 watts, the amount of solar energy available to drive the 4 diode generator will be (1500-200) or 1300 watts for a fixed thermal power input of 1500 watts. Using the 10 percent solar power to electrical power figure above yields only 130 watts output from the generator terminals.

To pay the price in thermal watts to heat the thyratrons three alternatives are open:

1. Accept limited power from generators at 130 watts.
2. Increase efficiency of solar collector to electrical power out of generator from 10 percent to 11.5 percent and obtain a generator output of 150 watts.
3. Increase energy collection of solar concentrator from 1500 to 1700 watts to obtain a generator output of 150 watts.

These alternatives are summarized in Table 4-I.

The choice of alternatives is obviously based on system needs but, except for the case where an absolute maximum electrical output is required regardless of weight, the choice can generally be made in terms of the figure of merit F for the thyratron.

**TABLE 4-I**

EFFECT OF THYRATRON ON HEAT SOURCE

| Solar Concentrator Thermal Power (watts) | Thyratron Heating Power (watts) | Solar Power to Electrical Power Efficiency | Power Out of Generator (watts) | Conditioned Power Output at 80% dc-dc Conversion Efficiency (watts) |
|---|---|---|---|---|
| 1500 | (solid state) | 10 percent | 150 | 120 |
| 1500 | 200 | 10 percent | 130 | 104 |
| 1700 | 200 | 10 percent | 150 | 120 |
| 1500 | 200 | 11.5 percent | 150 | 120 |

## 4.3 Thermal Analysis of a Cesium Vapor Thyratron

The thermal energy available from a solar-thermionic cavity is extracted for the operation of a cesium thyratron tube. The tube consists of a cathode, an anode, and a grid, all made of molybdenum.* It is anticipated that the cathode will be operated in the 1000-1300°C range. The problem is then to determine the cathode operating temperature and the thermal energy required to operate the device. In order to minimize back emission, the grid and anode will be operated at approximately 600°C. Radiator areas required to dissipate the heat intercepted by the two electrodes will be determined. The following thermal analysis is typical of that required for the thyratron development.

The output voltage of the 4 diode generator is typically 2.8 volts. For the generator output of 150 watts the current will be 54 amps.

The tube geometry considered will be cylindrical. For convenience, cesium reservoir temperatures of 294, 324 and 348°C will be considered. With the cathode temperature between 1273 and 1573°K and cesium pressures between 294 and 348°C the emission current density as shown in p. 4-13 of Ref. 16 will be between 18 and 2 amps/$cm^2$, respectively. The cathode area required will then be between 3 and 27 $cm^2$. The grid aperture was determined to be approximately 0.2 cm for the desirable spread discharge condition.

There are two thyratron operating modes. During the ON cycle, the thermal energy is transferred from the cathode to the anode by electron cooling, interelectrode radiation, cesium vapor conduction and conduction from the cathode envelope to the grid and then to the anode. In the ordinary thermionic converter the electron cooling accounts for 75 to 85 percent of the heat transfer. For the thyratron this

*The analysis has been made for a molybdenum emitter; a similar analysis will apply to tantalum or rhenium.

percentage will be even higher since the cathode-anode radiation will be restricted to the grid aperture; the cesium conduction is drastically reduced due to a large spacing and relatively low cesium pressure. The heat transfer from the cathode to grid follows the same mechanisms with the absence of electron cooling. During the OFF cycle, the electron cooling is also absent.

### 4.3.1 Cathode Anode Heat Transfer

#### 4.3.1.1 Electron Cooling

The thermal energy attributed to electron cooling is given by

$$P_e = I\left(\phi_c + 0.173\,\frac{T_c}{1000}\right) \qquad (1)$$

where

$P_e$ = electron cooling power
$I$ = current
$\phi_c$ = cathode work function
$T_c$ = cathode temperature

The electron cooling power as a function of the cathode temperature as calculated by Eq. 1 is shown in Fig. 4-1 for the three chosen cesium reservoir temperatures.

Figure 4-2 shows the cesium reservoir temperature, current density and cathode area as a function of the cathode temperature. It can be seen that the cathode temperature falls within a narrow band, i.e., between 1550 and 1650°K.

It should be noted that results in Figs. 4-1 and 4-2 were based on the thermionic converter optimized at 0.7 volt/converter to yield the output current of 54 amps.

#### 4.3.1.2 Interelectrode Radiation

The net energy interchange between two radiating surfaces can be approximated by

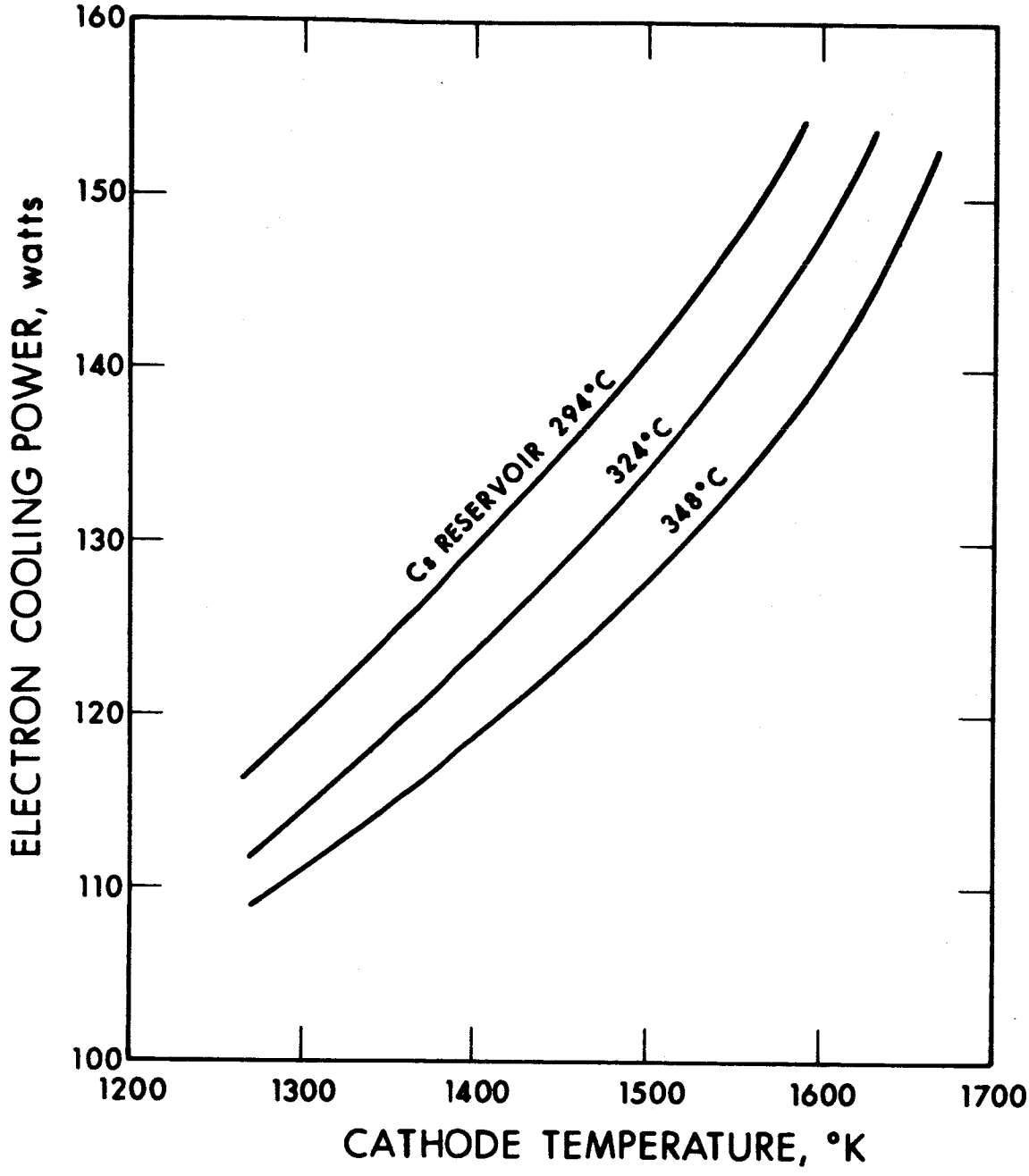


FIG. 4-1 ELECTRON COOLING POWER

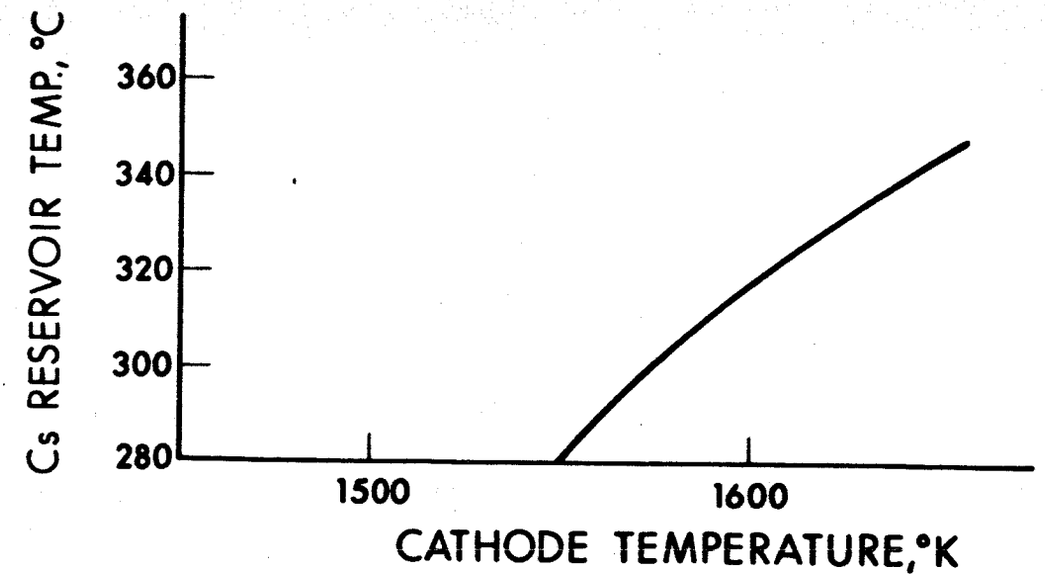


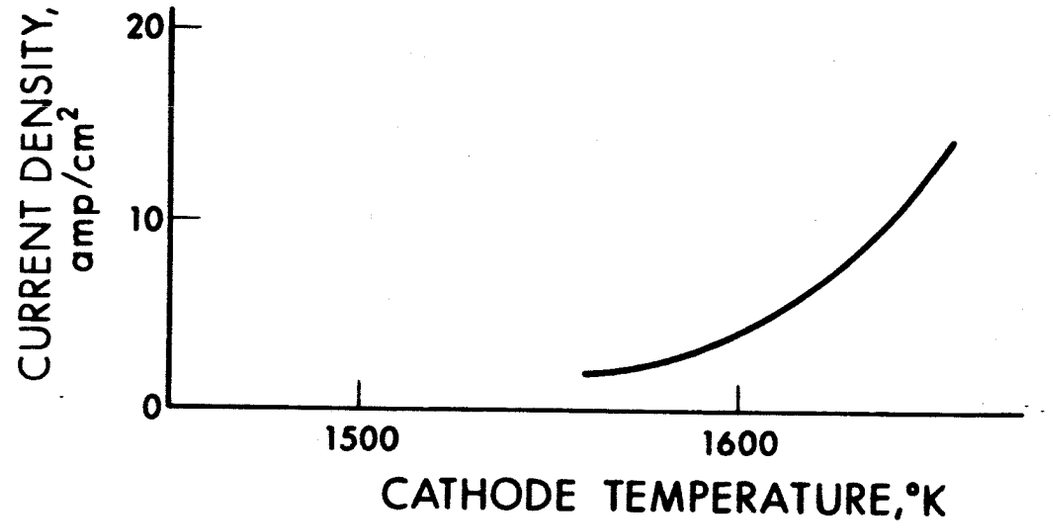


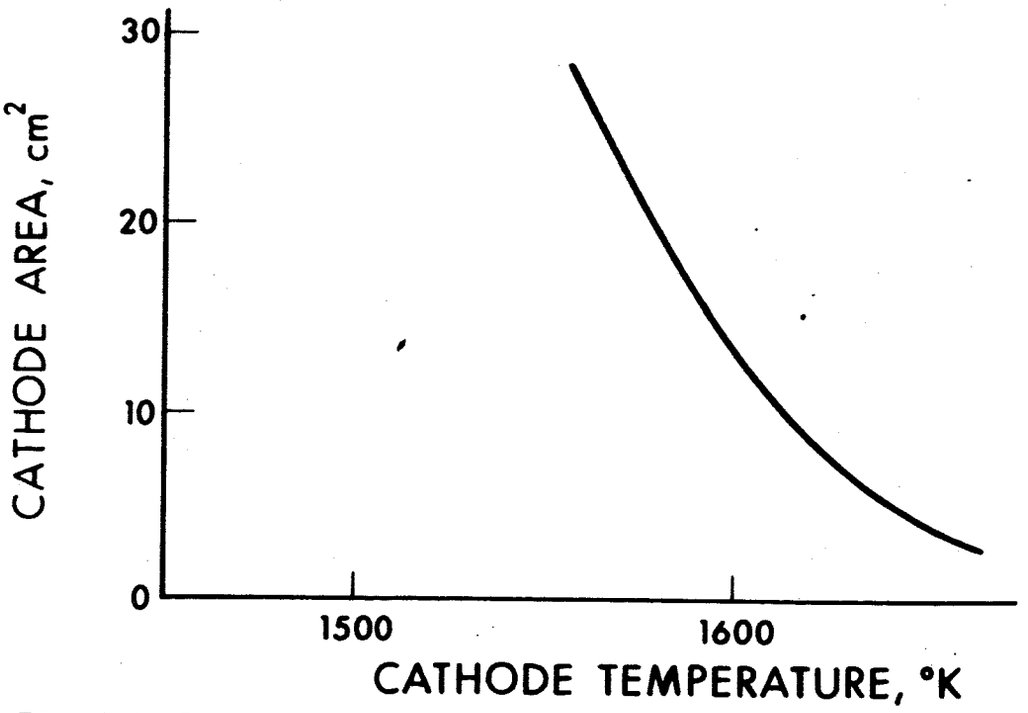


FIG. 4-2 Cs RESERVOIR TEMPERATURE, CURRENT DENSITY AND CATHODE AREA VERSUS CATHODE TEMPERATURE

$$Q = A_2 F_{21} F_\epsilon \sigma (T_1^4 - T_2^4) \quad (2)$$

where

$A_2$ = anode area

$F_{21}$ = view factor of cathode as seen by anode = 1

$$F_\epsilon = \text{emissivity factor} = \frac{1}{\frac{1}{\epsilon_1} + \frac{1}{\epsilon_2} - 1} \quad (3)$$

$\sigma$ = Stefan-Boltzmann constant = $5.67 \times 10^{-12}$ $\frac{\text{watts}}{\text{cm}^2 \left(^\circ\text{K}\right)^4}$

$T_1$ = cathode temperature

$T_2$ = anode temperature

It is anticipated that the anode will be operated at about 600°C. The emissivity of molybdenum as a function of temperature is tabulated below.

| | Temperatures - °K | | | | |
|---|---|---|---|---|---|
| Emissivity $\epsilon$ | 800 | 900 | 1550 | 1600 | 1650 |
| | 0.07 | 0.08 | 0.16 | 0.17 | 0.18 |

The emissivity factor $F_\epsilon$ is not sensitive to the cathode and anode temperatures in the range considered and will be assumed constant at 0.057 as calculated from Eq. 3 above.

The anode effective area will be taken as 125 percent of the grid aperture area. Assuming the grid diameter of 0.75 inch, the anode effective area $A_2$ is 1.5 $\text{cm}^2$.

#### 4.3.1.3 Cesium Conduction

The heat transfer coefficient for a close spacing (1 to 2 mils) diode operating in the pressure range of 0.5 torr is conservatively estimated at $1.0 \times 10^{-3}$ watts/$\text{cm}^2{}^\circ\text{K}$. With a larger spacing, say 10 mils, the coefficient will be reduced to approximately $0.5 \times 10^{-3}$ watts/$\text{cm}^2{}^\circ\text{K}$.

#### 4.3.1.4 Envelope Conduction

Heat is conducted away from the cathode to the grid through the cathode envelope. Since the grid will be approximately at the same temperature as the anode, there will be negligible heat transfer between grid and anode. The cathode-to-grid conduction will be calculated in the next section.

### 4.3.2 Cathode-Grid Heat Transfer

#### 4.3.2.1 Interelectrode Radiation

The grid area is approximately the cathode area minus the grid aperture. For the cathode operating at 1550, 1600 and 1650°K, the grid area will be about 28, 12 and 3 $cm^2$. Assuming the grid is at 900°K, the radiation loss from cathode to grid is 46 watts at a cathode temperature of 1650°K and 6.5 watts at a cathode temperature of 1550°K.

#### 4.3.2.2 Cesium Conduction

The same order of magnitude of heat flux estimated previously can be expected.

#### 4.3.2.3 Envelope Conduction

An estimate will be made, assuming a tantalum envelope thickness of 2 mils and the cathode and grid diameters of 0.75 and 2 inches, respectively. If the thermal resistance of the ceramic seal is neglected, the thermal resistance of the envelope can be computed from

$$R = \frac{1}{2\pi kt} \ln \frac{r_o}{r_i} \qquad (4)$$

where

$k$ = tantalum thermal conductivity = $0.18 \frac{cal}{sec\ cm^oK}$

$r_o$ = outer radius

$r_i$ = inner radius

$t$ = thickness of envelope

### 4.3.3 Thermal Energy From Cavity

The thermal energy extracted from the cavity during the ON cycle as a function of cathode temperature is tabulated below.

| | Thermal Power Intercepted in Watts/Tube | | | | | |
|---|---|---|---|---|---|---|
| | Cathode-Grid | | | Cathode-Anode | | |
| Cathode Temperature, $^{o}K$ | 1550 | 1600 | 1650 | 1550 | 1600 | 1650 |
| Electron Cooling | - | - | - | 150 | 150 | 150 |
| Interelectrode Radiation | 46.0 | 22.4 | 6.5 | 2.5 | 2.8 | 3.2 |
| Cesium Conduction | 9.2 | 4.2 | 1.1 | 0.5 | 0.5 | 0.6 |
| Envelope Conduction | 15.8 | 17.0 | 18.2 | - | - | - |
| Total | 71.0 | 43.6 | 25.8 | 153.0 | 153.3 | 153.8 |

During the OFF cycle, the thermal power required will be the same except electron cooling. Since the two thyratrons operate in a push-pull fashion, the total power required from the cavity will be as shown below.

| | Thermal Power, Watts | | |
|---|---|---|---|
| Cathode Temperature, $^{o}K$ | Thyratron No. 1 | Thyratron No. 2 | Cavity |
| 1550 | 224 | 74 | 298 |
| 1600 | 196.9 | 46.9 | 243.8 |
| 1650 | 179.6 | 29.6 | 209.2 |

Figure 4-3(a) shows the thermal power required to operate thyratron Nos. 1 and 2 and the power required from the cavity as a function of the cathode temperature. Figure 4-3(b) shows the thyratron thermal power as a function of time for a cathode temperature of $1650^{o}K$.

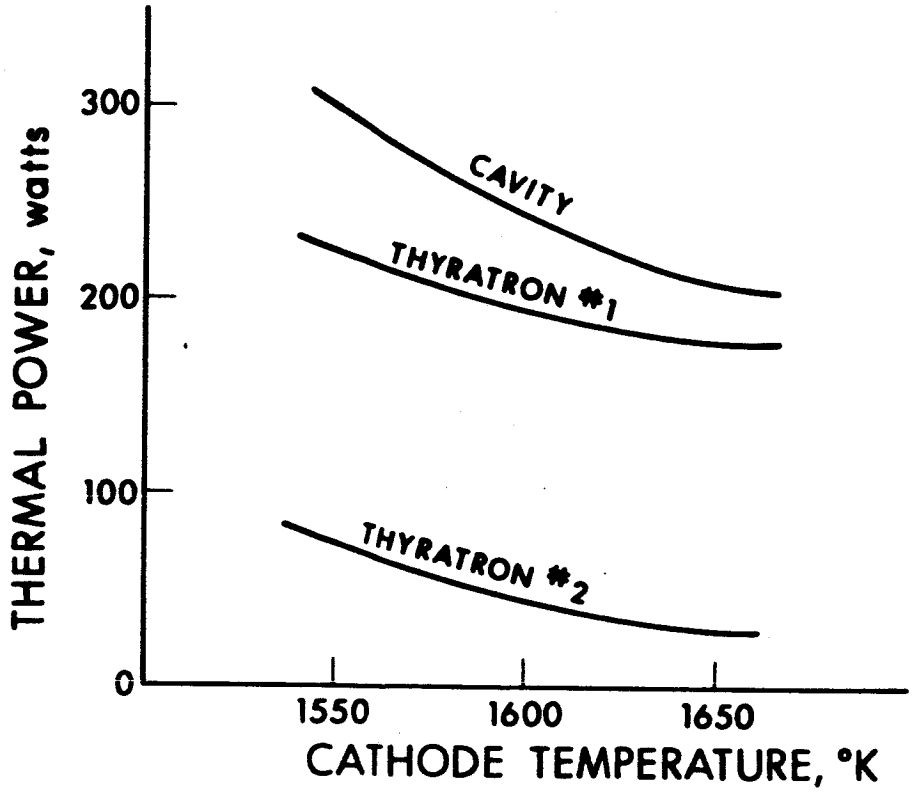


FIG. 4-3a THERMAL POWER REQUIRED TO OPERATE THYRATRONS 1 AND 2 AND THE TOTAL REQUIRED CAVITY THERMAL POWER AS A FUNCTION OF CATHODE TEMPERATURE

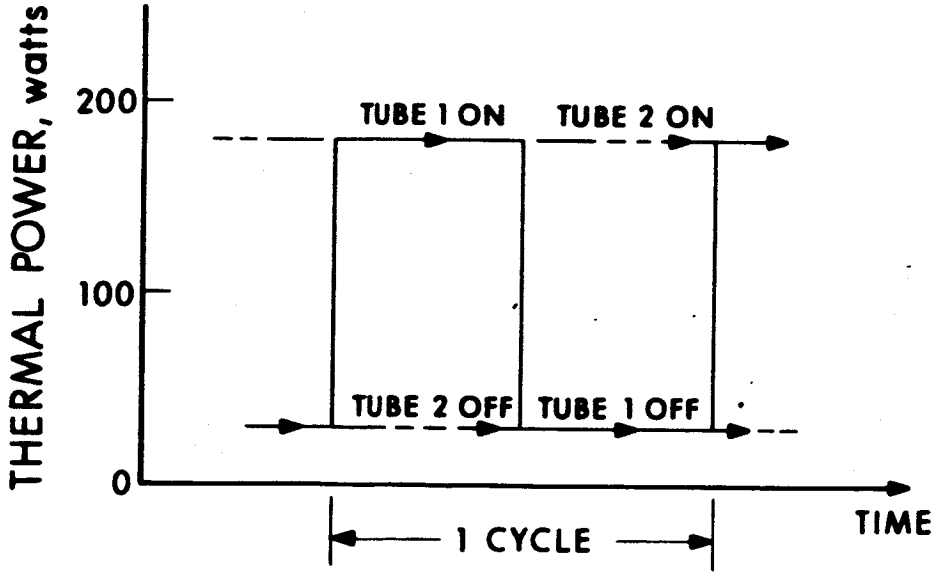


FIG. 4-3b THYRATRON THERMAL POWER AS A FUNCTION OF TIME FOR A CATHODE TEMPERATURE OF 1650°K

### 4.3.4 Radiator Area

It is recommended that the cathode be operated at 1650°K since it represents optimum conditions from the standpoint of a minimum thermal power required and a minimum weight. The grid and anode radiators must be sized to dissipate 26 and 154 watts, respectively. By employing Rokide "C" which has an emissivity of 0.95, we have for a view factor of unity required radiator areas of 7.3 and 43.2 $cm^2$ respectively.

### 4.3.5 Summary and Conclusions

Results of the thermal analysis indicated that, for a 150-watt, 4-converter generator with an output current of 54 amp, the cathode should be operated at 1650°K. The recommended operating point represents an optimum condition from the standpoint of a minimum thermal power required from the cavity and a near minimum weight thyratron. The important characteristics corresponding to the above recommendation are the following:

| | |
|---|---|
| Cathode | |
| Temperature | 1650°K |
| Area | 4.3 $cm^2$ |
| Emission Current Density | 13 amp/$cm^2$ |
| Anode | |
| Temperature | 900°K |
| Anode Area Radiator | 43.2 $cm^2$ |
| Grid | |
| Temperature | 900°K |
| Grid Radiator Area | 7.3 $cm^2$ |
| Cesium Reservoir Temperature | 343°C |
| Thermal Power | |
| Thyratron No. 1 (ON) | 180 watts |
| Thyratron No. 2 (OFF) | 30 watts |
| Cavity | 210 watts |

# 5. TRANSFORMER ANALYSIS

The development of a transformer that can be used in the high-temperature space environment required for the cesium thyratron, dc to dc converter is essentially a materials problem. The core material, for example, must have a Curie point above any core hot-spot temperature, must exhibit a high degree of magnetic stability, and must show no significant irreversible change in magnetic properties as a result of high-temperature, low-temperature cycling. The insulation materials used for the conductors and for layer insulation must possess good mechanical and dielectric strengths, and must be capable of withstanding long exposures to elevated temperatures. Since the transformers required for this application have voltages below 100V peak, no problems are anticipated due to loss of insulation dielectric strength and the problem of major concern becomes one of basic core material properties.

## 5.1 Core Materials

Iron-cobalt alloys with Curie temperatures greater than 900°C and saturation inductions over 23 kilogauss, have the most stable high temperature properties of all known alloys. Figure 5-1 shows the dc magnetization curves at room temperature for various materials with cobalt iron alloys demonstrating high induction level capabilities.

Pavlik,[17] while testing iron-cobalt, tape-wound cores in air, observed magnetic degradation of the material due to mechanical strains induced by oxidation and thermal expansion at elevated temperatures (300 to 600°C). However, when the same core was tested in a neutral atmosphere, the strains due to oxidation were minimized and the magnetic properties remained stable. Additional tests performed

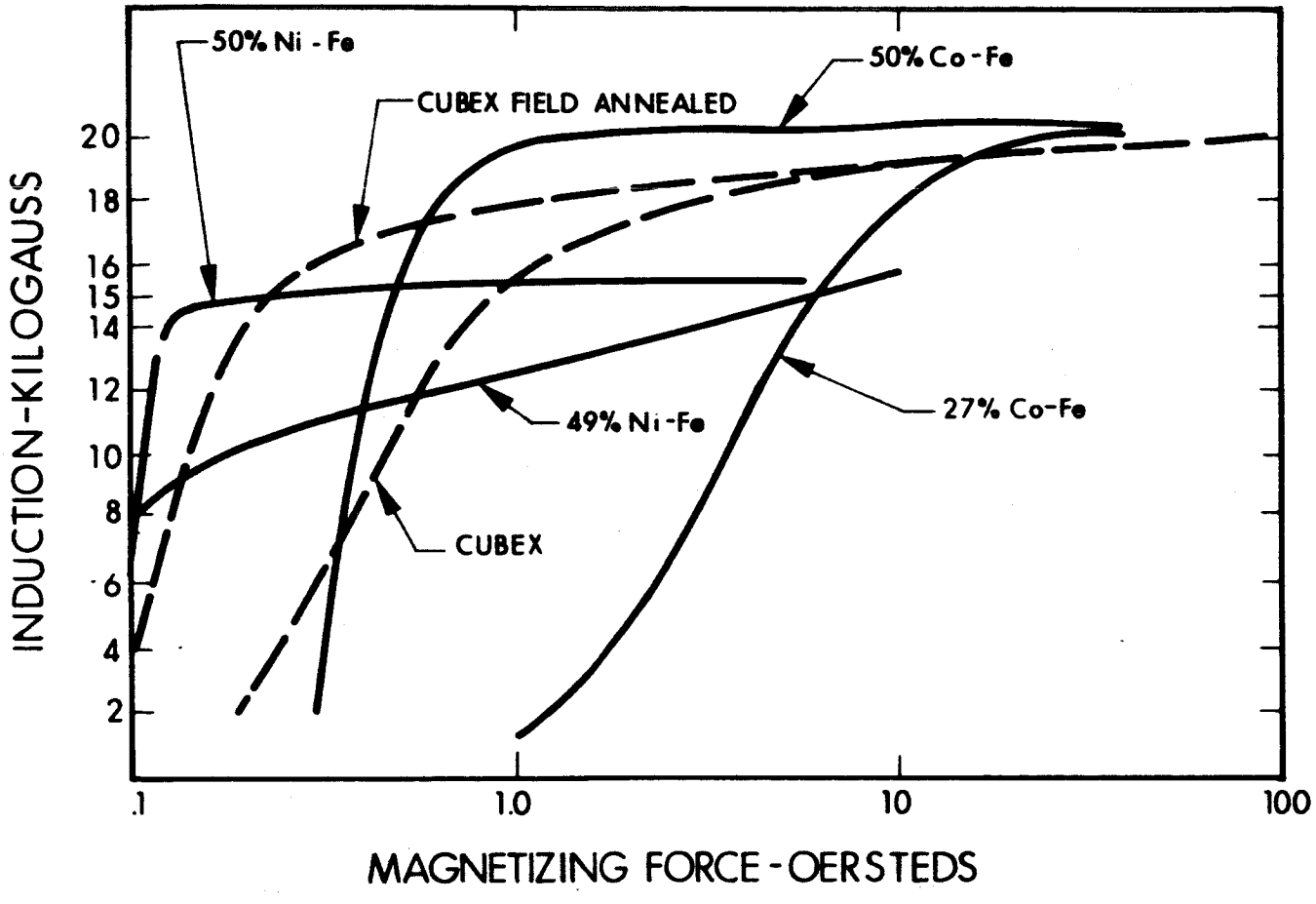


FIG. 5-1 MAGNETIZATION CURVES (dc), THIN TAPE MATERIAL AT ROOM TEMPERATURE

on laminated specimens in air revealed no change in magnetic properties at elevated temperatures, since the laminated structure was free to expand, thereby minimizing strains. Also, there was some indication that the lower percentage cobalt to iron alloys were more stable at 600°C for tape-wound cores.

Table 5-I is a tabulation of the change in dc magnetic properties for Hyperco 50 (49 percent Co-Fe) at elevated temperatures. Note that Hyperco 50 had a large increase in the room temperature coercive force after exposure to 760°C. This may be associated with the strain or with a new arrangement in the atom positions, both brought about by an atomic-ordering reaction which for 50 percent Co-Fe occurs at temperatures up to 732°C (Ref. 18). The ordering region does not extend to 27 percent cobalt iron alloys, and for this reason Hyperco 27 may be more desirable as the final core material choice. However, the core loss associated with Hyperco 27 is greater than that for Hyperco 50 as shown in Fig. 5-2 (Ref. 19).

Tables 5-II and 5-III tabulate the change in core loss for Hyperco 50 and Hyperco 27, respectively. After exposure to 760°C, the room temperature core loss increased. Since the magnetic properties for Hyperco 27 show an improvement after exposure to 760°C, Fig. 5-3, it was concluded that the interlaminar insulation had broken down at elevated temperatures. But, it should be noted that the magnetic properties for both materials are good up to at least 595°C (1100°F) with Hyperco 27 apparently superior at higher temperatures up to 760°C (1400°F).

Thus, the stability of iron-cobalt alloys at high temperatures depends upon the geometric configuration, the environmental atmosphere, and the percentage of cobalt to iron in the alloy.

## 5.2 Proposed Construction

Figure 5-4 shows the proposed transformer configuration for the dc to dc converter. The shell-type core configuration, having

TABLE 5-I

DC MAGNETIC PROPERTIES

Test Atmosphere: Air to 500°F, Argon at 800°F and above

| | R.T. | 500°F | 800°F | 1100°F | 1400°F | R.T. after 1400°F |
|---|---|---|---|---|---|---|
| | Hyperco 50 (50% Co-Fe) Ring Laminations, 0.004-in. thick | | | | | |
| Coercive Force* (oersteds) | 0.616 | 0.576 | 0.490 | 0.314 | 0.478 | 1.73 |
| Residual Induction* (Kilogauss) | 10.9 | 8.9 | 7.4 | 10.2 | 10.8 | 4.8 |
| Induction ($B_{tip}$) for H = 300 oersteds (Kilogauss) | 24.0 | 23.4 | 22.0 | 21.4 | 18.5 | 24.0 |

*Taken from $B_{tip}$ for H = 100 oersteds (Reference: NAS3-4162)

TABLE 5-II

CORE LOSS

Hyperco 50 (50% Co-Fe) Ring Laminations, 0.004 inch thick
Test Atmosphere: Air to 500°F, Argon at 800°F and above

| | Core Loss (Watts per pound) | | | | | |
|---|---|---|---|---|---|---|
| | R.T. | 500°F | 800°F | 1100°F | 1400°F | R.T. after 1400°F |
| Induction (Kilogauss) | | | 400 cps | | | |
| 12 | 6.03 | 5.6 | 5.04 | 4.03 | 9.28 | 8.76 |
| 14 | 7.65 | 7.14 | 6.33 | 4.81 | 11.29 | 11.09 |
| 16 | 9.55 | 8.74 | 7.63 | 5.6 | 13.34 | 13.64 |
| 18 | 11.46 | 10.37 | 8.88 | 6.5 | 16.77 | 16.37 |
| | | | 1600 cps | | | |
| 6 | 11.58 | -- | 9.5 | 9.8 | -- | -- |
| 8 | 18.57 | -- | 15.4 | 14.5 | -- | -- |
| 10 | 26.9 | -- | 22.6 | 19.8 | -- | -- |
| 12 | 36.6 | -- | 30.9 | 25.6 | -- | -- |

(Reference: NAS3-4162)

TABLE 5-III

CORE LOSS

Hyperco 27 (27% Co-Fe) Ring Laminations, 0.008 inch thick
Test Atmosphere: Air to 500°F, Argon at 800°F and above

| Induction (Kilogauss) | Core Loss (Watts per pound) | | | | | |
|---|---|---|---|---|---|---|
| | R.T. | 500°F | 800°F | 1100°F | 1400°F | R.T. after 1400°F |
| | | | | 400 cps | | |
| 18 | 30.9 | 24.97 | 21.0 | 20.57 | 31.4 | 46.1 |
| 12 | 17.3 | 14.2 | 11.86 | 11.6 | 14.5 | 22.5 |
| | | | | 800 cps | | |
| 12 | 43.7 | -- | 28.6 | 31.54 | 53.65 | 64.7 |
| | | | | 1600 cps | | |
| 12 | 117 | -- | 73.0 | 94.25* | 183* | 204.5* |
| | | | | 3200 cps | | |
| 8 | 106 | -- | 100 | 141* | 295* | 283* |

*Interlaminar insulation probably damaged. Samples being reinsulated.

(Reference: NAS3-4162)

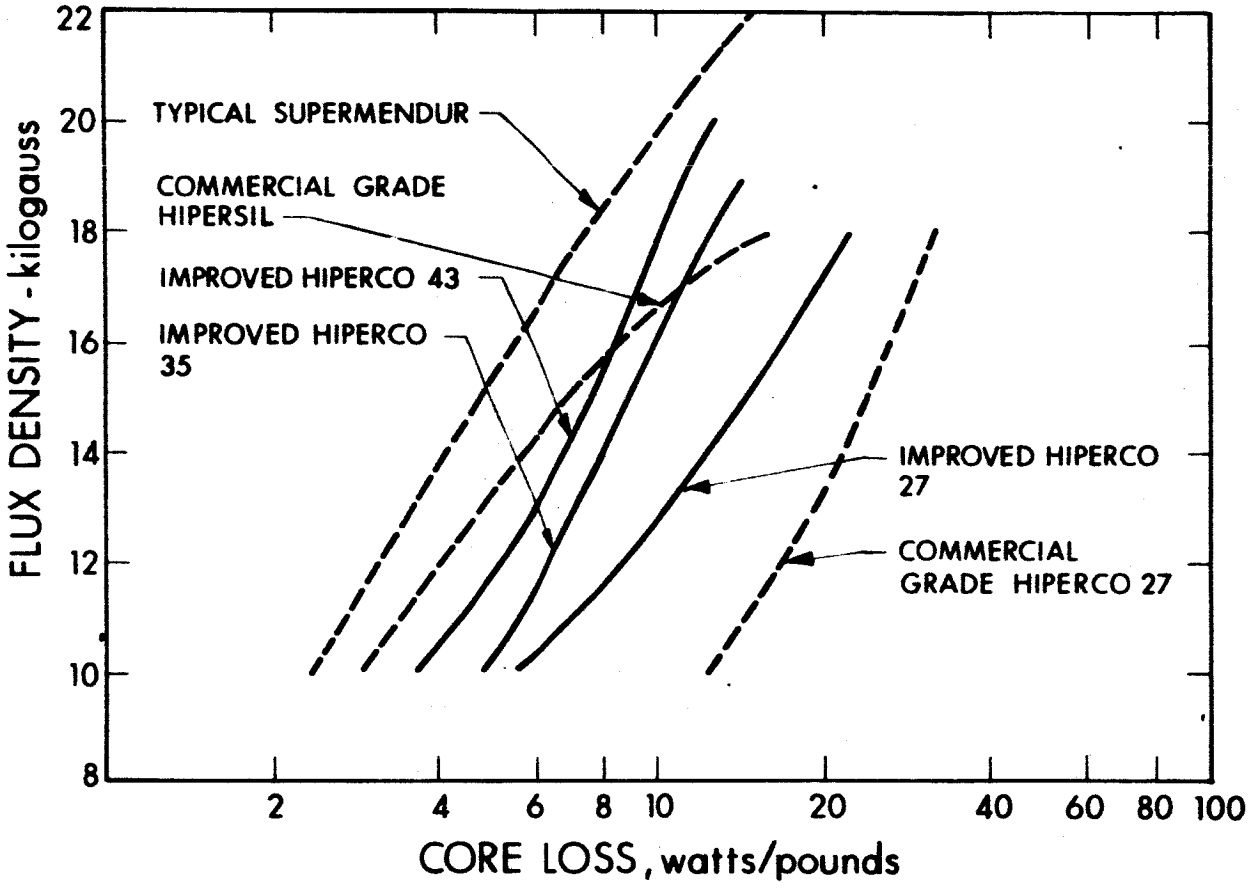


FIG. 5-2 CORE LOSS AT 400 Hz OF SEVERAL IMPROVED HIGH-PURITY IRON-COBALT ALLOYS, WITH DATA ON OTHER MATERIALS FOR COMPARISON (all curves are for 0.004-inch thick material)

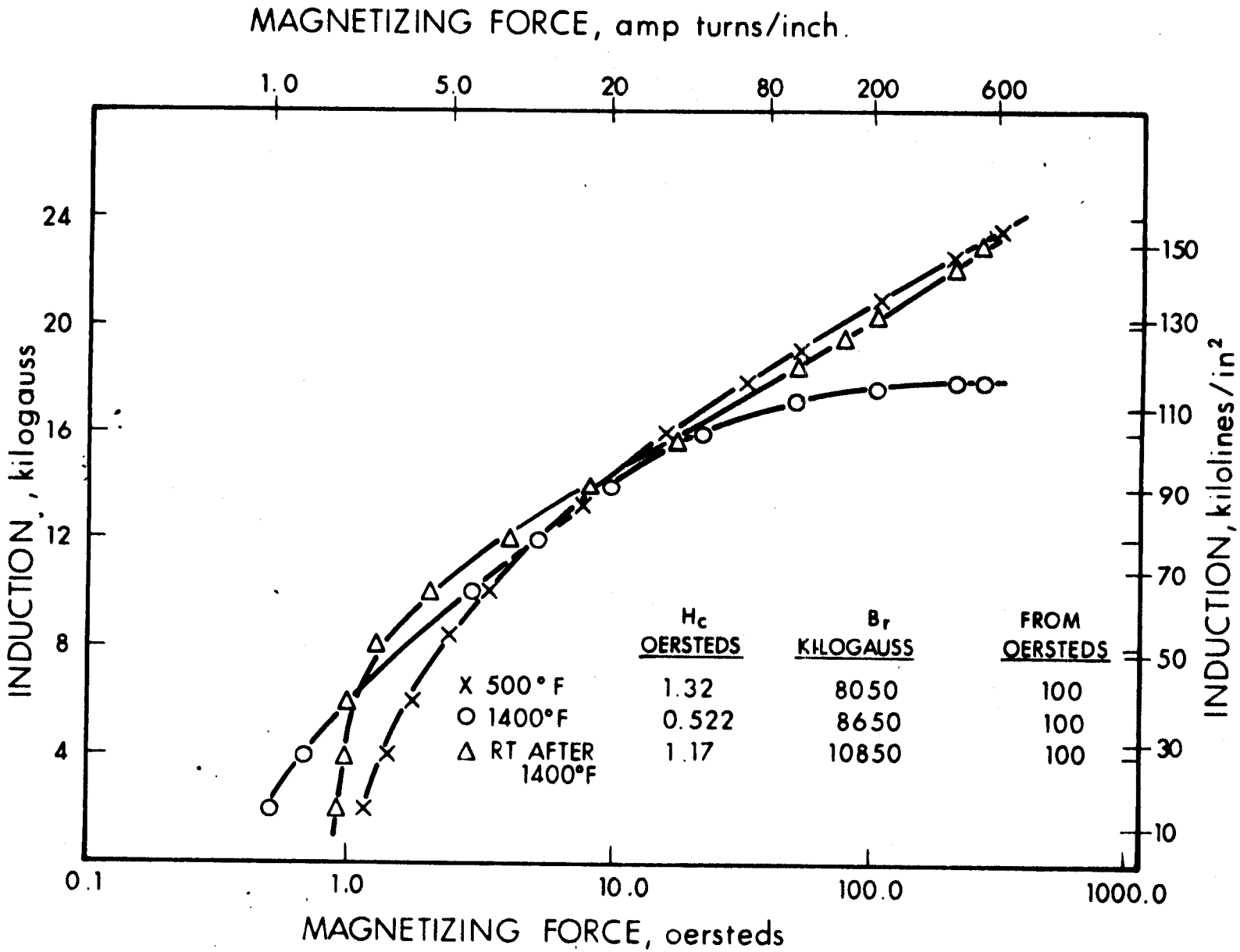


FIG. 5-3 MAGNETIZATION CURVES (dc) FOR HYPERCO 27, RING LAMINATIONS, 0.008-INCH THICK
TEST ATMOSPHERE: AIR TO 600°F, ARGON 600°F

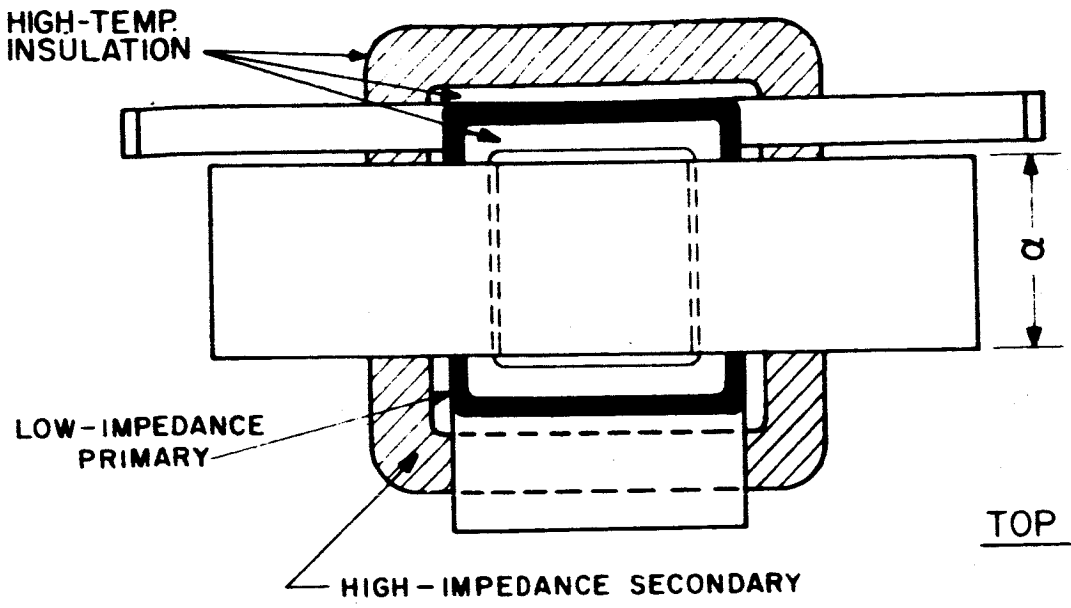


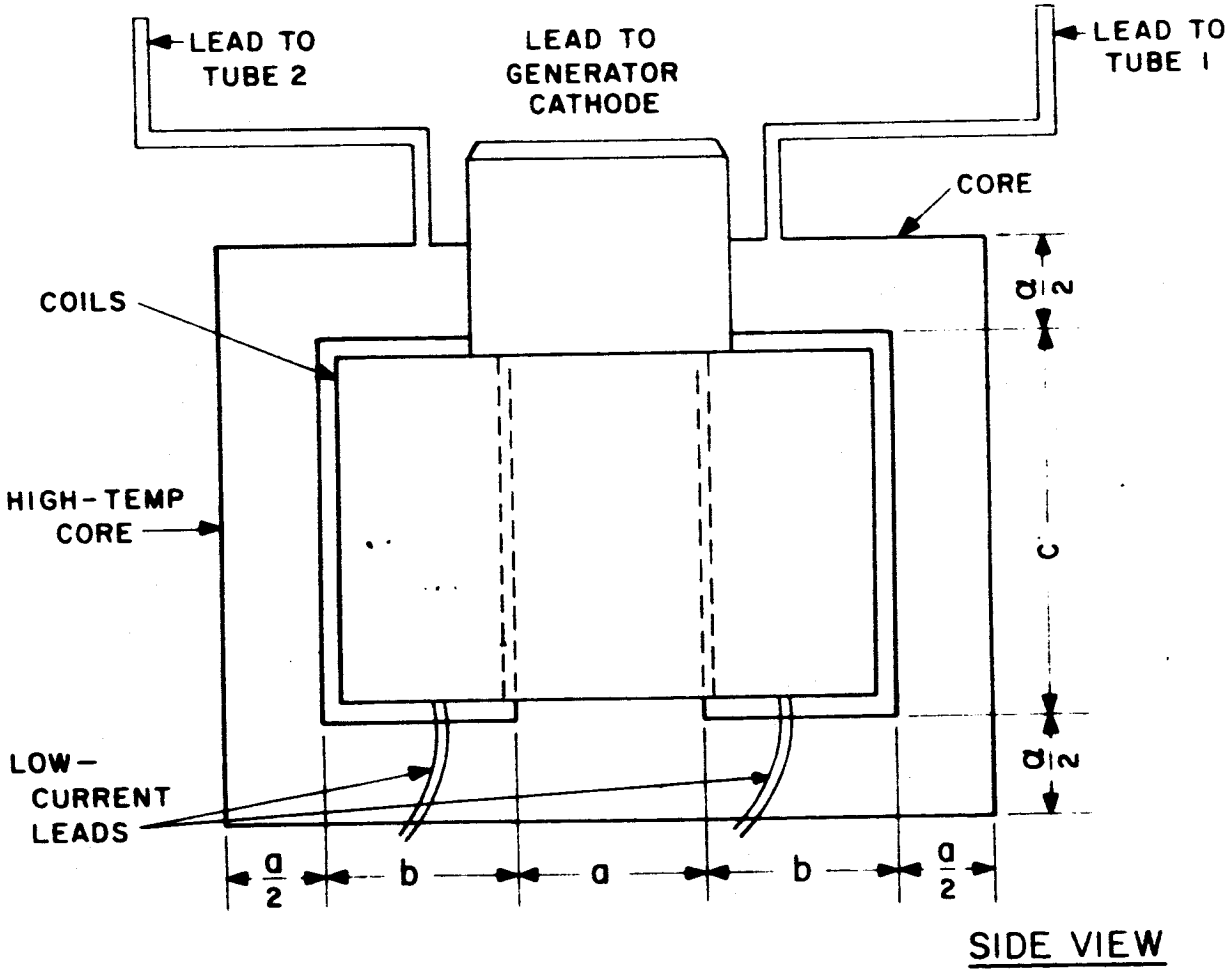


FIG. 5-4 TRANSFORMER CONFIGURATION FOR DC TO DC CONVERTER

over 50 percent more surface area for heat rejection than a comparable C-type or single window core, will probably consist of 0.004 inch thick laminations insulated with magnesium methylate. Silver wire is the best conductor for high-temperature transformer windings (Ref. 20 and 21), but, since oxidation will not be a problem, copper or nickel-clad copper would be more practical from both an availability and economic viewpoint. Copper strip, preferably OFHC grade copper, can be used for the primary winding with strip dimensions on the order of 0.75 inch wide and 0.050 inch thick, insulated with alumina. The secondary winding will consist of commercially available, high-temperature wire possibly coated with DuPont's "H-film" to provide a good dielectric strength per unit of thickness (6,000 volts/mil at 150°C) and a temperature tolerance to 800°F. The insulation to ground and core tube can be fabricated from mica paper (Ref. 21), and at present it does not appear that an additional layer of insulation will be necessary between primary and secondary windings.

Table 5-IV lists the core materials evaluated for use in the present transformer. Assuming a 600°C ambient operating temperature, only cobalt-iron alloys will be considered as possible core materials. Of these, the specifications for Hyperco 50 will be used in the initial design considerations due to its availability over Supermendur and its lower core loss, as compared to the lower percentage cobalt to iron alloys.

### 5.2.1 Leakage Inductance

Leakage inductance is caused by magnetic flux which does not link both primary and secondary windings. There are generally three ways to reduce leakage inductance, and they must be considered in the initial design; they are: (1) minimizing insulating spacing between windings, (2) reducing coil radial build by increasing coil height, and (3) interleaving primary and secondary windings (Refs. 22 and 23). The low voltages requires (below 100V peak) will

TABLE 5-IV

CORE MATERIALS

| Material | Composition | Curie Point | Remarks |
|---|---|---|---|
| Hyperco 50 | 49 percent Iron<br>49 percent Cobalt<br>2 percent Vanadium | 940°C | Readily available |
| Supermendur | 49 percent Iron<br>49 percent Cobalt<br>2 percent Vanadium | 940°C | Refined version of Hyperco 50 with magnetic anneal, not readily available, expensive |
| Magnesil | 97 percent Iron<br>3 percent Silicon | 740°C | Single-oriented grain, readily available |
| Cubex | 97 percent Iron<br>3 percent Silicon | 740°C | Double-oriented grain, not commercially available |

enhance the reduction of leakage inductance provided the insulation thicknesses do not become excessive and the primary to secondary turns ratio (function of voltage wave shape) remain relatively low. At present, it appears that the insulation thicknesses will be on the order of 0.002 to 0.006 inch maximum, and the required turns ratio will be less than 25 to 1. Also, with sufficient initial consideration, the effect of leakage inductance becomes one of reactance and is not expected to constitute a problem for the proposed frequency range of 500 to 1600 cps (Ref. 24).

## 5.3 Computer Design Program

A computer program based upon a mathematical model representation of Fig. 5-4 was written to provide transformer parametric data for design and tradeoff information purposes. The computer program allows the variation of many parameters including the physical constants of materials as well as electrical specifications. Transformer dimensions, weight, and efficiency (as functions of flux density, frequency, volt-turn ratio, and temperature) were examined. The transformer design criteria and tradeoff information obtained should hopefully encompass thyratron performance. However, the final design will be dependent upon measured thyratron characteristics, in particular, parameters to determine final operating frequency and voltage wave shape.

### 5.3.1 Initial Considerations

The transformer performance curves to follow reflect electrical parameters initially selected to provide a rectified output of 28 volts dc at a power level of 150 watts and an operating temperature of 600°C. Square voltage and current wave shapes were assumed throughout with the following associated magnitudes:

$E_p$ (primary voltage) = 3V peak
$I_p$ (primary current) = 66A peak
$E_s$ (secondary voltage) = 36V peak
$I_s$ (secondary current) = 5.5A peak

A secondary, open-circuit voltage of 36 volts was estimated as that required to produce a rectified 28V dc output including 2 volts, rectifier drop and 15 percent voltage regulation at 600°C. Voltage regulation is considered to be the percentage change in no-load voltage as the secondary terminal voltage drops from no-load to full-load (defined differently for convenience). If the source is power limited, i.e., designed to operate at 150 watts output, the transformer performance curves may still be used to obtain useful information.

Wire gauges were determined by using 500 circular mils per amp to establish required area. This consideration dictates an impractical No. 5 gauge wire for the primary winding. Commercially available, high-temperature wire was examined with a resulting No. 16 gauge selection; thus, the primary winding was considered to consist of 12 parallel No. 16 gauge wires, and the secondary winding composed of a single No. 16 gauge strand. If copper strip instead of wire is used in the primary winding, the strip dimensions would probably be on the order of 0.75 inch wide by 0.050 inch thick, less insulation.

### 5.4 Size and Weight

Both transformer size and weight are affected by variations in either flux density, frequency, or volt-turn ratio. Figure 5-5 shows transformer weight as a function of volt-turn ratio at frequencies of 500 and 1600 cps and flux densities of 4, 8, and 12 kilogauss. The 12 kilogauss curves are included only to establish a general trend. For reliability considerations, 8 kilogauss would be a maximum design level.

A volt-turn ratio of 1.5 appears to be the probable design point established from minimum loss considerations. Transformer efficiency, discussed in a later subsection, indicates that flux densities of 8 kilogauss at 500 cps and 4 kilogauss at 1600 cps are desirable. Thus, the expected range of transformer weight is 2 to 4 pounds.

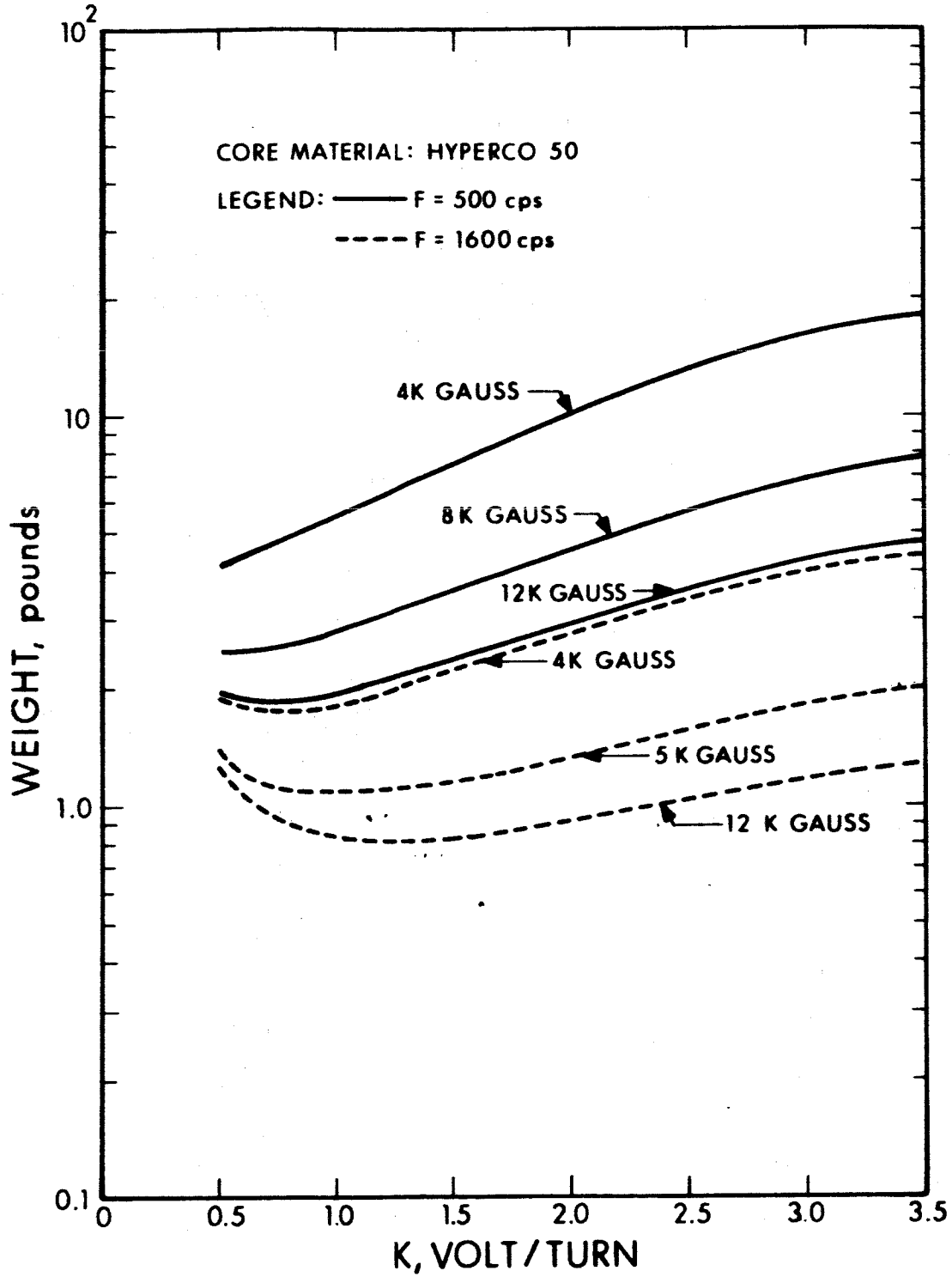


FIG. 5-5 TRANSFORMER WEIGHT VERSUS VOLT/TURN RATIO FOR VARIOUS FREQUENCIES AND FLUX DENSITIES

Transformer sizes under the same conditions range from 4.75 inches long by 2.6 inches high at 500 Hz to 4.25 inches long by 2.33 inches high at 1600 Hz.

### 5.5 Effect of Frequency

The effects of increased operating frequency are: (1) decrease transformer weight as shown in Fig. 5-5, (2) improve transformer efficiency shown in Fig. 5-8, and (3) improve voltage regulation, Fig. 5-6. The improvement in voltage regulation through higher frequency and higher flux density operation is caused by a reduction in core cross-sectional area - hence, a reduction in total wire length. The expected range in voltage regulation at 600°C is 8 to 10 percent.

### 5.6 Effect of Temperature

The overall effect of increased operating temperature is to decrease transformer efficiency and voltage regulation as shown in Figs. 5-7 and 5-8. The reduction in core loss at higher temperatures is overshadowed by the increase in wire resistivity.

If a lower operating temperature could be obtained, transformer efficiency would be improved through the use of other core materials and lower wire resistivities as indicated in Fig. 5-9. The material comparison is based upon a frequency of 500 cycles, a flux density of 8000 gauss, and a volt-per-turn ratio of 1.5. With reference to minimum loss, the above conditions do not demonstrate the maximum capabilities of lower temperature materials, but they do demonstrate a relative trend toward 95 percent efficiency at reduced temperatures (possibly 98 percent for good designs). Also, Fig. 5-9 as well as additional parametric data indicate that Hyperco 27 is not a desirable core material from an efficiency viewpoint- generally 10 to 30 percent less efficient than transformers using Hyperco 50.

### 5.7 Efficiency

Assuming that a 600°C temperature tolerance is desirable, Fig. 5-8 shows transformer efficiency versus temperature for various

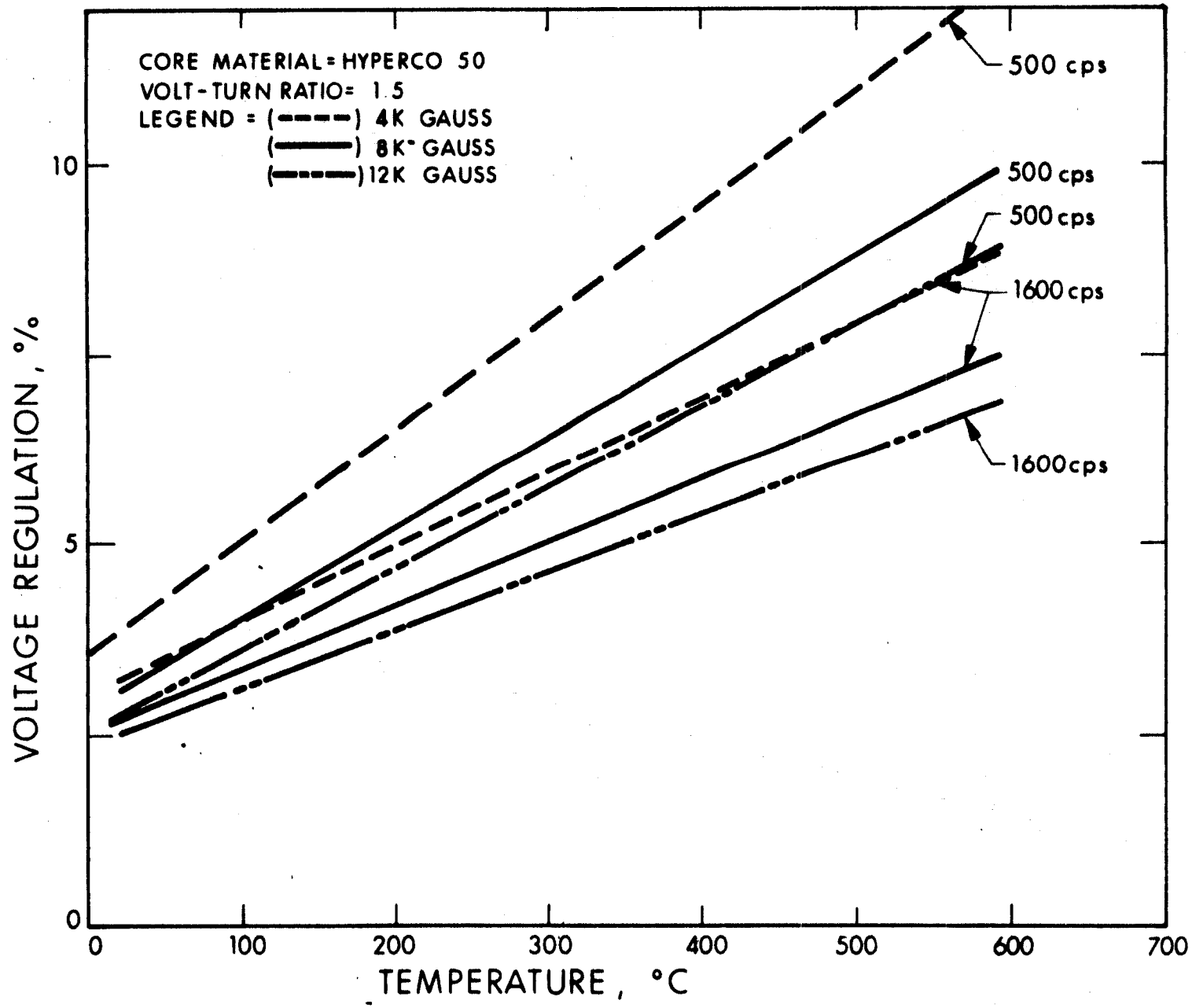


FIG. 5-6 TRANSFORMER VOLTAGE REGULATION VERSUS TEMPERATURE FOR VARIOUS FREQUENCIES AND FLUX DENSITIES

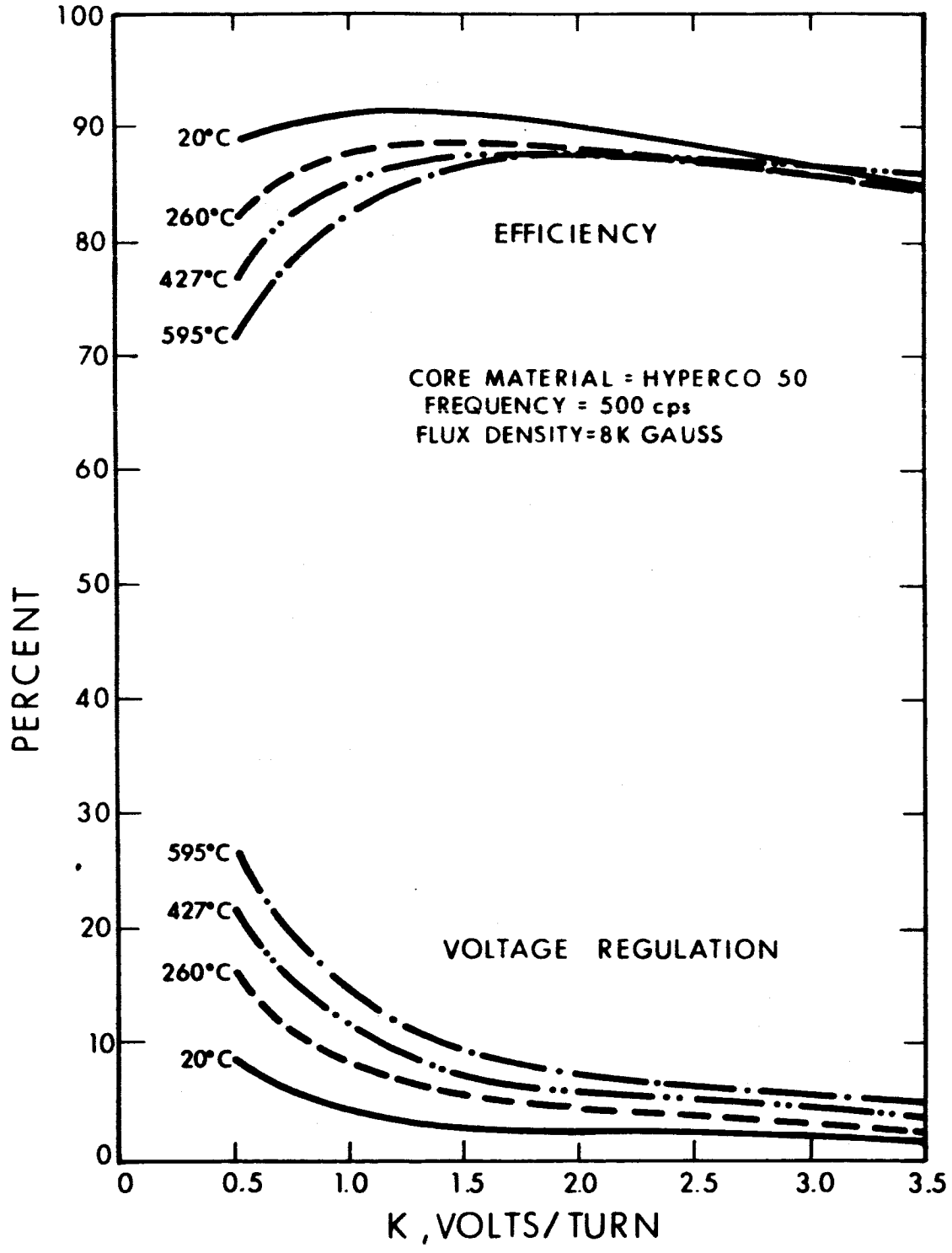


FIG. 5-7 TRANSFORMER EFFICIENCY AND VOLTAGE REGULATION VERSUS VOLT/TURN RATIO FOR VARIOUS TEMPERATURES

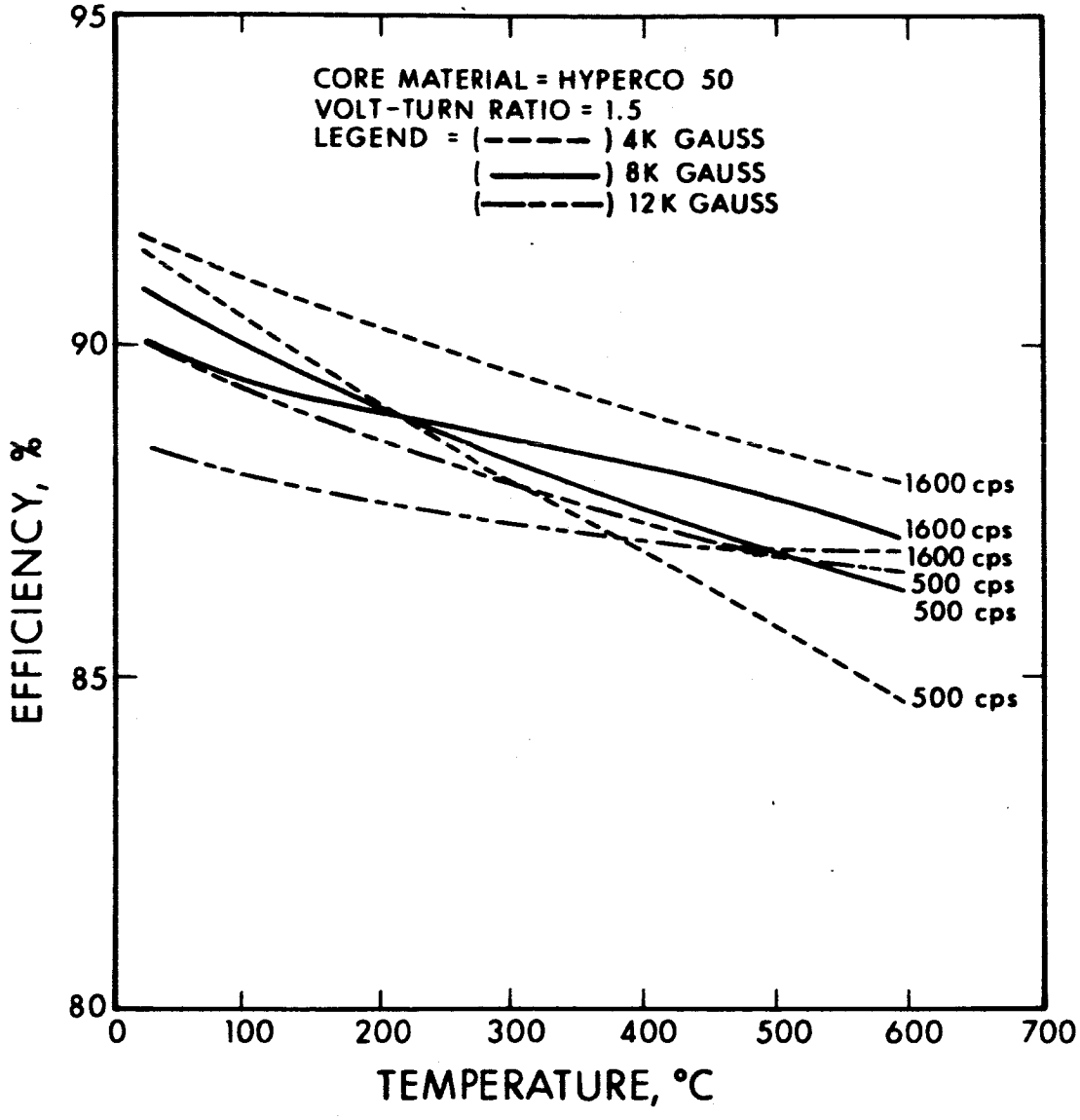


FIG. 5-8 TRANSFORMER EFFICIENCY VERSUS TEMPERATURE FOR VARIOUS FREQUENCIES AND FLUX DENSITIES

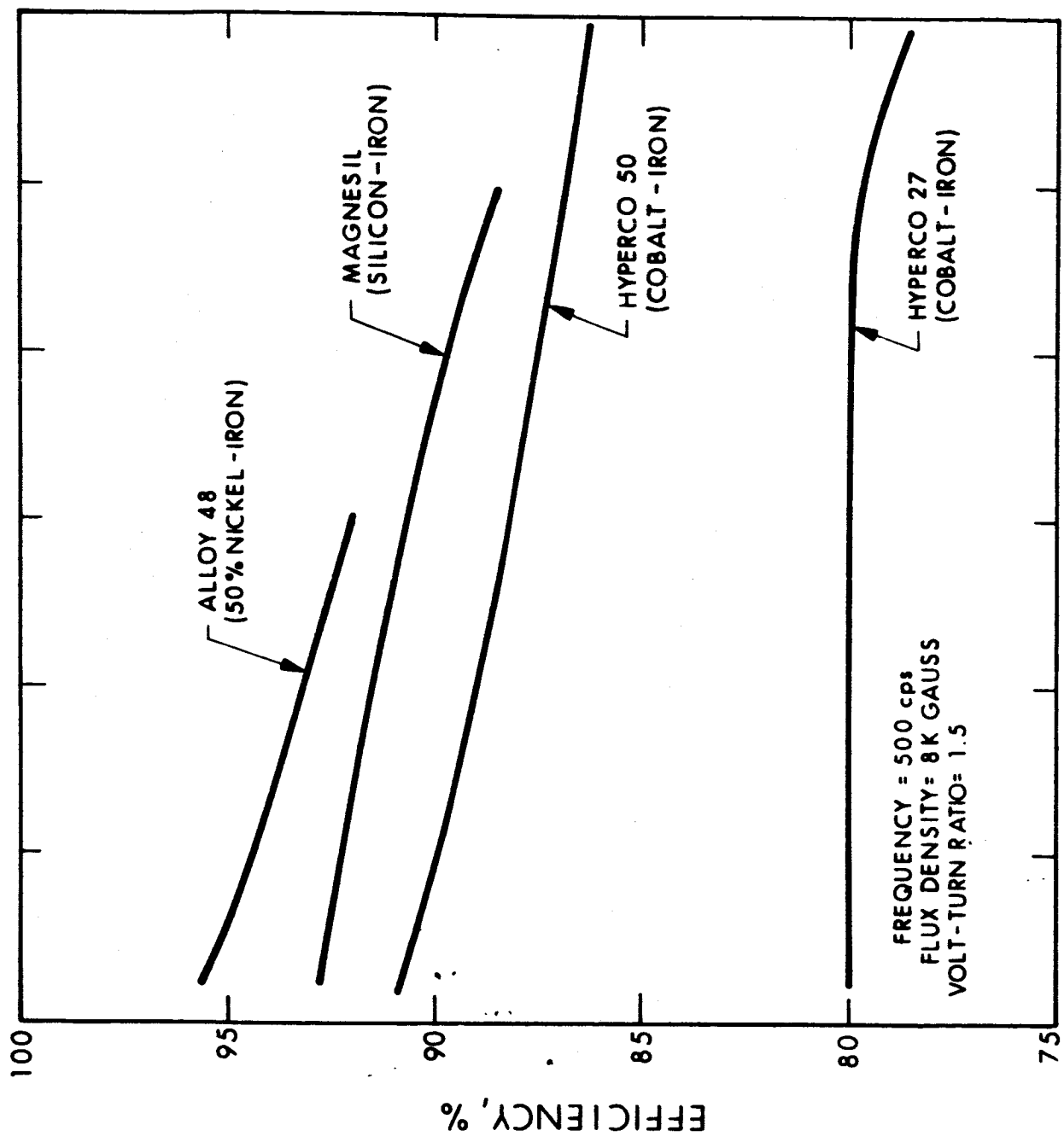


FIG. 5-9 TRANSFORMER EFFICIENCY VERSUS TEMPERATURE FOR VARIOUS CORE MATERIALS

operating frequencies and flux densities centered about a design point of 1.5 volts per turn. For the values considered, maximum efficiency exists at a frequency of 1600 cycles and a flux density of 4000 gauss; 8000 gauss would be the desirable flux density for 500 cycle operation. Thus, the expected range of transformer efficiency at 600°C is 86 to 88 percent.

### 5.8 Thermal Considerations

A complete thermal analysis will require final design definition (contingent upon measured thyratron characteristics) and heat transfer through associated structures. However, a few cursory calculations can be made to establish the feasibility of transformer radiation cooling. Figure 5-10 shows the assumed heat transfer configurations for a copper strip primary and shell core. Temperature calculations are for heat transfer only in the directions indicated from the surfaces indicated. Emissivities of 0.6 and 0.5 are assumed to be those of the core material and a coated copper surface, respectively (Ref. 25). The two cases considered are the maximum efficiency conditions listed in Subsection 5.7, and dissipated heat is limited to transformer loss, i.e., no additional heat inputs. Table 5-V is a summation of the resulting calculations.

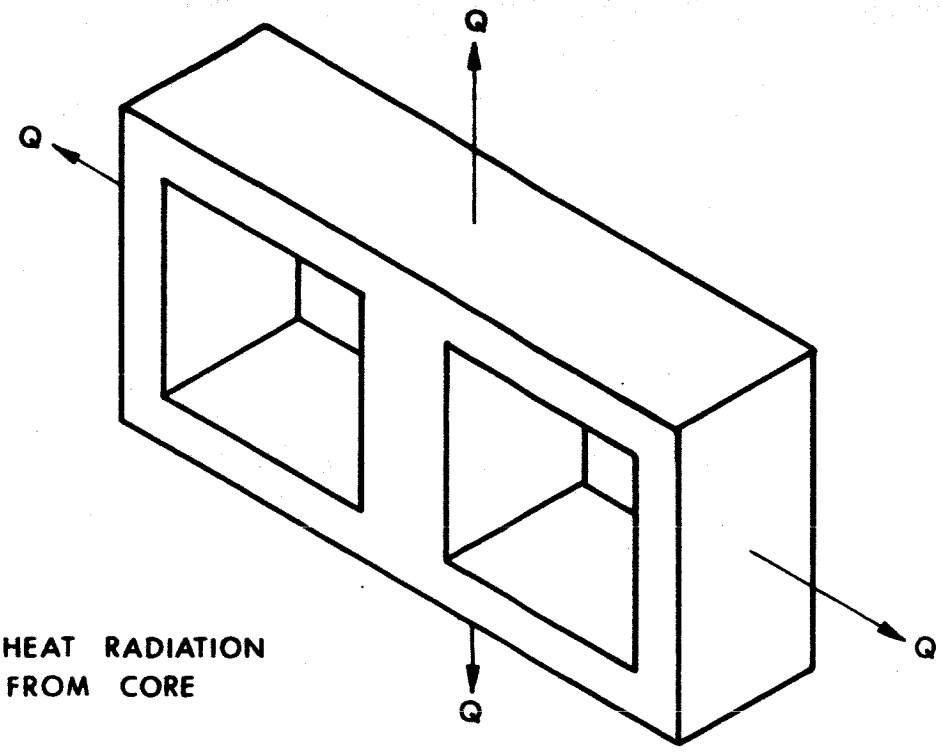


(A) HEAT RADIATION FROM CORE

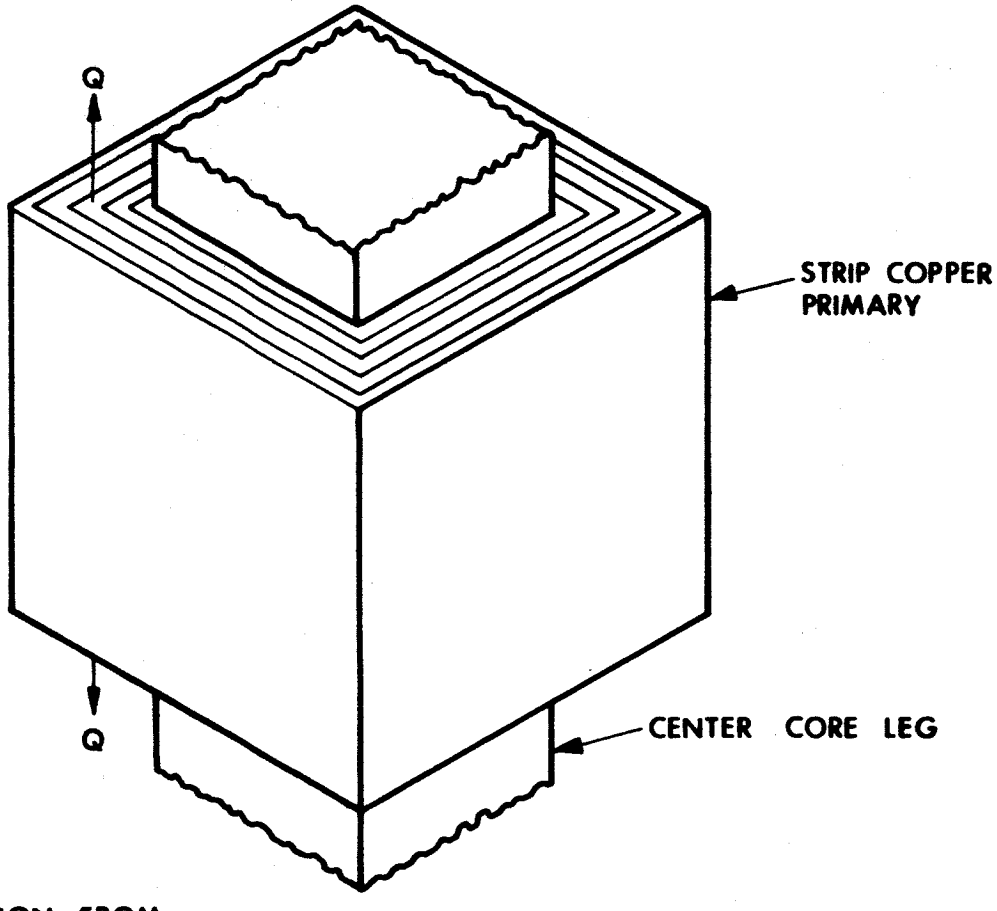


(B) HEAT RADIATION FROM COPPER STRIP PRIMARY

FIG. 5-10 ASSUMED HEAT TRANSFER CONFIGURATION

## TABLE 5-V

THERMAL CALCULATIONS

| Frequency | Surface Area | | Emissivity | | Loss* | | Temperature | |
|---|---|---|---|---|---|---|---|---|
| | Core | Copper | Core | Copper | Core | Copper | Core | Copper |
| 500 cps | 114 $cm^2$ | 17 $cm^2$ | 0.6 | 0.5 | 13.18W @ 20°C | 6.75W @ 600°C | 156°C | 339°C |
| 1600 cps | 80 $cm^2$ | 15 $cm^2$ | 0.6 | 0.5 | 11.06W @ 20°C | 5.83W @ 600°C | 177°C | 336°C |

Note: Loss figures are highest values which for the core occur at 20°C and for the copper occur at 600°C; i.e., approach has been to use worst-case values.

# 6. CIRCUIT ANALYSIS

## 6.1 Thyratron Inverter Circuits

Inverter circuits for thyratrons have been developed and used for many years. However, the cesium thyratron differs from conventional thyratrons in that the conduction drop is very low (0.1V), the current capability high (50 amps), and the peak reverse voltage rating low (20V). In selecting and comparing inverter circuits for the cesium thyratron, circuits for silicon controlled rectifiers (SCR) and transistors are more directly applicable than many of the conventional thyratron circuits. The main differences between SCR and the cesium thyratron are the slower turn-on time and the long deionization time of the thyratron. While the SCR recovers quickly when back biased, a reverse current surge occurs which uses some power. This is not expected to occur with the thyratron. In general, the circuits for thyratron (and SCR) inverters can be divided into two categories, series and parallel. There are other single tube types but they have not been considered because of low efficiency, lack of a common cathode connection, or other incompatibility features.

### 6.1.1 Parallel Inverter Circuits

A typical circuit of a parallel thyratron inverter is shown in Fig. 6-1. Commutation or shut-off of a conducting thyratron is accomplished by the commutating capacitor C. This capacitor can be placed on the primary or secondary side of the transformer.

Operation of the circuit is as follows: Assume that Tube 1 is conducting. A firing pulse is applied to the grid of Tube 2. Tube 2 rapidly turns on and the anode voltage falls to nearly ground potential (+0.1V). Since the capacitor was charged to twice the supply voltage (positive at Tube 2 side) the voltage at the anode of Tube 1

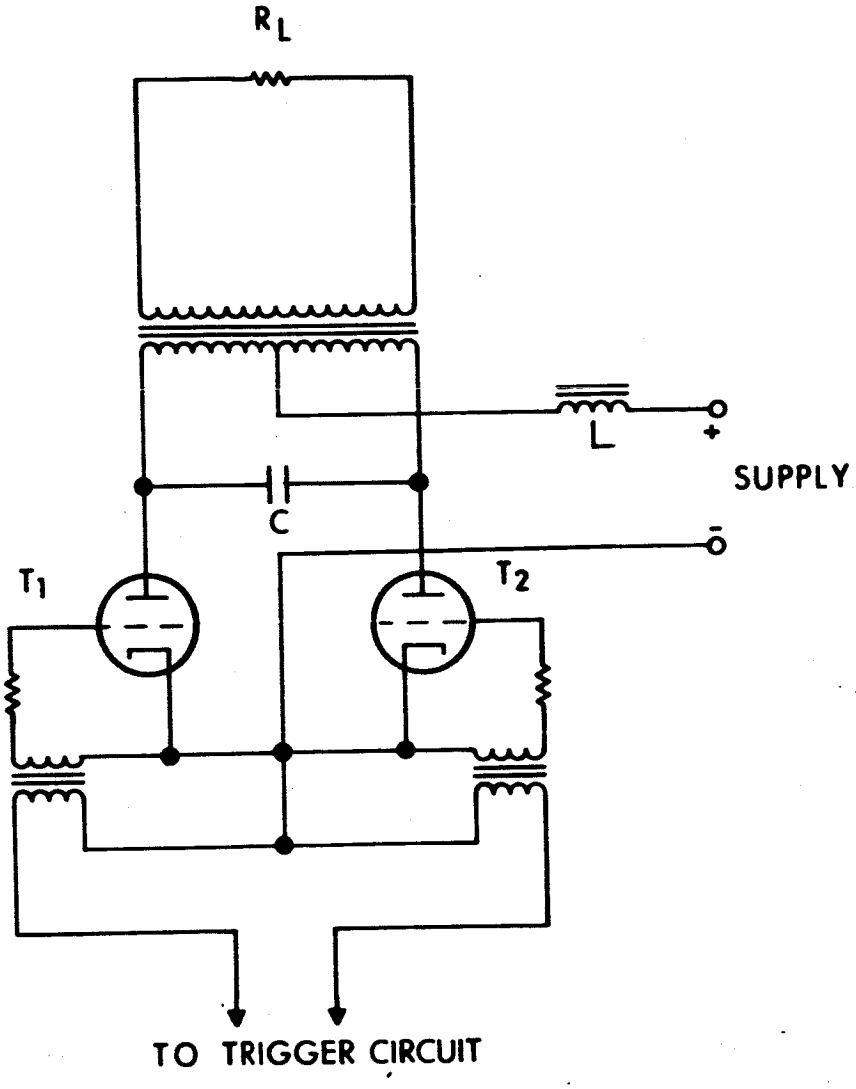


FIG. 6-1 TYPICAL PARALLEL INVERTER CIRCUIT

is now about twice the supply voltage below ground potential (less the Tube 2 drop). Note that at this point the voltage across the transformer has not yet changed in polarity. The capacitor discharges through the transformer into the load, and at the same time is being charged in the reverse direction by the supply voltage. Thus, the discharge rate is faster than the $R_LC$ time constant alone. The time that the anode of Tube 1 is held below ground level must be as long or longer than the deionization time of the tube. The voltage waveform across the transformer (and load) is the same as the capacitor voltage waveform. Tube 2 is now conducting and Tube 1 is off. A firing pulse is applied to the grid of Tube 1 and the commutation process repeats in the reverse direction.

Voltage and current waveforms for the parallel inverter are shown in Fig. 6-2. A variety of waveforms can exist at the load depending upon inverter component values and load characteristics. As previously mentioned, the commutating capacitor can be placed on the secondary side of the transformer or split between primary and secondary. The Inductance L serves as a ballast to prevent excessive current flow during switching. During the switching interval, high currents can flow in the primary to the commutating capacitor and to the anode of the thyratron which has been turned on. If this current is not limited, the charging time for the capacitor will be very short and the tube which is to be turned off will not be reverse-biased long enough for deionization to occur.

Another type of parallel inverter is shown in Fig. 6-3. This is known as a counter EMF inverter. An external voltage is applied to the commutation transformer at the same instant that the grid trigger voltage is applied to the opposite tube to reverse the voltage on the conducting tube. Detailed operation of this circuit was not found in the literature and several problem areas can be seen. First, the power transformer should be in the plate circuit because of the desirability of having the cathodes common and at ground potential. Second, the

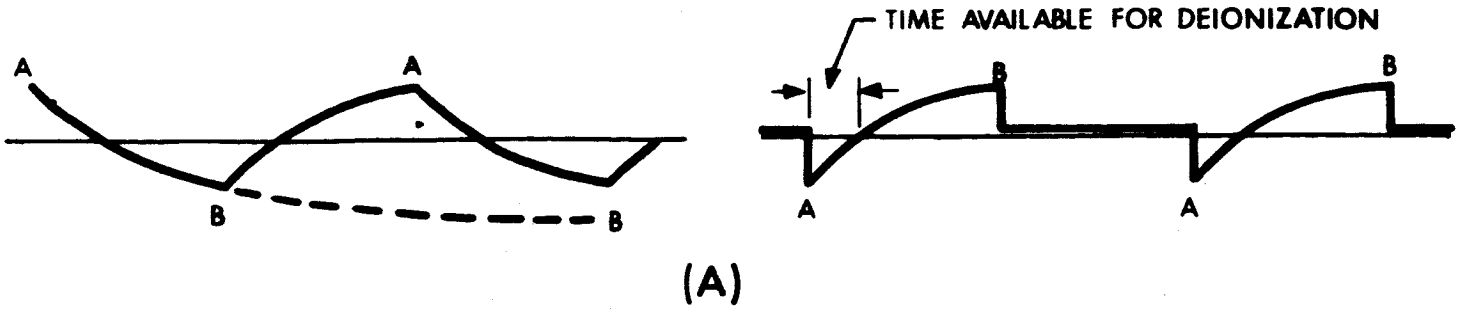


(A)

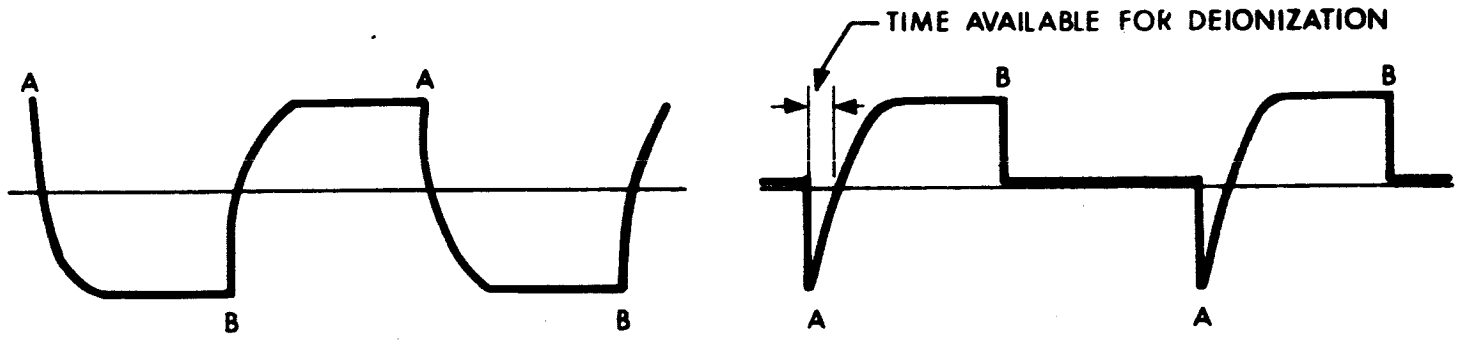


(B)

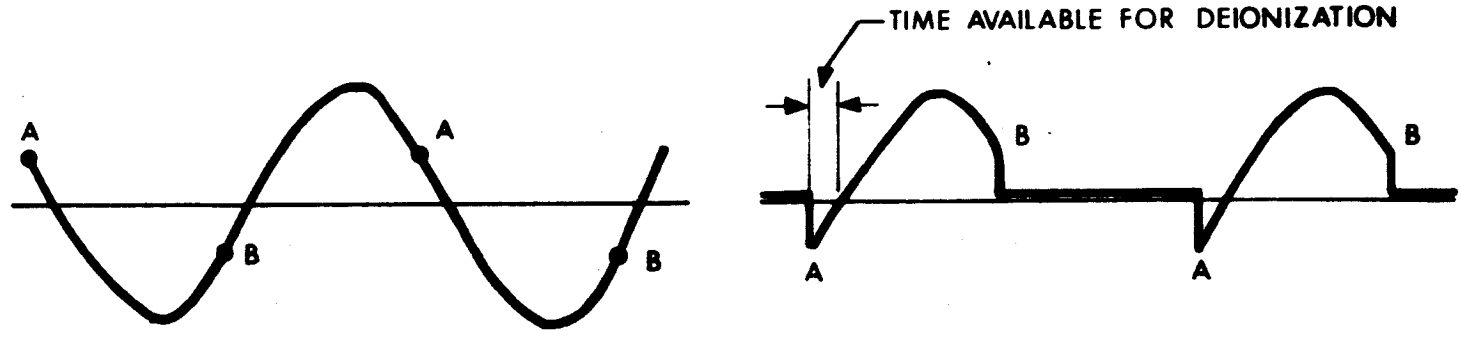


(C)

LOAD WAVEFORM PLATE VOLTAGE WAVEFORM

A- LIGHT RESISTANCE LOAD
B- HEAVY RESISTANCE LOAD
C- PARTIALLY INDUCTIVE LOAD

FIG. 6-2 PARALLEL INVERTER WAVEFORMS

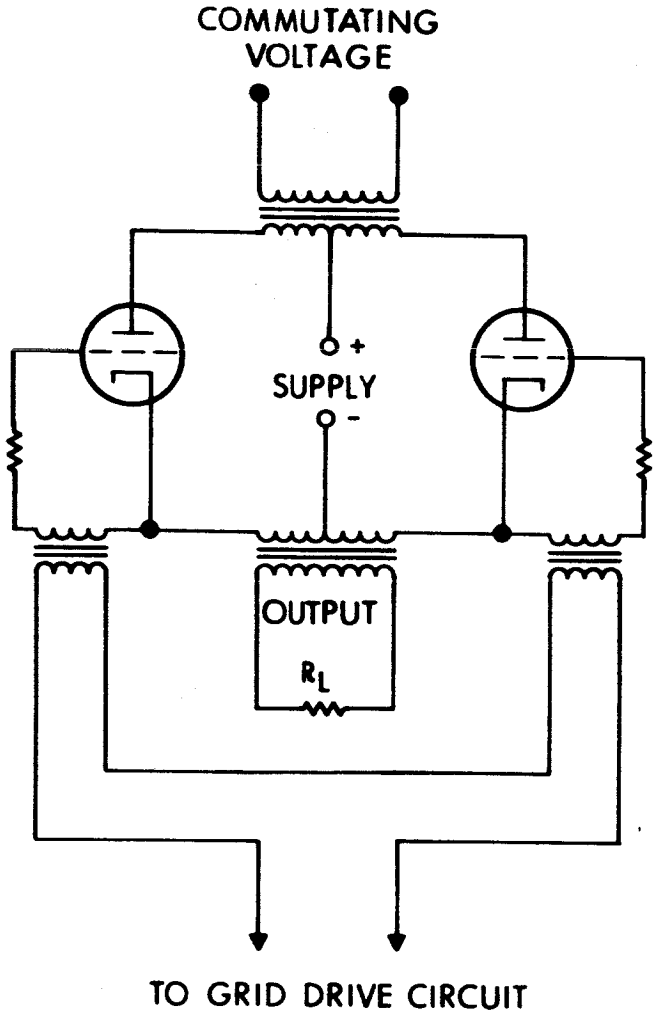


FIG. 6-3 COUNTER EMF PARALLEL INVERTER

commutating transformer must handle large currents with extremely low dc drop and be able to supply over twice the supply voltage to reverse bias the thyratron. The commutation transformer would also have to be a high temperature type. The driving power required for commutation appears to be high with this circuit. Due to the limited information available and the number of potential problem areas mentioned above, this circuit will not be considered for use on this program. If information obtained later in the program shows that this circuit has a significant advantage over existing ones, it will be reconsidered.

### 6.1.2 Series Inverter Circuits

Several series inverter circuits are shown in Fig. 6-4. The circuit in A is a sine wave-type inverter. That is, when the natural frequency of the inverter and load is the same as the grid excitation frequency, the output is coupled through Capacitors $C_1$ and $C_2$. The circuit B is a load capacitor commutated series inverter and is shown with a shunt load and a series load. In C is a dc chopper circuit which has the advantage over A and B in that the commutating capacitor only has to store enough energy to turn off the conducting thyratron, and not carry the full load power. It should be noted that commutation of the series inverters is also done by using a charged capacitor.

Expected efficiencies of the series inverter are lower than the parallel type. In addition, the cathodes cannot be at ground potential, and high temperature, high capacity capacitors would be required. For these reasons, the series inverter is not applicable to the high temperature tube program and will not be discussed further.

### 6.1.3 Analysis of the Selected Circuit

#### 6.1.3.1 Circuit Selection and Justification

The circuit selected is the capacitor commutated parallel inverter. This type of circuit was selected

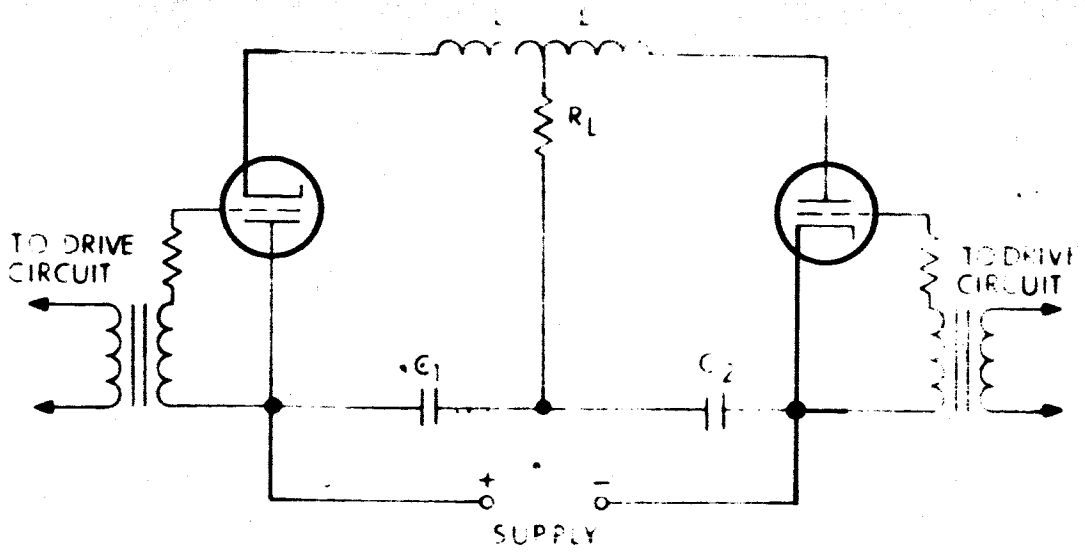


A. SINE WAVE SERIES INVERTER

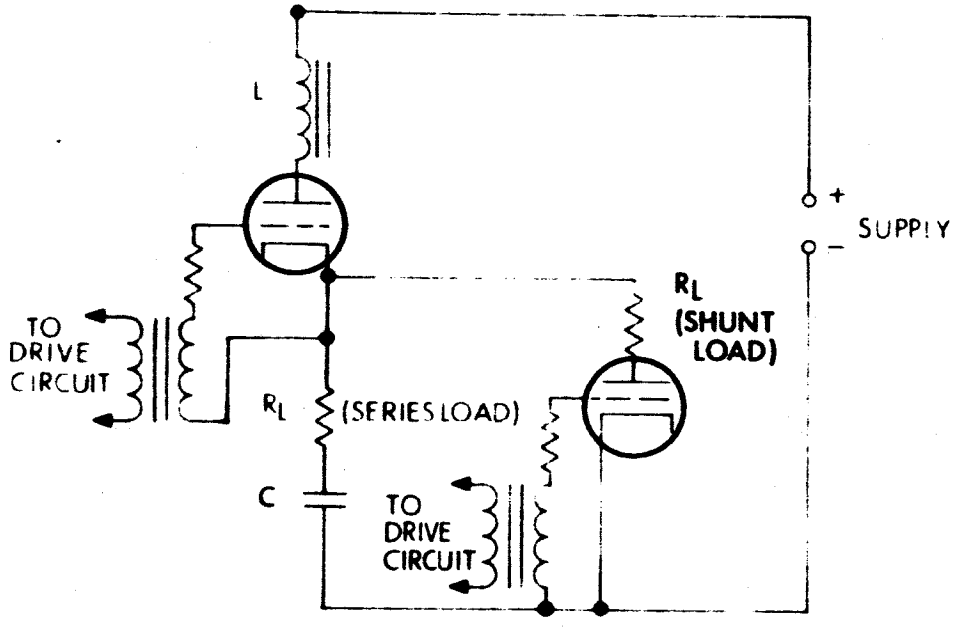


B. LOAD CAPACITOR COMMUTATED

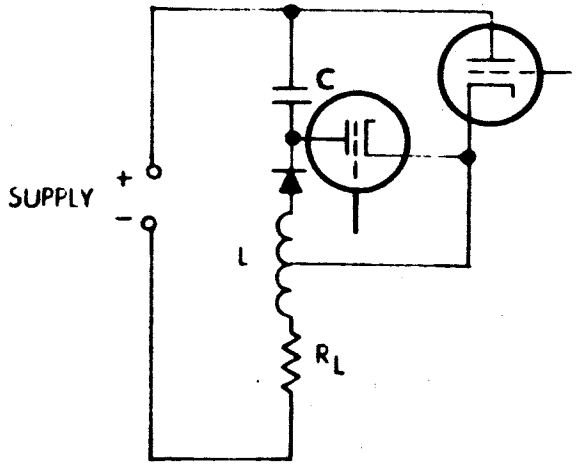


C. D.C. CHOPPER CIRCUIT

FIG. 6-4 SERIES INVERTER CIRCUITS

for several reasons. First, since it is highly desirable to have the thyratron cathodes electrically common, and at circuit ground, the parallel circuit meets this requirement. Second, much work has been done with parallel type of inverters, and the expected efficiencies are higher. Also, should grid control of the thyratron be possible, this circuit is readily adaptable for this type of operation. The circuit of the parallel inverter and a possible drive circuit are shown in Fig. 6-5.

6.1.3.2 Determination of Circuit Values

In order to select circuit values, the operating conditions must be known or assumed. For the first cut, it will be assumed that the inverter load will be a constant resistive load. This type of load provides a constant load on the thermionic generator and thyratrons and would alleviate possible thermal transient problems. Although a constant resistive load seems, at first, rather optimistic, it may actually be quite close to an actual system. Since the output waveform of the inverter will probably be a poor square wave, in all probability it would be rectified and only the dc output used. If a shunt regulator is used on the dc output the load would then be constant. Further power conditioning would provide other needed spacecraft voltages and waveforms. For these calculations the power output will be assumed as 130W less the power consumed in the inverter. The operating frequency has been assumed to be 1600 Hz.

No actual thyratron data for turn on or deionization time has been obtained. A deionization time of 125 microseconds has been assumed for these calculations. The high temperature transformer has been covered in Section 5 where the maximum turns ratio is shown to be 12 to 1. Voltage regulation of the transformer is about 10 percent.

First, the value of the commutation capacitor will be determined. The commutation ratio, defined as the fraction of

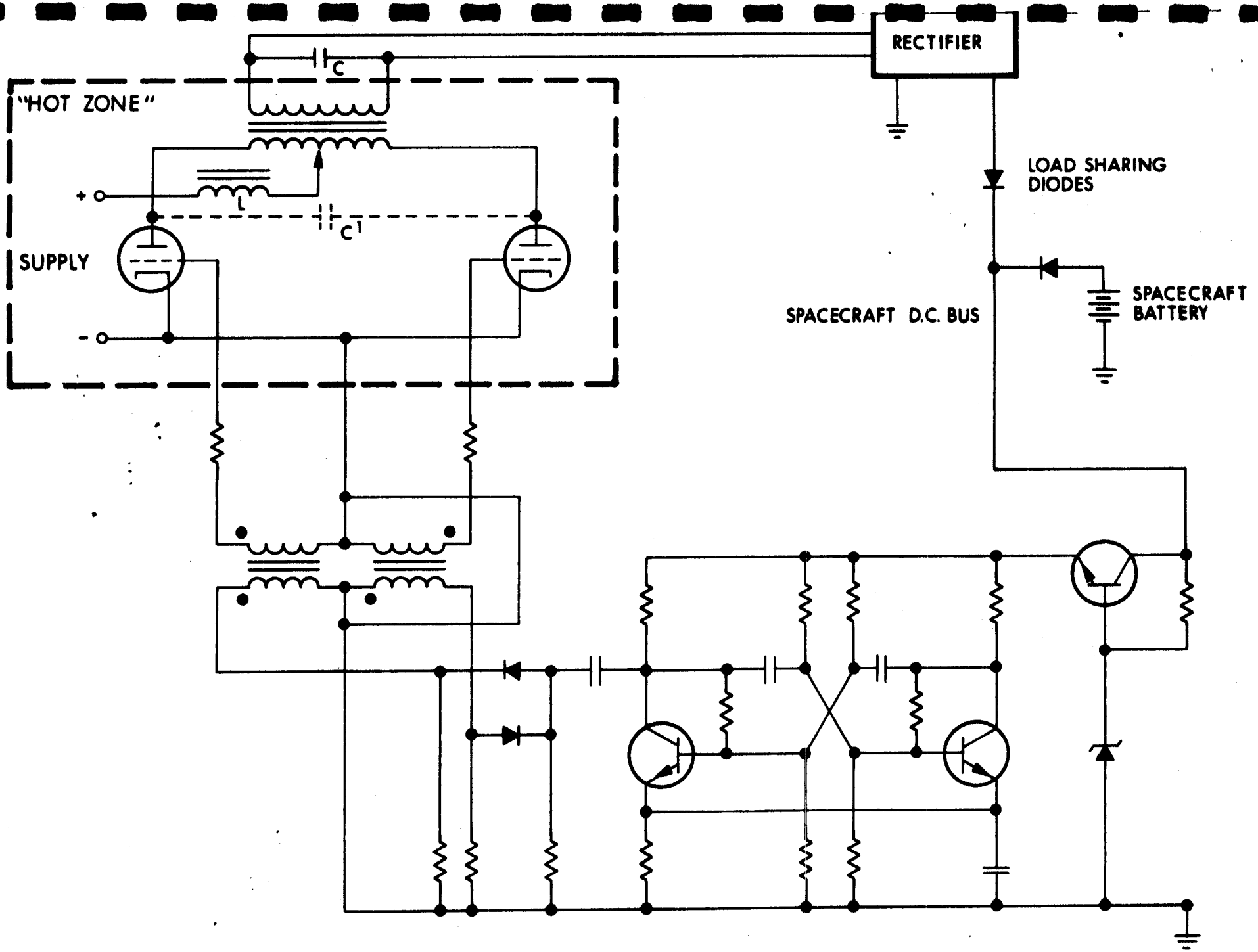


FIG. 6-5 PREFERRED INVERTER CIRCUIT WITH DRIVER CIRCUIT

the total cycle during which the thyratron anode is negative, for an operating frequency of 1600 Hz is 125/625 = 0.2. Referring to Fig. 6-6, for a power factor of 1 (resistive load) K = 2. K is defined as a dimensionless number equal to $4(2\pi fC)|Z|$, where $|Z|$ is the secondary impedance reflected to the primary side of the transformer. Assuming an overall inverter efficiency of about 80 percent, the output power will be 130 (0.8) = 104 watts. With an input voltage of 2.8V and an output of 30.3V (2.8 x 12 with 10 percent regulation), the load resistance for 104 watts is 8.83 ohms. $|Z| = R/N_1^2$, where $N_1$ equals the ratio of total secondary turns to one-half of the primary turns or N = 12.

Solving the equation for C

$$C = \frac{K}{4(2\pi f)|Z|} = \frac{KN_1^2}{8\pi fR}$$

$$C = \frac{2(12)^2 10^6}{8\pi 16008.83} \text{ microfarads}$$

$$= 812\ \mu f$$

Thus, 812μf is the value for the commutating capacitor. However, the commutating capacitor can also be placed on the secondary of the transformer. The value to be used on the secondary is $C/N_2^2$ where $N_2$ is the ratio of secondary turns to total primary turns or 812μf/36 = 22.5μf. A value of 30μf should be adequate.

To compute the value of L required so that current flows continuously from the supply, we must estimate a value for J. J is a dimensionless parameter defined as $2\pi fl(4N_1^2/R)$ where $N_1$ is the total turns ratio or 6 in this case. For current to flow continuously $J \geq K/3.24$ or $J > 0.62$. Therefore,

$$L \frac{JR}{2\pi f 4N^2} = \frac{0.62\ (8.83)}{2\pi 1600(4)36} \times 10^6\ \mu h = 3.78\ \mu h$$

The Inductor L should be greater than 3.78 microhenry.

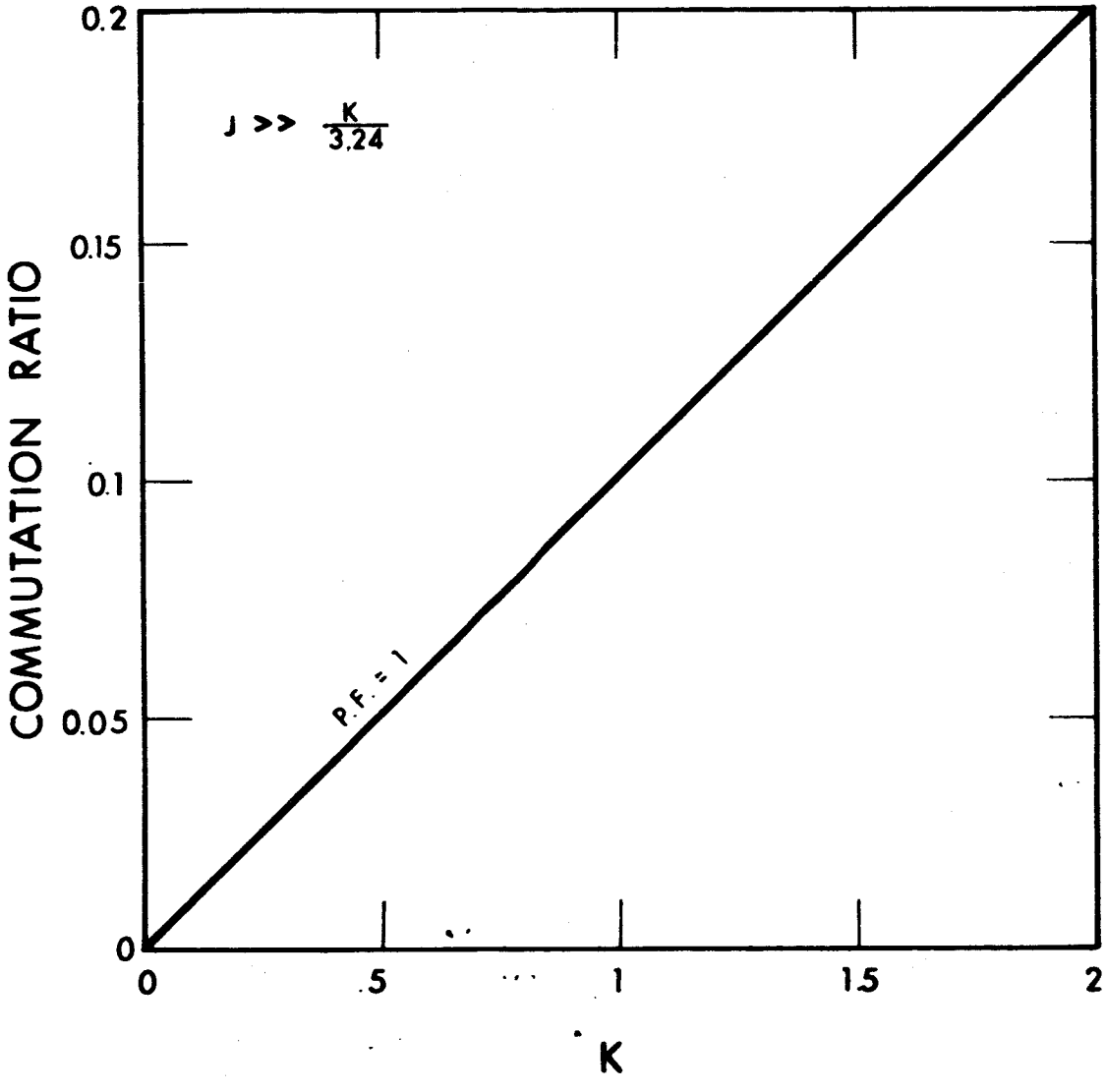


FIG. 6-6 COMMUTATION RATIO OF PARALLEL INVERTER

### 6.1.4 Calculated Circuit Efficiency

#### 6.1.4.1 Thyratron Losses

The thyratrons will contribute to circuit losses in three ways. First, when a tube is conducting, a voltage drop of about 0.1V is expected. At a current of 46.5 amps (2.8V x 46.5A = 130W) the power losses for both tubes will be about 4.65 watts average. Second, some power will be consumed by the drive circuit. The drive requirements of the tube have not been measured as yet, but a power consumption of 3 watts for the driver circuitry has been assumed. Thirdly, the turn-on and deionization times contribute to the circuit losses. The turn-on time is in the order of 10 micro-seconds. The average power loss due to turn-on time will be 1.8 watts. During deionization the anode of the thyratron is negative with respect to the cathode. The anode load current drops to zero instantly when the anode becomes negative. Since any reverse current will be due to leakage currents and will therefore probably be negligible, the power loss in the tube during deionization will be essentially zero and will be neglected in the calculations. The main loss during deionization is the loss in the commutating capacitor.

#### 6.1.4.2 Commutation Capacitor Power Loss

The loss in the capacitor is due to the series resistance (effective series resistance, or ESR). For this calculation an actual capacitor will be assumed. The capacitor could be made of three Sprague 260P, 10 microfarad units in parallel. The maximum dissipation factor at 1 KC is 0.3 percent at 25°C. The ESR is equal to the dissipation factor D divided by $2\pi fC$. The ESR of these capacitors is about 0.03 ohms. Assuming that the short circuit of the thermionic generator is 150 amps or less, the maximum surge current at the secondary would be 12.5 amps. This would be divided between the three capacitors or a maximum inrush of 4.1 amps. However, since the capacitors are also discharging in the direction of charge and an

additional current of 3.43 amps maximum could be flowing out of the capacitors through the load, the peak current into one capacitor is therefore 12.5 + 3.43/3 = 5.31 amps. This only occurs for a fraction of a cycle, but assuming it occurs for a time twice the deionization time or 250 microseconds, the power loss would be 2.0 watts.

The total circuit losses (neglecting choke loss) then are 4.65 watts average due to thyratron voltage drop, 3 watts, drive circuit losses, 1.8 watts average due to thyratron turn-on time and 2.0 watts average loss in the commutating capacitor (see Table 6-I). The total circuit power loss is 11.4 watts. The expected transformer efficiency is 88 percent which means a power loss of about 15.8 watts for a total of 27.2 watts. This gives an estimated overall current efficiency of 79.1 percent. If the output is rectified an additional loss will occur in the diodes with a resulting overall dc to dc efficiency of 77.4 percent.

TABLE 6-I

THYRATRON CIRCUIT LOSSES

| Item | Power Loss Watts |
|---|---|
| Thyratron Forward Drop | 4.65 |
| Thyratron Tube ON Time | 1.80 |
| Drive Circuit Losses | 3.00 |
| Commutating Capacitor Losses | 2.00 |
| Transformer | 15.80 |
| Total Losses | 27.25 |

### 6.1.5 Construction of Proposed Circuit

No difficulties are foreseen in constructing the proposed circuit. Construction of the two main components, the thyratrons and the transformer have been covered in separate sections. At present it is not known if the Choke L (Fig. 6-5) will actually be needed. Since the value of L is small and the thermionic generator is current

limited, the choke may not be required for current limiting. If, however, current is not drawn for the full cycle, then it will be necessary to fabricate a high temperature choke. As previously mentioned, the commutating capacitor will be made up of three (or more) Sprague Type 260P, 10 μf units in parallel. The commutating capacitor will be located on the secondary side of the transformer out of the hot zone. These particular capacitors can be operated at temperatures up to 105°C so that the actual distance or lead length can be minimized somewhat.

### 6.1.6 Problem Areas

As discussed previously, the proposed circuit cannot readily be operated under varying loads, particularly with changing power factor. Thus, the restriction of a constant resistive load has been imposed. However, inverter circuits have been developed for operation under these conditions.

A circuit diagram of an improved type of parallel inverter is shown in Fig. 6-7. Note, however, that the choke has been placed in the cathode circuit and that diodes and a capacitor are used. The capacitor across the supply is required because the supply should have a low transient impedance so it can accept power as well as supply power. The inductance is chosen to resonate with the commutating capacitor C to provide a short impulse to turn off the thyratron. The inductor also serves as a ballast to limit the current flow during switching. The diodes prevent the voltage across either half of the primary from exceeding the supply voltage.

The improved circuit cannot readily be adapted for use in a solar-thermionic power system using thyratrons. First, the cathodes are not at ground potential in this circuit, as this feature is highly desirable. Secondly, the commutating interval is very short and would need to be lengthened to allow for deionization time. Third, the filter capacitor should be located at the inverter to minimize lead inductance, and this would mean a high temperature, high capacity

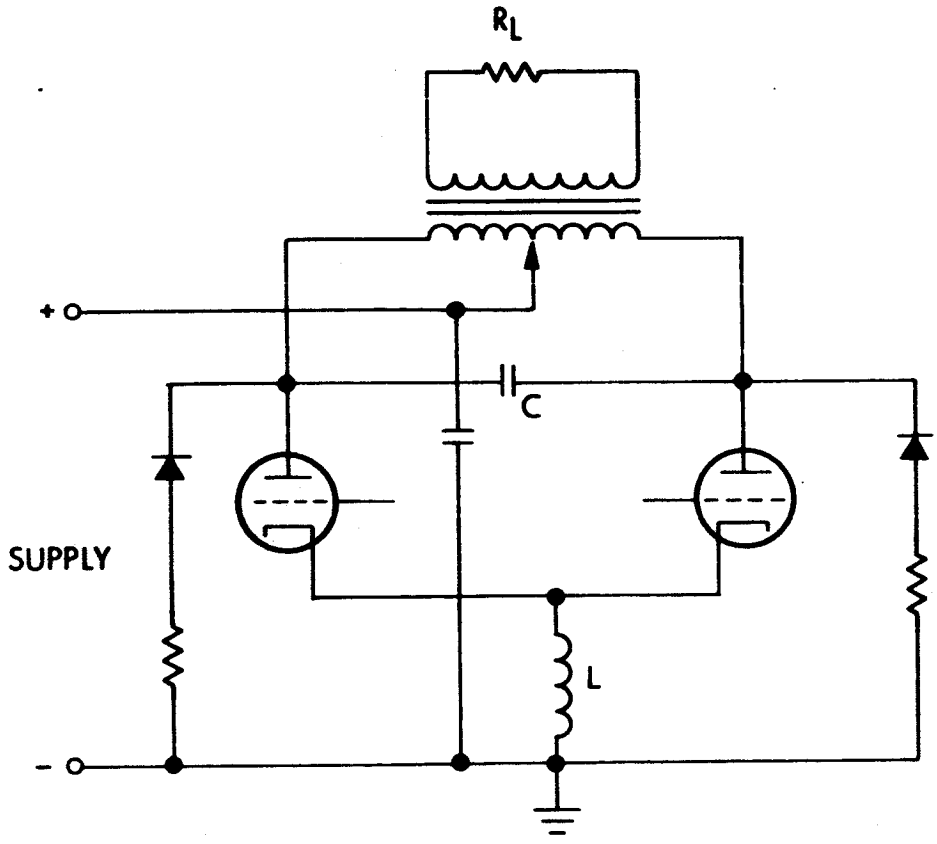


FIG. 6-7 IMPROVED INVERTER CIRCUIT

unit. The diodes do not present a great problem; a cesium diode, or some other high temperature diode, could be developed for this application.

Another possible problem area is starting of the inverter. If, for example, one thyratron is conducting when the circuit is deenergized and the same tube is fired first when it is turned on, the transformer may be driven into saturation. If this occurs, commutation will not occur and both tubes would be left in a conducting state. This problem can be alleviated in several ways. First, the transformer can be designed to have a saturation capability far in excess of startup conditions. However, this requires a larger and heavier unit than is necessary for normal operation. Second, a circuit can be designed such that the initial flux in the transformer is always opposite to the direction of the startup flux. This requires adding circuitry to always bias the transformer in one direction at turnoff, and to always fire one tube first at startup.

## 7. POWER CONVERSION SYSTEMS

There are a variety of low voltage power conversion systems that can be applied to thermionic generator systems. The main criterion of suitability is the voltage drop of the active inverter circuit element i.e., transistor, switching diode, or thyratrons. Germanium transistors are ideal because of their low drop but suffer from a temperature limitation of 30 to 50°C. Silicon transistors will work at a higher temperature (75 - 80°C) but have a drop so high as to lower the efficiency to an undesirably low level. Therefore, the only solution producing a practical dc-dc converter with usable efficiency is to use transistors at the proper temperature or to design a thyratron which will work at high temperature with very low forward tube drop.

### 7.1 High Temperature Integrated Tube and Transformer Approach

The high temperature integrated tube and transformer approach constitutes a high power density, low volume, power conditioning system which can result in quite an improvement in solar thermionics in terms of watts per pound and overall system simplicity. One of the biggest problems in the use of thermionic converters is that the power output terminals have temperatures of 1700°C at the emitter and 700°C at the collector. Making high current connections to these terminals requires heat chokes in the leads to bring the temperature down to a safe value. If the low temperature ends of the connector leads are at 500 or 600°C instead of 30°C, for the same thermal resistance the heat loss will be reduced as follows

$$\frac{Q_1}{Q_2} = \frac{K}{K} \frac{\Delta T_1}{\Delta T_2} = \frac{\Delta T_1}{\Delta T_2}$$

where $Q_1$ = thermal lead loss for high temperature system

$Q_2$ = thermal lead loss for low temperature system

T = temperature drop through lead

K = thermal resistance

$$Q_1 = Q_2 \frac{\Delta T_1}{\Delta T_2}. \quad (1)$$

For the temperatures mentioned above, $Q_1 = 0.3\ Q_2$ and the lead loss for the thyratron is thereby reduced by 70 percent from that for the solid state device. The thermal resistance K cannot be reduced indefinitely because the electrical conductivity would suffer too much. That is, a compromise value of L/A must be used to maximize electrical output and minimize thermal losses. (L = bus length and A = conductor cross sectional area). For the high temperature circuit, on the other hand the electrical power connection between the 500°C and the 30°C low temperature section is made very efficiently by the transformer coupling while at the same time, a high thermal impedance can be maintained.

A diagram of the integrated generator/power conditioning system as it might be applied to a five foot mirror is shown in Fig. 7-1. It differs from the usual five foot system in several significant ways. All components required for the dc-dc conversion are mounted along the system axis and directly in front of the four diode generator. The thyratron cathode cavity connects directly with the absorber cavity. (The exact configuration of the absorber cavity to include the thyratron cathode heating has not been shown since it must be coordinated with the diode and generator support structure.) The other end of the dual thyratron cathode cylinder forms both the mounting for the thyratrons and the electrical connection for the circuit ground return. The transformer core is located approximately at the center of gravity of the electrical system and is therefore the logical support point to which the support struts can be securely fastened by means of the transformer brackets. Because the struts

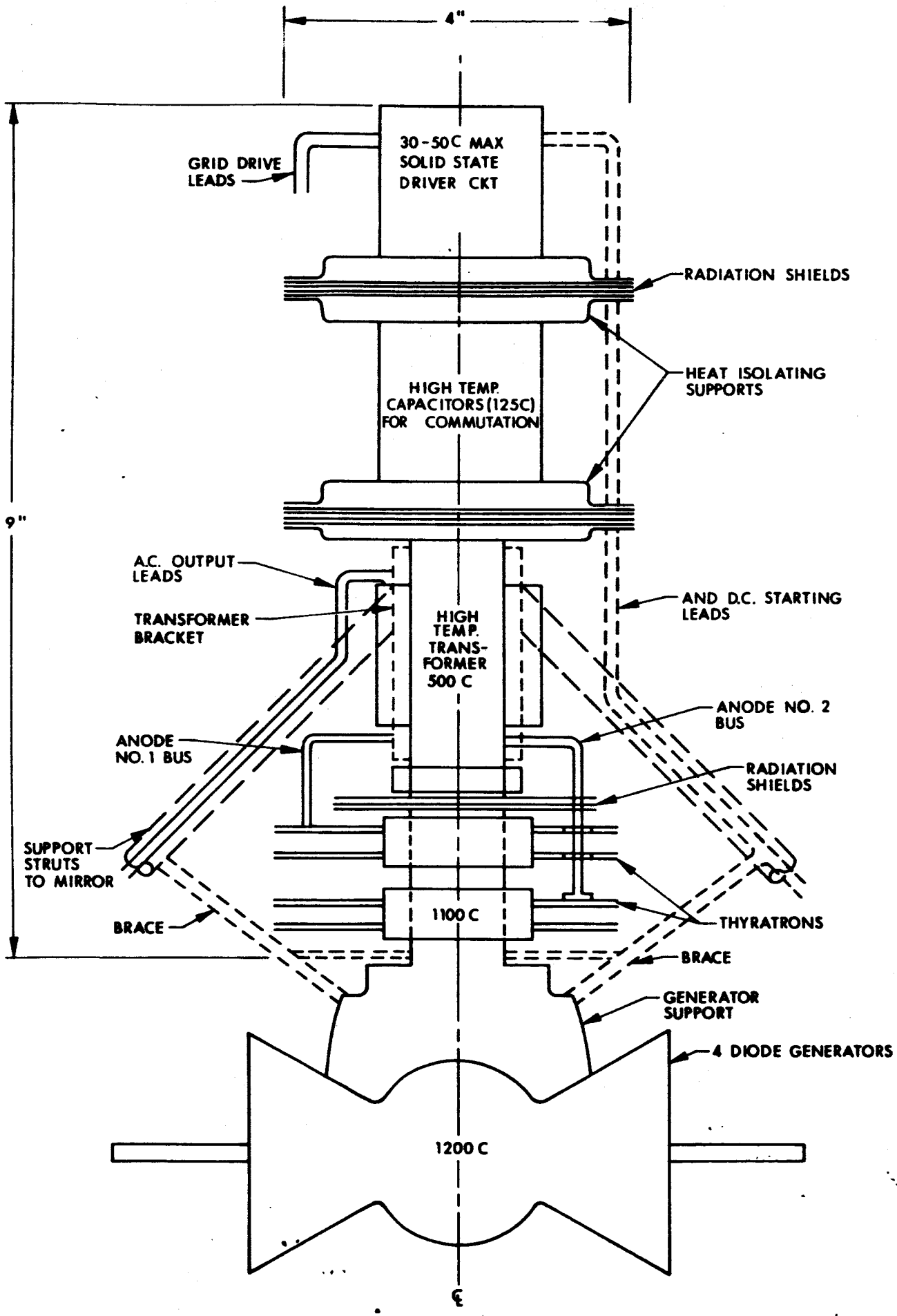


FIG. 7-1 POWER CONDITIONING SYSTEM - INTEGRATED TUBE

do not carry current they can all be at the circuit ground potential and do not require insulating from the transformer core. The struts and their terminations at both the generator and mirror are therefore extremely simple since no coaxial lines or double electrical connectors are required.

Attached to the transformer core opposite the end at the cathode is a lightweight, thermally insulating support for the commutating capacitors. The capacitor mounting region can safely operate at 125°C since commercial capacitors of the required capacity and voltage rating are readily available. Although not shown, the capacitor connections are easily made.

Beyond the capacitor section is another lightweight thermally insulating support to serve as a mounting for the solid state thyratron driver circuit. A radiator section can be added if necessary to maintain the proper operating temperature. However, since all the components are low current the system as shown in Fig. 7-1 is designed primarily for a.c. output since it appears that ac power transmission is more desirable for space vehicles than dc transmission. However, it would be quite feasible to add solid state rectifiers in the same region as the driver circuit, feed the transformer secondary into it and obtain a dc output. The output leads consisting of a pair of No. 16 wires can be brought out as shown and can utilize the hollow support struts as a shielding conduit.

Mechanically, the entire assembly is mounted rigidly at the center of gravity by the lightweight struts. Braces from the struts to the generator support will stabilize the entire assembly, since the generator is the other heavy member of the system. The relatively lightweight capacitors and driver circuit can easily be cantilevered from the transformer without serious vibration problems.

Optically, all components will fit within a four or four and one-half inch diameter obscuration circle which is no larger than the present obscuration circle and therefore will not affect the

input radiation in any way. If anything, the support struts can be made with a cross-section of moment of inertia comparable to the electrically conducting struts but with narrower profile to intercept thermal radiation so that the obscuration efficiency is actually improved.

### 7.2 High Temperature Tube and Low Temperature Transformer Approach

This approach was discussed in the proposal and mentioned in the work statement. However, it was to be used only in the event the high temperature transformer appeared to be unattainable. Since the high temperature transformer does appear to be quite practical, the usefulness of the low temperature transformer approach is less attractive and perhaps should be limited to testing the thyratrons in the laboratory. The main reason of course, is that three bus bar lengths would be required under the same conditions that two are required for the completely solid state approach. In order for the low temperature transformer approach to be competitive, the 8 to 10% increase in efficiency of the low temperature transformer over the high temperature version must offset any losses in system electrical efficiency due to bus bar losses. In addition, the additional weight of the bus bars should not lower the figure of merit of the system even if electrically the efficiency is improved.

### 7.3 Low Temperature dc to dc Converters

Many types of solid state dc-dc converter circuits have been designed and built for use with low input voltages. The thermionic generator presents an unusually difficult problem because the output voltage is so low, being less than 3 volts. Efficiencies for dc-dc conversion of over 90% can be achieved for 2.8V input, but only by the accumulation of circuit weight. Fig. 7-2 shows how the efficiency of germanium and silicon transistors operating at a temperature of 30°C and 85°C respectively and a power level of 150W varies with the converter weight. When the data are converted into the figure of merit F,

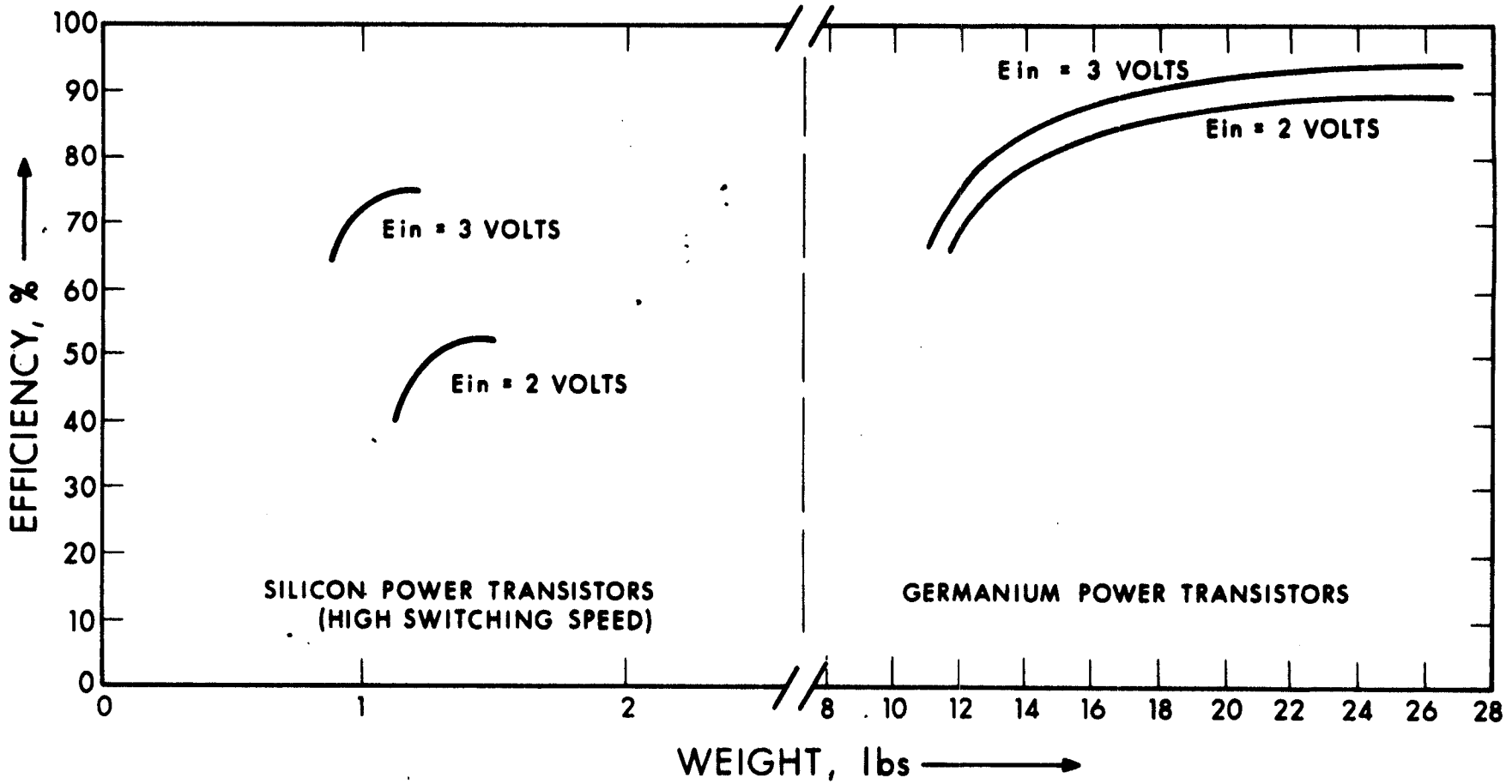


FIG. 7-2. CURVES OF dc-dc CONVERTER EFFICIENCY AS A FUNCTION OF WEIGHT FOR $P_{out}$ = 150 WATTS

of watts per pound, it is seen that F is highest when the efficiency is poorest. As will be shown later, the transistor circuit efficiency at maximum F is less than the calculated efficiency of the high temperature tube circuit.

Associated with the low temperature circuits is the necessity to isolate the converter from the high temperature zones and to run high current bus bars from the generator to the conditioning system. Fig. 7-3 and 7-4 show the weights and efficiencies of the bus bars. By clever design, both the weight and deleterious effects such as magnetic fields can be minimized, but only by increasing the system complexity and cost considerably. For example, coaxial conductors, which also serve as structural members, must be devised with reliable insulating techniques and double connector terminations. In addition, it is usually necessary to add radiators to the low temperature circuit housing to make sure that the transistors remain at a low temperature. This type of circuit is also subject to runaway conditions where a temporary thermal overload will cause the solid state device drop to increase which increases the internal dissipation, which further increases the temperature.

## 7.4 Overall Comparison of dc to dc Conversion Systems

As discussed in section 4, the figure of merit, F, is the most meaningful criterion for judging one system against another because it includes not only circuit efficiencies, but also thermal effects and the weight necessary to achieve a given efficiency. If any one parameter is an absolute necessity regardless of cost or weight then it becomes the criterion which determines system acceptability. For example, if the maximum number of electrical watts output are required from a fixed thermal source then a solid state system would be required even though system weight and complexity is high. Thus, F does not serve as a universal criterion for judgment of system excellence but for most cases it is a good all around indicator for such judgment because it does include a variety of system parameters.

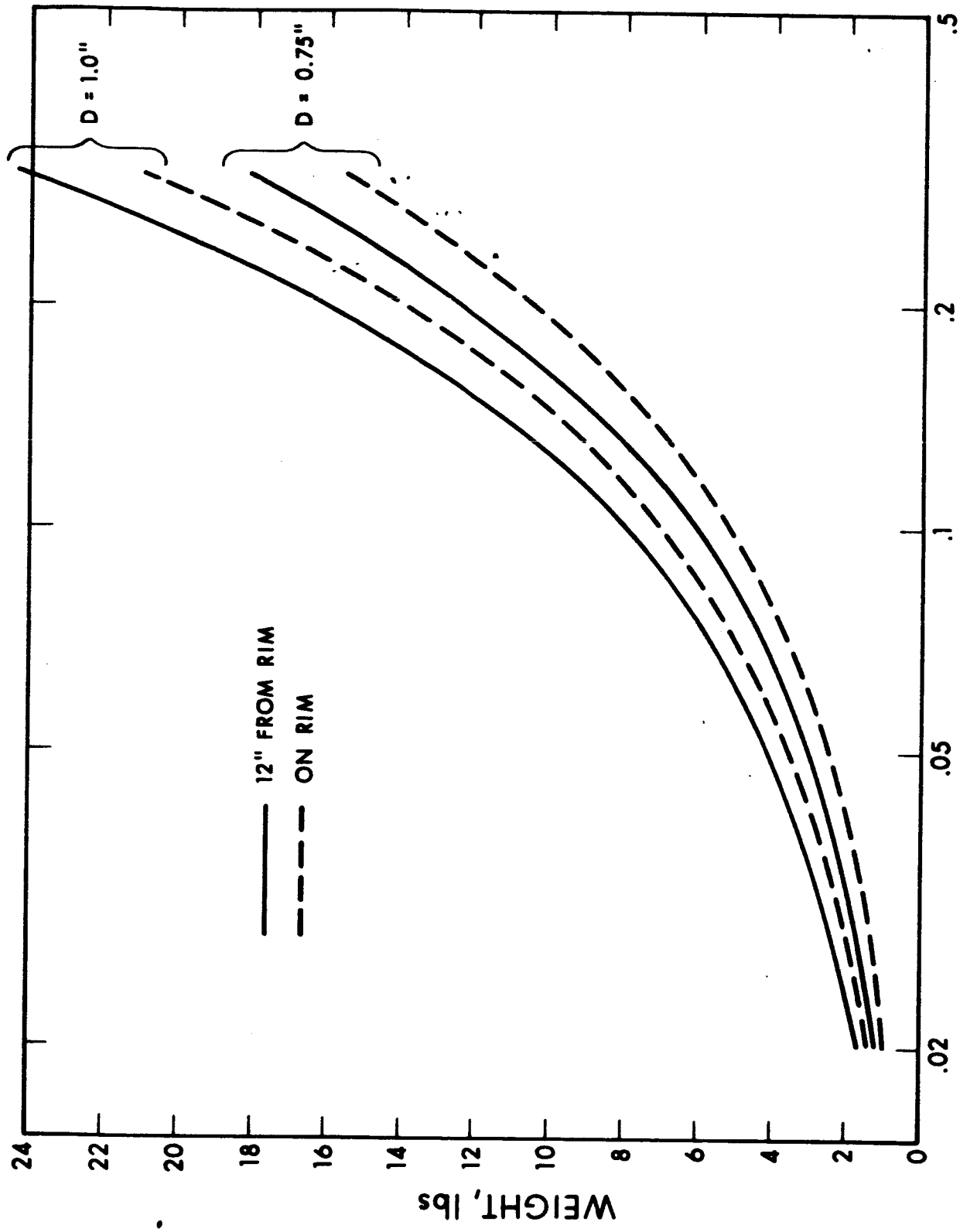


FIG. 7-3. CURVES OF BUS BAR/REGENERATOR SUPPORT WEIGHT AS A FUNCTION OF BUS BAR THICKNESS FOR 1.0" and 0.75" DIA. (AVERAGE LENGTH TO RIM = 74.4")

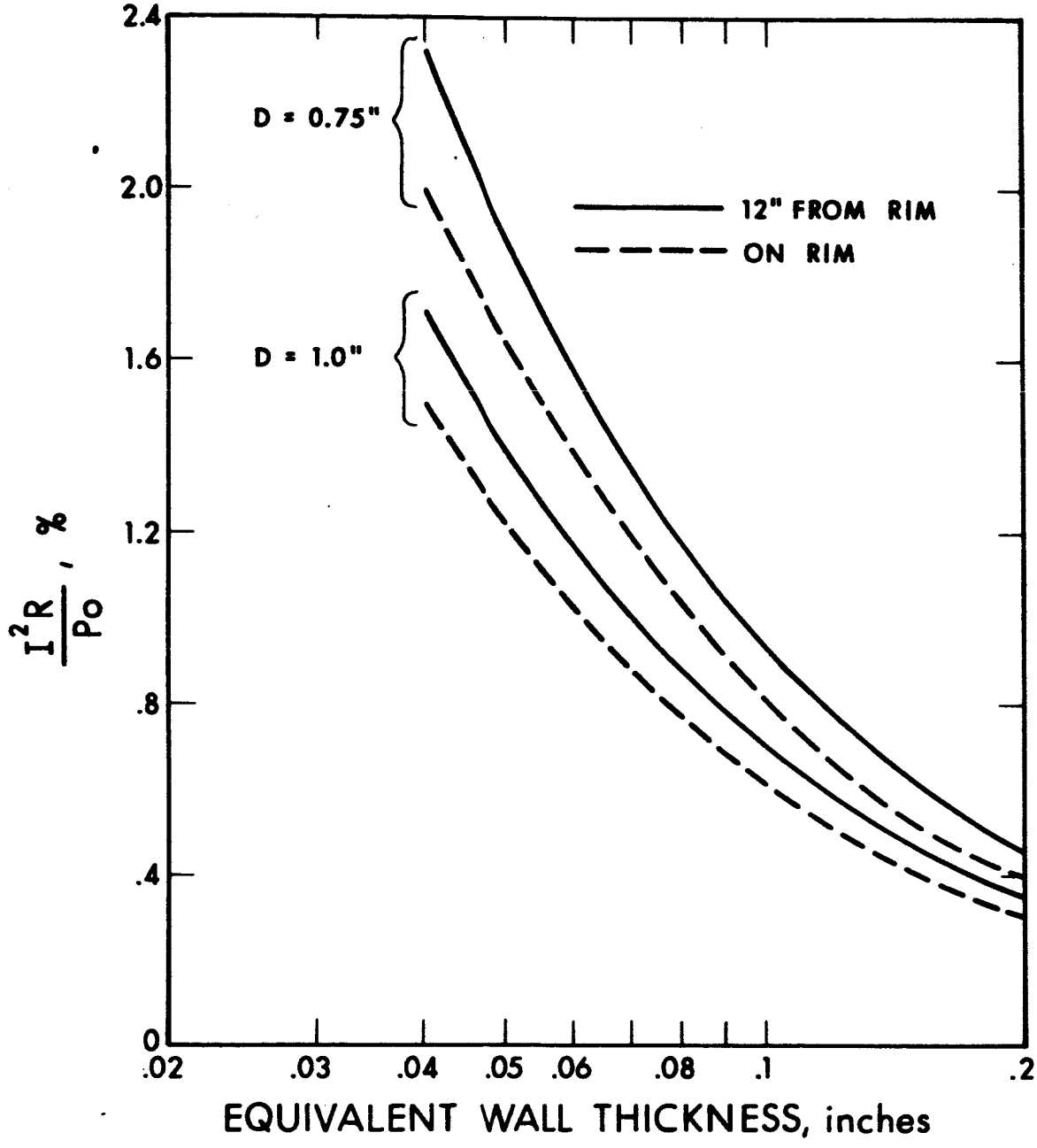


FIG. 7-4. CURVES OF BUS BAR/GENERATOR SUPPORT LOSSES, %, AS A FUNCTION OF BUS BAR THICKNESS FOR 1" AND 0.75" DIA. (AVERAGE LENGTH TO RIM = 74.4") $P_{out}$ = 150 WATTS

For comparison of various power condition systems, the various forms of low temperature dc-dc conversion schemes are represented schematically by (a) and the high temperature system by (b) in Fig. 7-5. Before making actual comparisons, some definitions of efficiencies and the system area to which they apply are required.

### 7.4.1 Efficiencies

A block diagram of a solar thermionic system is shown in Fig. 7-6. This is a rather simplified diagram, since it omits solar flux controls, cesium reservoir controls, shunt load regulators and energy storage, but it is quite adequate for a reliable comparison since the omitted items are essentially independent of those shown as far as efficiency is concerned. The efficiencies shown on the diagram are defined in Table 7-I. To simplify the comparison further, the analysis is based on a generator-mirror efficiency of 10 percent, i.e., $\eta_{c-a}$ $\eta_{obs}$ $\eta_{gen}$ = 0.1 with a total power into the mirror of 1500 watts. Thus, for the low temperature system, the electrical power out of the 4 diode thermionic generator is 150 watts. For the high temperature system, however, some thermal power is required to supply the electron emission and thermal losses for the thyratrons. The extremes in required thermal power absorbed from the cavity for the thyratrons are 200 to 300 watts depending upon the thyratron cathode temperature. A detailed tabulation of weight and efficiencies for both the solid state and thyratron systems is given in Table 7-II. The two columns on the right refer to the two extremes of thyratron power absorbed from the thermal cavity. A detailed discussion of the thyratron thermal power requirements is given in Subsection 4.3.

### 7.4.2 System Weights

The system weights are tabulated in Table 7-II. They are based on measured or calculated values for the existing five foot mirror system including the solid state dc-dc converter. Thyratrons, transformer, and high temperature weights are calculated from estimated parameters.

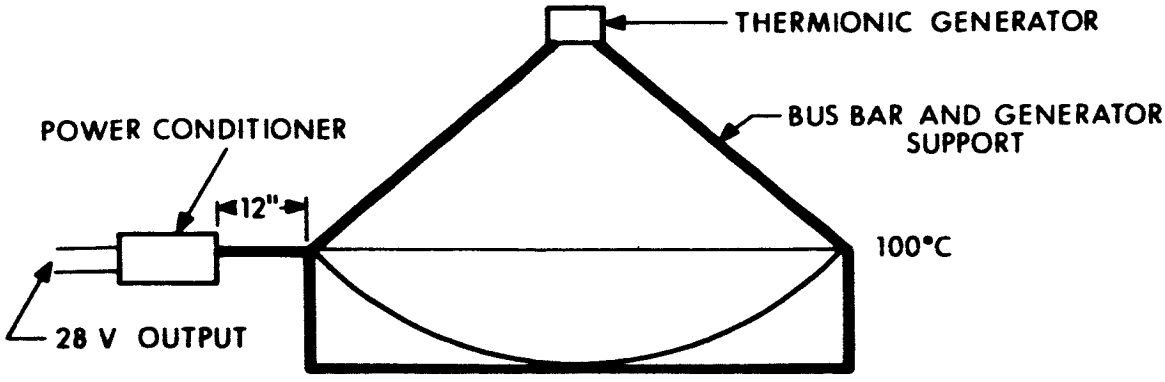


(a) TYPICAL LOW TEMPERATURE SYSTEM CONFIGURATION

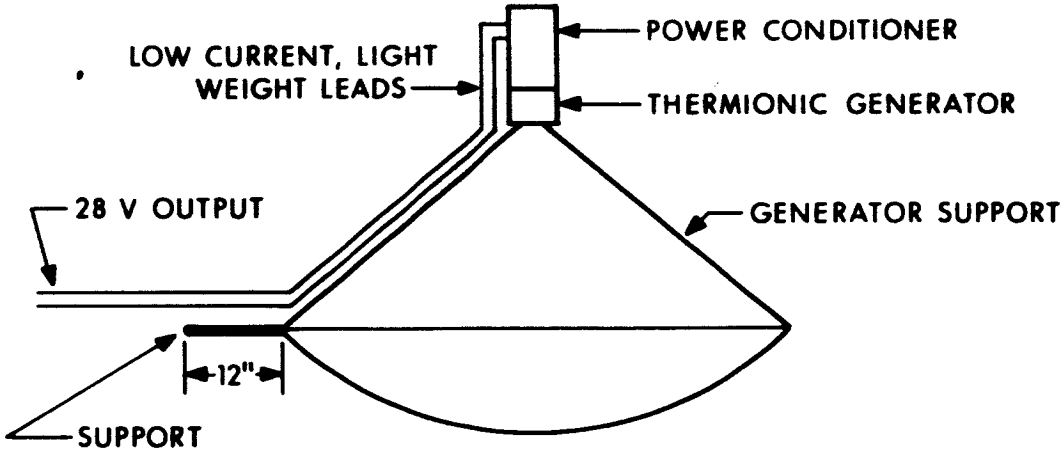


(b) INTEGRATED HIGH TEMPERATURE TUBE AND TRANSFORMER CONFIGURATION

COMMON SPECIFICATIONS

5' COLLECTOR
55° RIM ANGLE
150 WATT GENERATOR OUTPUT

FIG. 7-5. SOLAR POWER SYSTEMS

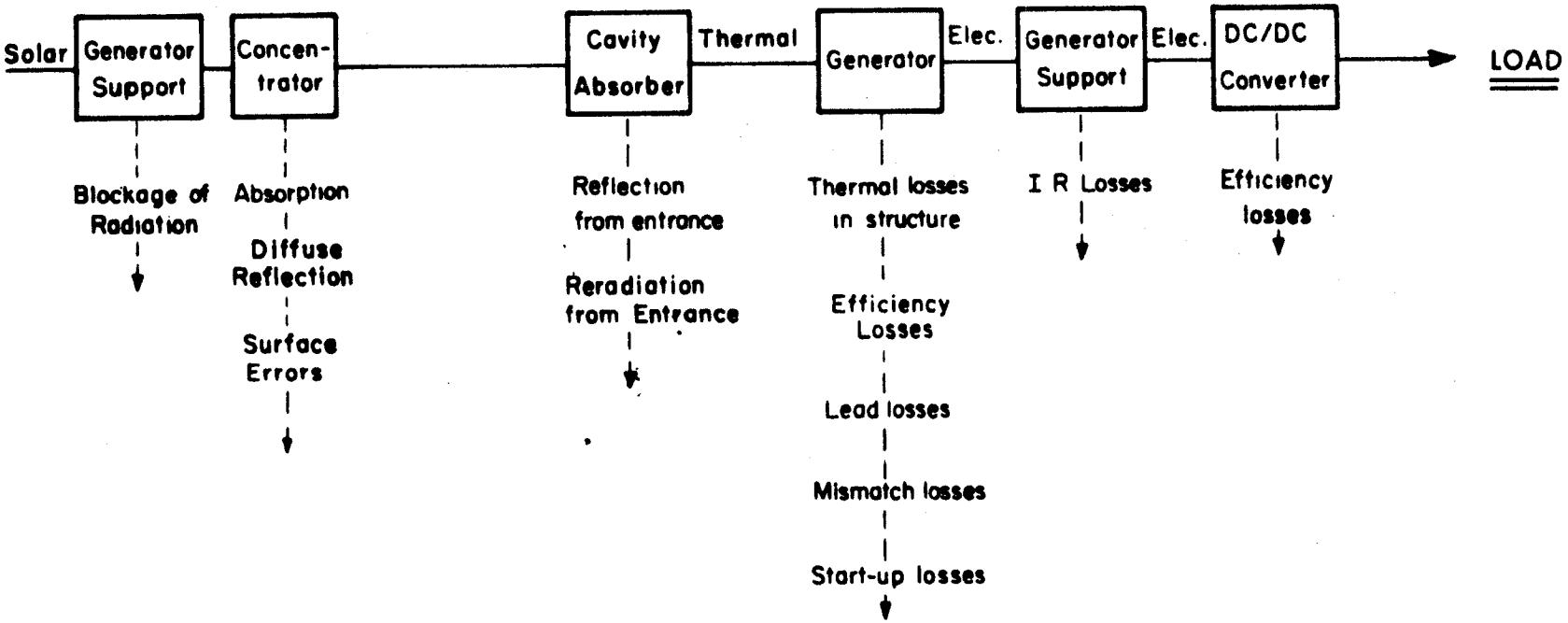


**System Efficiency**

$$\eta_{sys} = \underbrace{\eta_{obscr}}_{\text{Obscuration}} \times \underbrace{\eta_{c-a}}_{\text{Concentrator-Absorber Efficiency}} \times \underbrace{\eta_{gen}}_{\text{Generator Efficiency}} \times \underbrace{\eta_{BB}}_{\text{Lead eff.}} \times \underbrace{\eta_{BD}}_{\text{DC/DC Converter Efficiency}}$$

FIG. 7-6. SOLAR-THERMIONIC SYSTEM BLOCK DIAGRAM AND ENERGY LOSSES

**TABLE 7-I**

DEFINITION OF EFFICIENCIES

| | | | |
|---|---|---|---|
| (1) | $\eta_s$ - system | = | $\eta_{BB}\ \eta_{DD}\ \eta_{gen}\ \eta_{a-c}\ \eta_{obs}$ |
| (2) | $\eta_{obs}$ - obscuration | = | $\frac{\text{area mirror - area obsc}}{\text{area mirror}}$ |
| (3) | $\eta_{c-a}$ - absorber/collector | = | $\frac{\text{Useful output power of cavity}}{\text{(incident mirror power)}\ \eta_M}$ |
| (4) | $\eta_{gen}$ - thermionic gen. | = | $\frac{\text{Electrical power out}}{\text{thermal power in}}$ |
| (5) | $\eta_{DD}$ - dc-dc Conversion | = | $\frac{\text{power out}}{\text{power in}}$ |
| (6) | $\eta_{BB}$ - Bus Bar | = | $\frac{\text{power out of bus - } I^2R \text{ in bus}}{\text{power into bus}}$ |

TABLE 7-II

WEIGHTS AND EFFICIENCIES

| System | Solid-State | | | Thyratron-500°C | | | |
|---|---|---|---|---|---|---|---|
| | Low Eff Germ Syst. (30°C) | High Eff Germ Syst. (30°C) | High Freq Silicon Syst. (85°C) | ***Low Thermal Power | | ***High Thermal Power | |
| Item Weight (lb) | | | | 1600 Hz | 500 Hz | 1600 Hz | 500 Hz |
| Concentrator | 10.0 | 10.0 | 10.0 | 10..0 | 10.0 | 10.0 | 10.0 |
| Generator + Ring | 5.0 | 5.0 | 5.0 | 5.0 | 5.0 | 5.0 | 5.0 |
| Generator Support | 1.5 | 1.5 | 1.5 | 1.0 | 1.0 | 1.0 | 1.0 |
| Add. Bus | 2.5 | 2.5 | 2.5 | --- | --- | --- | --- |
| Connections | 0.25 | 0.25 | 0.25 | --- | --- | --- | --- |
| Add. Radiator | 1.0 | 1.0 | ---- | --- | --- | --- | --- |
| **Low Current Leads | ----- | ----- | ----- | 0.16 | 0.8 | 0.16 | 0.8 |
| dc-dc Converter | 12.0 | 27.0 | 1.0 | 4.0 | 6.0 | 4.0 | 6.0 |
| Total System Weight (lb) | 32.25 | 47.25 | 20.25 | 20.16 | 22.8 | 20.16 | 22.8 |
| $\eta_{c-a}$ $\eta_{obs}$ $\eta_{gen}$ | 10 | 10 | 10 | 10 | 10 | 10 | 10 |
| *$\eta_{BB}$ | 97 | 97 | 97 | 99.3 | 99.8 | 99.3 | 99.8 |
| $\eta_{DD}$ | 74 | 93 | 70 | 77.4 | 77.4 | 77.4 | 77.4 |
| $\eta_e = \eta_{BB}\,\eta_{DD}$ | 72 | 90 | 63 | 77 | 77 | 77 | 77 |
| Watts In | 150 | 150 | 150 | 130 | 130 | 120 | 120 |
| Watts Out | 108 | 135 | 94 | 100 | 100 | 92 | 92 |
| Figure of Merit F W/Lb | 3.34 | 2.86 | 4.65 | 4.95 | 4.40 | 4.5 | 4.0 |

*$\eta_{BB}$ includes 0.050 Volt loss for multiple series connections.

** Weights calculated for 10 feet total of no. 16 and no. 10 copper wire respectively and doubling for insulation.

*** Low thermal power = 200 watts thermal drive for thyratron
High thermal power = 300 watts thermal drive for thyratron

### 7.4.3 Summary of System Characteristics

Table 7-III summarizes the salient parameters and characteristics of both low and high temperature systems. For the worst case of the thyratron and the best case of the solid state system the watts per pound are almost equal, being slightly better for the thyratron. The best case for the thyratron is significantly better than the solid state. However, several other features must be considered before deciding which system is actually superior, as pointed out in section 7.4.

#### 7.4.3.1 Short Circuit Protection

The solid state device needs protection from load short circuits. The thyratron does not.

#### 7.4.3.2 Over-Voltage Protection

The solid state device needs protection from over-voltages which are possible in the circuit. The thyratron does not.

#### 7.4.3.3 Shunt Regulation

The entire circuit must be shunt regulated to maintain constant generator load currents. Without it the generator operating point shifts from optimum with resulting performance degradation. Both systems will therefore utilize shunt regulation.

#### 7.4.3.4 Magnetic Field Problems

Many of the satellite instruments, particularly the magnetometer will suffer if generator bus bar power conditioner current loops are not eliminated. The acceptable field strengths are a few gammas (1 gamma = $10^{-6}$ gauss). The solid state bus bar system requires, therefore, high current coaxial leads and connectors. The thyratron output can be a low current, lightweight, flexible coax or a shielded, twisted pair to minimize electrical interference.

#### 7.4.3.5 System Complexity

One of the most significant features of the high temperature systems is the reduction in overall system complexity.

TABLE 7-III

SUMMARY OF SYSTEM CHARACTERISTICS

| Feature of System | Solid State | | | Thyratron | | |
|---|---|---|---|---|---|---|
| | Ge Low Eff | Ge High Eff | Si | 1600 cps | 500 cps | 500 cps |
| Total Weight | 32.2 | 47.2 | 20.3 | 20.2 | 22.8 | 22.8 |
| Solar Power Input - Watts | 1500 | 1500 | 1500 | 1500 | 1500 | 1500 |
| Electrical Power Into Dc-Dc Converter - Watts | 150 | 150 | 150 | 130 | 130 | 120 |
| Electrical Power Out - Watts | 108 | 135 | 94 | 100 | 100 | 92 |
| Dc-Dc Conversion Efficiency | 72 | 90 | 63 | 77 | 77 | 77 |
| Figure of Merit, F - Watts/lb. | 3.3 | 2.9 | 4.6 | 4.9 | 4.4 | 4.0 |

| | | |
|---|---|---|
| Short Circuit Protection Rqd. | Yes | No |
| Overvoltage Protection Rqd. | Yes | No |
| Shunt Regulation Rqd. | Yes | Yes |
| Magnetic Field Problems | Severe | Slight |
| System Complexity | High | Low |
| Maximum Operating Temp. | 30°C to 85°C | 500°C to 600°C |

High current coaxial-leads and their two terminal connectors are quite complex mechanically, and are potentially electrical problems. As can be seen from Fig. 7-1, the entire generator support structure in the case of the high temperature system is at ground potential with no multitude of high current connections. This mechanical simplicity should result in overall improvement in system reliability, lowered cost, and ease of assembly.

## REFERENCES


1 H. Fotz, Annalen der Physik, 37, (1940) pp. 1-40

2 J. A. Kok, Appl. Sci. Research, Section B, 5 (1956) pp. 445-453

3 J. A. Kok, Appl. Sci. Research, Section B, 6 (1956) pp. 207-221

4 J. T. Tate and P. T. Smith, Phys. Rev., 46 (1934) pp. 773-776

5 A. W. Hull, E. E. Burger, and J. H. Westbrook, Final Report, Contract W-36-039-56-14604 (Aug 1950)

6 W. J. Kearns and J. O. Pehek, WADC Report 57-422 (Mar 1958)

7 D. H. Pollock, A. O. Jensen, and J. A. Duarte, Report on Thermionic Specialist Conference, Gatlinburg, Tenn. (1963) p. 94

8 A. O. Jensen, WADC Report 58-621 (Jan 1959)

9 S. C. Brown, Basic Data of Plasma Physics, p. 47ff, J. Wiley and Sons, New York, 1959

10 L. M. Chanin and R. D. Steen, Phys. Rev., 132 (1963) p. 2554

11 L. M. Chanin and R. D. Steen, Phys. Rev., 136 (1964) p. A138

12 P. Dandurand and R. B. Holt, Phys. Rev., 82 (1951) p. 278

13 C. L. Chen and M. Raether, Phys. Rev., 128 (1962) p. 2679

14 P. Langevin, Ann. Chim. et Phys., 5 (1905) p. 245

15 A. von Engel, Ionized Gases, p. 100, Oxford, 1955

16 A. O. Jensen, Research Program Related to Vapor Thermionic Converters for Nuclear Application, EOS Report 3410, Oct 1963

17 N. Pavlik, "High Temperature Stability of Magnetic Materials," J. Appl. Phys., 32 (1961) p. 372 S

18 P. E. Kueser et al, "Research and Development Program on Magnetic, Electrical Conductor, Electrical Insulation, and Bore Seal Materials," Third Quarterly Report, Report NASA-CR-54089, Contract NAS3-4162, Jun 1964

19 D. S. Shull, "Improved Magnetic Properties of High-Purity Iron-Cobalt Alloys Containing 27-43% Cobalt," J. Appl. Phys., 32 (1961) p. 356 S

20 W. W. Wareham, "Magnet Wire for 600°C Temperature Transformers, AIEE Transactions, Applications and Industry, Mar 1959

21 Harold M. Nordenberg, Electronic Transformer, Reinhold Publishing Corporation, 1964

22 Ruben Lee, Electronic Transformers and Circuits, John Wiley and Sons, 1955

23 J. G. Howe, Final Report for High Power, High Voltage, Audio Frequency Transformer Design Manual, Navy Department Bureau of Ships, Electronics Division, Contract BSR-87721, Aug 31, 1964

24 A. E. Fitzgerald and C. Kingsley, Electric Machinery, McGraw-Hill Book Company, 1961

25 William H. McAdams, Heat Transmission, McGraw-Hill Book Company, 1954